Combating Nonlinear Power Amplifier Effects in Multicarrier Systems

BY

GUOGUANG CHEN
B.E. in Electronic Engineering, Tsinghua University, Beijing, 1999
M.S. in Electronic Engineering, Tsinghua University, Beijing, 2002
M.S. in Mathematics, University of Illinois at Chicago, Chicago, Illinois, 2005

THESIS

Submitted as partial fulfillment of the requirements
for the degree of Doctor of Philosophy in Electrical and Computer Engineering
in the Graduate College of the
University of Illinois at Chicago, 2014

Chicago, Illinois

Defense Committee:

Rashid Ansari, Chair and Advisor
Milos Zefran
Jezekiel Ben-Arie
Daniela Tuninetti
Ajay Kshemkalyani, Computer Science

Copyright by

Guoguang Chen

2014

To my family

ACKNOWLEDGMENTS

Completion of this thesis would not have been possible without the help and support of so many people in my life and through my eduction. I am indebted to all those directly and indirectly helped me complete my thesis.

First, I would like to express my gratitude to my advisor, Dr. Rashid Ansari, who has not only supervised this thesis and provided guidance and encouragement, but also has most kindly supported and advised me in every aspect of my life. I am so grateful for him sharing with me his knowledge and wisdom and providing countless efforts in my growth.

I would like to thank the other members of my dissertation committee, Dr. Milos Zefran, Dr. Jezekiel Ben-Arie, Dr. Daniela Tininetti and Dr. Ajay Kshemkalyani, for reviewing the thesis and providing insightful suggestions. I would like to thank Dr. Yingwei Yao and Dr. Ashfaq Khokhar for providing close guidance and answering my many questions.

I am grateful to Department of Electrical and Computer Engineering, Department of Physics, and College of Engineering for the financial support.

My sincere thanks also go to my colleagues and friends, Dr. Lucia Valbonesi, Dr. Ahmet Murat Bagci, Dr. Xiaobo Zhang, Dr. Songqing Zhao, Dr. Huan Xu, Dr. Wei Qu, Gregory Nash and Xi Xu for all interesting research and technical discussions.

Some portions of Chapter 3, 4 and 6 in this work have been published previously in papers that I am the primary author by IEEE. I would like to thank my co-authors and also thank IEEE to allow me to reuse them.

ACKNOWLEDGMENTS (Continued)

Last but not least, I would like to express my deepest gratitude to my beloved wife, my beloved parents, my beloved brother and sister. I would like to appreciate their unconditional and endless love, support and blessing, without which I would not have achieved this successfully. Their encouragement has given me the strength to accomplish this and will be always with me.

GC

TABLE OF CONTENTS

CHAPTER | PAGE

TABLE OF CONTENTS (Continued)

LIST OF TABLES

LIST OF FIGURES

LIST OF FIGURES (Continued)

FIGURE **PAGE**

LIST OF ABBREVIATIONS

3GPP	3rd Generation Partnership Project
4G	4th Generation
ACE	Active Constellation Extension
ACPR	Adjacent Channel Power Ratio
ADC	Analog-to-Digital Converter
AWGN	Additive White Gaussian Noise
BER	Bit Error Rate
CA	Carrier Aggregation
CCDF	Complementary Cumulative Distribution Function
CIR	Channel Impulse Response
CP	Cyclic Prefix
CS	Compressed Sensing
DAC	Digital-to-Analog Converter
DMT	Discrete MultiTones
DPD	Digital Pre-Distortion
EPS	Erasure Pattern Selection
FAP	Frame-based Alternating Projection

LIST OF ABBREVIATIONS (Continued)

FDM	Frequency Division Multiplexing
FIR	Finite Impulse Response
IBO	Input Back-Off
ICI	InterCarrier Interference
IFFT	Inverse Fast Fourier Transform
IMD	InterModulation-Distortion
ISI	Inter-Symbol Interference
LASSO	Least Absolute Shrinkage and Selection Operator
LP	Linear Programming
LS	Least Square
MB-OFDM	Multi-Band Orthogonal Frequency Division Multiplexing
MCM	MultiCarrier Modulation
MIMO	Multiple Input Multiple Output
MSE	Mean Square Error
OBO	Output Back-Off
OFDM	Orthogonal Frequency Division Multiplexing
OFDMA	Orthogonal Frequency Division Multiple Access
OOB	Out-Of-Band

LIST OF ABBREVIATIONS (Continued)

PA	Power Amplifier
PAPR	Peak-to-Average Power Ratio
POCS	Projection Over Convex Sets
PTS	Partial Transmit Sequences
RCE	Relative Constellation Error
RX	Receiver
SDR	Software Defined Radio
SISO	Single Input Signal Output
SLM	SeLective Mapping
STBC	Space Time Block Coding
TR	Tone Reservation
TX	Transmitter
ZF	Zero-Forcing

SUMMARY

Multicarrier modulation is widely accepted as a powerful technology to satisfy the increasing demand of high data rate transmission, whether in wireless or in wireline systems. The inherent large envelope fluctuations of multicarrier signals necessitate the use of power amplifiers with large dynamic range. However, the incompatibility between linear amplification and power efficiency poses challenges in deployment of practical systems. When high power efficiency is mandatory, e.g. in mobile systems, nonlinear power amplifier effects are inevitable. The goal of this research is to explore signal design and processing techniques to enhance the performance of transmission and reception in multicarrier communications that employ nonlinear power amplifiers at the system front-end, specifically focusing on boosting power efficiency and improving bit error rate in orthogonal frequency division multiplexing (OFDM) and orthogonal frequency division multiple access (OFDMA) systems.

In this dissertation, several novel methods are proposed to combat the nonlinear power amplifier effects in multicarrier systems. With emphasis on easy implementation and low cost at the transmitter, two novel peak windowing schemes, with asymmetric window functions and simple coefficient optimization respectively, are proposed to handle the case of successive peaks in transmitted signals. Numerical results validate their effectiveness in overcoming the flaws of excessive attenuation and ill-conditioning window weights in existing schemes.

Receiver-oriented methods are explored to provide power efficiency improvement with simple direct clipping at the transmitter while clipping noise is estimated and compensated at the receiver. To tackle the intrinsic challenge in OFDMA reception where an individual user has insufficient information of other users' modulation to apply conventional decision-aided schemes, a novel method is proposed to estimate the clipping noise using two steps: improved peak localization and magnitude estimation with frame-based alternating projection. The proposed method does not require modulation information of the entire OFDM symbol, and has significantly enhanced performance compared with existing schemes in terms of bit error rate, especially in the high signal-to-noise regime.

With focus on the power efficiency improvement without sacrificing system performance in terms of bit error rate, we propose a joint design of transmitter-oriented scheme of tone reservation with clipping and receiver-oriented scheme of frame-based alternating projection which opens up a novel way to deal with the nonlinear power amplifier effects. The tight requirement of sparsity level in clipping noise imposed by compressed sensing framework is relaxed with a novel formulation based on frame theory and projection over convex sets and thus significant bit error rate performance improvement is achieved compared with the signal recovery scheme based on compressed sensing. In addition, the proposed scheme provides increased flexibility in balancing the computational load between the transmitter and the receiver, which gives more leeway to system designers.

For multicarrier systems with multiple antennas, the large fluctuations of signals that are prone to nonlinear power amplifier effects still remain an issue. In this research, a hybrid scheme that combines two existing single-antenna schemes, namely erasure pattern selection and Fourier projection algorithm, is designed to address the issue for the multi-antenna case and simulations demonstrate it outperforms a popular existing scheme. Signals in generalized multicarrier modulated systems such as multi-band OFDM, software defined radio and carrier aggregation, still face the issue of combating nonlinear power amplifier effects, which drives future research in this field.

CHAPTER 1

INTRODUCTION

Multicarrier modulation (MCM) is a parallel data transmission scheme in which data is split into several components and used to modulate subcarriers spaced within an available bandwidth.

MCM has a long history over decades as an effective technology for data transmission [1] [2]. Initially it was developed in analog military communications. With recent advances in digital signal processing technology, MCM such as orthogonal frequency division multiplexing (OFDM) and discrete multitones (DMT) exhibit rising popularity for the implementation of wireless and wireline communication systems [3]. Many international standards make use of OFDM or DMT as the physical layer technology, such as Asymmetric Digital Subscriber Line (ADSL), Very high bit-rate Digital Line Subscriber (VDSL), Digital Audio Broadcasting (DAB), Digital Video Broadcasting (DVB), IEEE 802.11a/g wireless LAN [4, 5], IEEE 802.16 [6, 7], IEEE 802.11n [8], IEEE 802.11ac [9] and the 3rd generation partnership project (3GPP) pre-4G long term evolution (LTE) (3GPP Release 8) [10] and 4G LTE-Advanced (3GPP Release 10) [11]. Orthogonal frequency division multiple access (OFDMA) that evolved from OFDM as a multiple access scheme is widely known to be the predominant air interface of next-generation mobile broadband wireless systems. Increased adoption of multicarrier modulation is envisioned in the future standards beyond official 4th generation (4G) systems.

MCM is basically a method of frequency division multiplexing (FDM). In classical FDM, the available bandwidth is divided into many non-overlapping subbands; each subcarrier is modulated with a data stream and then all subcarriers are frequency-division multiplexed. The basis pulse function for each subcarrier is rectangular in frequency domain obtained by band-limited filters. When the number of subcarriers increases, increasingly sharp filters are required to separate the subbands. This makes the implementation of such systems impractical. It is also necessary to use some extra bandwidth between subcarriers to prevent intercarrier interference (ICI). To overcome the inefficiency in bandwidth usage and the difficulty in implementation, OFDM adopts $sinc$ functions as the basis pulse functions for subcarriers. Orthogonality among subcarriers is maintained and multiplexed subcarriers are separable at the receiver, while the scalability within the assigned bandwidth increases.

There are other forms of multicarrier modulation depending on the orthogonal basis pulse function used in the system, such as filter bank based multicarrier (FBMC) systems [12] and wavelet packet modulation (WPM) [13]. In terms of FDM, Multi-Band OFDM (MB-OFDM) divides the spectrum into several bands and then transmits the information using OFDM modulation in each band. The spectrum can be continuous with multiple neighboring subbands, or discrete with different spectrum gaps among the subbands. The advantages of MB-OFDM were exploited in the proposal of the IEEE 802.15.3a standard developed for ultra wide band (UWB) communication systems [14]. Since bands in MB-OFDM are still multiplexed, it can be viewed as generalized multicarrier modulation. Another form of generalized multicarrier modulation arises in software defined radio (SDR) signals [15]. Each subband signal in SDR can be a single carrier signal or an orthogonal multicarrier signal, while the overall SDR signal is composed of all subband signals as FDM. Carrier Aggregation (CA) that utilizes SDR as another form of multicarrier modulation was firstly introduced into 3GPP LTE standard and it aims to bring multiple subbands together into a total bandwidth greater than 100MHz for wireless broadband communications. Considering that the major advantages for OFDM or DMT multicarrier signals lie in quick and easy practical implementation of fast Fourier transform (FFT) algorithms, the term MCM is often used in the telecommunication field synonymously as OFDM or DMT, and sometimes they are interchangeable.

1.1 Multicarrier Modulation: Advantages and Disadvantages

Advantages of MCM over single carrier modulation are reflected in the widespread acceptance of MCM in various standards. An OFDM-based system can provide high spectral efficiency and high flexibility in supporting adaptive loading according to channel conditions. It also provides greater immunity to multipath fading and impulse noise, and simplifies the structure of equalizers with efficient hardware implementation using FFT techniques [16]. In addition, it makes single frequency networks possible which is especially attractive in broadcasting applications [17].

While it has many advantages, OFDM also has some drawbacks such as susceptibility to frequency dispersion and phase noise, which makes it very critical to have accurate synchronization in multicarrier systems. In OFDM, subcarriers are perfectly orthogonal only if the transmitter and the receiver use exactly the same frequencies. Any frequency offset affects the orthogonality consequently resulting in ICI at the receiver. Random phase jitter between the phase of the carrier and the phase of the local oscillator may cause the frequency, which is the time derivative of the phase, not to be perfectly constant, thereby causing ICI.

The drawback that most affects multicarrier systems is due to large fluctuations in transmitted signals caused by superposition of multiple subcarrier signals. The nonconstant signal envelope affects performance due to the presence of nonlinear devices in the communication path such as digital-to-analog converter (DAC), analog-to-digital converter (ADC) and power amplifiers. The design of a power-efficient system becomes challenging since high signal peaks produce severe impairments due to nonlinear distortions. A power amplifier (PA) with a large dynamic linear range is required in order to magnify the peaks without distortions, but the required sophisticated and expensive PA leads to dramatically increased system complexity and cost. An alternative is to force the operation of the PA into the linear range with high input back-off (IBO), that is, offsetting the input signal so far away from PA saturation as to accommodate the peaks and amplify the large peak linearly. The high IBO forces the PA to work in lower power region most of the time, thereby causing power efficiency to be severely reduced and energy to be unacceptably wasted. Low power efficiency significantly shortens the battery lifetime in mobile devices and also leads to undesirable reduction in the range of signal transmission in mobile systems.

In order to combat nonlinear effects without sacrificing power efficiency, many schemes have been proposed in the literature [18–20]. Most of them use the ratio between the peak power to the average power, Peak-to-Average Power Ratio (PAPR) as a measure of fluctuations of the input signals, and attempt to reduce nonlinear distortions by reducing PAPR to the extent possible. PAPR reduction schemes are mostly focused on the transmitter (TX) side, either in a distortionless way or with acceptable distortion. Distortionless transmitter-oriented schemes apply signal transformations to alter the input signal in a way that PAPR of the transformed signal is reduced, while the inverse transformation is applied at the receiver to restore the original signal without any impairment, so system performance is not degraded. Such schemes include multiple signal representation, probabilistic methods, dummy signal insertion and coding based methods. Distortion transmitter-oriented schemes modify the signal directly to satisfy PAPR requirements of TX PA, such as clipping and filtering, peak windowing, compounding transforms, and constraint constellation shaping. The signal with reduced PAPR at TX tends to incur less in-band distortion and smaller out-of-band emission. However, the gain of reduced PAPR comes with penalties such as increased transmission power, loss of data rate, extra computational complexity, spectral inefficiency and so on, which impacts the overall system performance negatively [21]. Depending on system requirements and user applications, different criteria rule the system design, especially when high power efficiency is demanded in a multicarrier system with a large number of subcarriers like OFDMA.

Besides PAPR, bit error rate (BER) has also been used as a figure of merit to evaluate the influence of signal transformation schemes on the system performance [22], [23]. The interference caused to other channels in these schemes is also a major concern in real-world system design [7]. While BER performance can be improved by some techniques at the receiver (RX), interference to other channels at the transmitter is relatively hard to control in practical systems. This challenge becomes especially important when high power efficiency is mandatory and the high back-off condition is unavailable, e.g. when sensor lifetime needs to be prolonged, or when limited interference can be tolerated to boost power efficiency. It is shown [24] that BER increases when PAPR further decreases assuming PAPR-reduced signals are entirely confine to PA linear range. Operating PA close to saturation to achieve high power efficiency makes PAPR reduction largely ineffective as the PAPR-reduced signals still drive PA to nonlinear amplification.

Beyond the considerations of performance metrics, simple implementation and fine controllability of the system are also important criteria for system designers to choose an appropriate scheme. In some low-cost applications, easy compatibility even outweighs other factors in complying with the standards.

After assessing different PAPR schemes, some popular PAPR reduction schemes are identified as lacking fine control on the performance and hard to maintain or upgrade. Some other schemes like peak windowing [25] permit fine control, are easy to implement and have excellent compatibility with other schemes.

Recently with the coming era of mobile Internet, the increasing demand of high data rate transmission pushes OFDM system design to employ more and more subcarriers. High order OFDM increases the complexity of PAPR reduction and the implementation cost at the transmitter. In the meanwhile, system capacity is demanded to provide services to more and more users. With more attention on BER performance in multiuser access scenario, interest has recently shifted to receiver-oriented schemes and is rapidly growing with the goal of tackling the nonlinear PA effects, especially when limitations on power consumption, implementation cost or computational complexity exist at the transmitter. Receiver-oriented methods may take an advantage of combating nonlinear effects with reduced dimension of signals on own subcarriers. However, a new challenge is posed by lack of information of other users which invalidates existing decision-aided methods.

Through the identification of key features of various schemes, integration of different schemes to achieve better performance can be envisioned accordingly. Previous schemes mostly were developed for single-antenna system. The implementation of OFDM in conjunction with multi-antenna techniques is a promising way to efficiently use the radio spectrum extending the capacity of mobile communication systems [26]. However, in a multiple input multiple out (MIMO) OFDM system, the high peak power issue still exists. Improvements obtained by combining different single-antenna PAPR reduction schemes are shown to be effective in enhancing the system performance in multiple antenna systems.

As generalized multicarrier modulation, multi-band signals like MB-OFDM or SDR or CA also exhibit high peak power due to the superposition of subcarrier signals. The trade-off between nonlinear distortions and the system power efficiency is still a major concern in that scenario which provides fertile ground for future work.

Therefore, this research is strongly motivated by the need to address the long-standing issue of balancing the conflict of power efficiency and nonlinear distortions in multicarrier modulated systems.

1.2 Research Contributions

The goal of this research is to explore signal design and processing techniques to enhance the performance of transmission and reception in multicarrier communications that employ nonlinear power amplifiers at the system front-end, specifically focusing on boosting power efficiency and improving BER in the PAPR issue in OFDM(A) systems. We develop new methods to alleviate nonlinear effects before signal transmission and/or to mitigate nonlinear effects by compensating received signals. We consider techniques suitable for implementation at the transmitter and at the receiver, and hybrid solutions with both ends involved together. We evaluate the performance through theoretical analysis and numerical simulations. Techniques are also extended to multicarrier systems with multiple antennas. Other considerations in practical systems such as block synchronization, phase jitter, I/Q imbalance, PA linearization and channel estimation are not addressed in this research.

By introducing the formulation of clipping noise estimation in terms of frame theory and projection over convex sets (POCS), we propose a new solution which very efficiently handles estimation and compensation of clipping noise in OFDMA systems, successfully resolving the new challenging issue that modulation information of other users is not known to any individual users in OFDMA. We cast the problem under frame theory and utilize POCS to achieve reliable results and better performance without increasing complexity.

We exploit the full potential of reserved bandwidth available in practical systems, and investigate the dual sparsity in frequency domain and time domain to jointly design the schemes in TX and RX. In this way we make it feasible to balance the load between TX and RX, and provide more flexibility in utilizing the reserved bandwidth. System performance is significantly improved by overcoming the sparsity limitations imposed in the existing schemes based on compressed sensing.

1.2.1 Transmitter-Oriented Approach: Improved Peak Windowing

We start with investigating the peak windowing scheme that is widely used in practice because of its simplicity of not requiring transmission of side information and neither modifying receiver structure nor incurring loss of data rate. More importantly, peak windowing does not impose heavy computational burden which is highly desirable for high order OFDM with limited resources at the transmitter. Despite of its relative simplicity of processing at TX, the specific challenge of peak windowing lies in the consecutive peaks in one OFDM symbol. We discovered the existing conventional methods treat multiple peaks in one OFDM symbol simply as isolated peaks without factoring in neighborhood context in the formulation, which results in over-attenuation from closely spaced windowed segments generated from neighboring peak window functions. Thus it leads to severe performance degradation. Meanwhile, the window shape is restricted to be symmetric and with limited flexibility.

For preserving the attractive features of low complexity of peak windowing while addressing the shortcoming of excessive attenuation of closely spaced peaks, as a solution, we propose two new peak windowing schemes, called Sequential Asymmetric Superposition (SAS) and Optimally Weighted Windowing (OWW) respectively, to overcome the disadvantages in previous schemes. We utilize asymmetric windows and propose to optimize coefficients of consecutive window functions with a novel formulation under convex optimization. Thereby we rectify the over-attenuation condition and incorrect coefficient calculation due to ill-conditioned matrix inversion. Although the cost of complexity is slightly higher than directly clipping, improved peak windowing incurs lower penalty in out-of-band distortion and meanwhile it provides a way to control the spectral mask to comply with the requirements of standards.

1.2.2 Receiver-Oriented Approach: Frame-based Clipping Noise Estimation and Compensation

We exploit the schemes of further reducing the processing cost at the transmitter which apply direct clipping at the transmitter and on the other hand estimating and recovering the distortion at the receiver. The existing schemes like decision-aided methods that require iterative computational load over the entire OFDM symbol are not suitable for high order OFDMA and meanwhile OFDMA poses a new challenge because individual users do not have modulation information of other users, which makes it infeasible to reconstruct the whole OFDM symbol to reevaluate the clipping scenario at TX,and therefore decision-aided schemes are invalidated.

We analyze the key factors in reconstructing the clipping noise at the receiver, and note that the accuracy of peak localization is crucial to the success of the whole scheme. We also identify the drawback of existing band-limited signal recovery scheme. Based on that, we propose a novel method of estimating peak locations with the help of oversampling and spectrogram analysis, in conjunction with predicting peak magnitudes with a combination of frame iteration algorithms and alternating projection over convex sets. The BER performance is significantly improved over existing schemes while the complexity is kept on the same level.

1.2.3 Design of Joint Transmitter-Receiver-Oriented Schemes

We identify the advantages of fully exploiting the degree of freedom of reserved bandwidth available in practical systems, and emphasize the necessity of balancing the complexity between TX and RX to provide flexibility to adapt to different system design requirements. Recently receiver-oriented approaches based on compressed sensing have attracted a lot of attention and a promising approach based jointly on TX and RX in conjunction with compressed sensing has been newly proposed. We investigated the performance of this TX-RX-based scheme and identified its limitations due to sparsity level and weak immunity against noise contamination. When high power efficiency is demanded and severe clipping happens at the transmitter, the performance of compressed sensing based schemes is diminished.

Recently receiver-oriented approaches based on compressed sensing have attracted a lot of attention and a promising approach of joint TX and RX with compressed sensing is proposed. We examine the performance of the existing scheme and identify its limitations due to sparsity level and weak immunity against noise contamination. When high power efficiency is demanded and severe clipping happens at the transmitter, the performance of compressed sensing based schemes is limited.

In our approach we examine the partition of the available reserved subcarriers into two sets, and utilize one set for tone reservation at the transmitter and the other set with frame-based signal recovery at the receiver. In our design we further incorporate a clipping step with tone reservation to boost power efficiency at the transmitter, and the clipping noise is recovered and compensated with frame-based alternating projection at the receiver. The proposed joint design overcomes the drawback of existing schemes that depend on light clipping and impose restrictions of only a few clips being allowed. The performance enhancement is significant especially for the high order OFDMA systems.

1.2.4 Extension on Multiple Antenna Systems

We examine the still-existing problem of high PAPR in the front-end of multicarrier systems with multiple antennas. High peaks can appear on any antenna. Direct application of PAPR reduction schemes for single input signal output (SISO) to each antenna individually in MIMO requires extensive computations to reach a final solution for all antennas, thus causing undesirable increase in complexity and redundancy.

We develop a frame-based algorithm erasure pattern selection to reduce the maximal peak power simultaneously over all antennas and utilize spatial diversity from space-time coding as well. Through the proposed scheme, more reliable communications over MIMO-OFDM is accomplished.

1.3 Organization of Dissertation

The remainder of the dissertation is organized as follows.

In Chapter 2 the concept of multicarrier signals specifically OFDM and the system model is first introduced and extended to discuss the PAPR issue. Typical methods of PAPR reduction are then surveyed. After introducing the power efficiency of PA, the importance of boosting power efficiency in multicarrier systems is emphasized.

In Chapter 3 an improved signal design based on peak windowing with the aim of simplifying transmitter processing while not severely penalizing system performance is presented. An optimization formulation is proposed as well to address the issue of multiple consecutive peaks in one OFDM symbol. Numerical results validate the proposed ideas.

In Chapter 4 a new idea is presented to handle clipping noise estimation and compensation at the receiver side after further reducing the transmitter processing to simple clipping only. The new method consists of two major steps: improved peak localization with analysis of run-length and spectrogram on oversampled sequences, and alternating projection over convex sets formulated with frame theory to further enhance the accuracy of signal recovery. Complexity analysis and simulation results reveal the advantages of the proposed method.

Efforts are taken in Chapter 5 to jointly design schemes at both the transmitter and the receiver, namely tone reservation with clipping at TX and frame-based alternating projection at RX. The new hybrid scheme provides flexibility in balancing load between TX and RX, in the meanwhile, simulations results demonstrate its superiority over the existing scheme based on compressed sensing.

Next the PAPR issue in multi-attenna multicarrier systems is explored with erasure pattern selection (EPS) method in Chapter 6.

Finally the major remarks in this dissertation are concluded in Chapter 7 and directions of future work are outlined.

CHAPTER 2

MULTICARRIER SIGNALS

2.1 System Model

In high-speed wireless communications, time-dispersive channels often cause severe inter-symbol interference (ISI), and also make the traditional symbol-to-symbol equalization complicated, especially when the number of time-dispersive channel taps become large. Multicarrier modulation like OFDM is a block transmission mechanism and it has been introduced to simplify the equalizer structure and also provide high spectral efficiency and robustness against time-dispersive channels. MCM is performed to group the data stream on a block-by-block basis with guard intervals inserted between blocks. Several symbols in one block are transmitted in parallel and therefore each symbol duration is increased thus reducing ISI. If the guard interval is larger than the channel delay spread, the received frequency-domain signal is simply the input signal multiplied with the frequency domain channel coefficients, which makes a simple single-tap equalizer feasible for each subcarrier.

OFDM systems can be efficiently implemented by using an Inverse Fast Fourier Transform (IFFT) at the transmitter while applying FFT at the receiver. The block diagram in Figure 1 shows a conventional OFDM system.

In an OFDM system with N subcarriers, the sequence of input bits are first aggregated into N parallel groups and then each group is mapped onto appropriate symbols based on the constellation

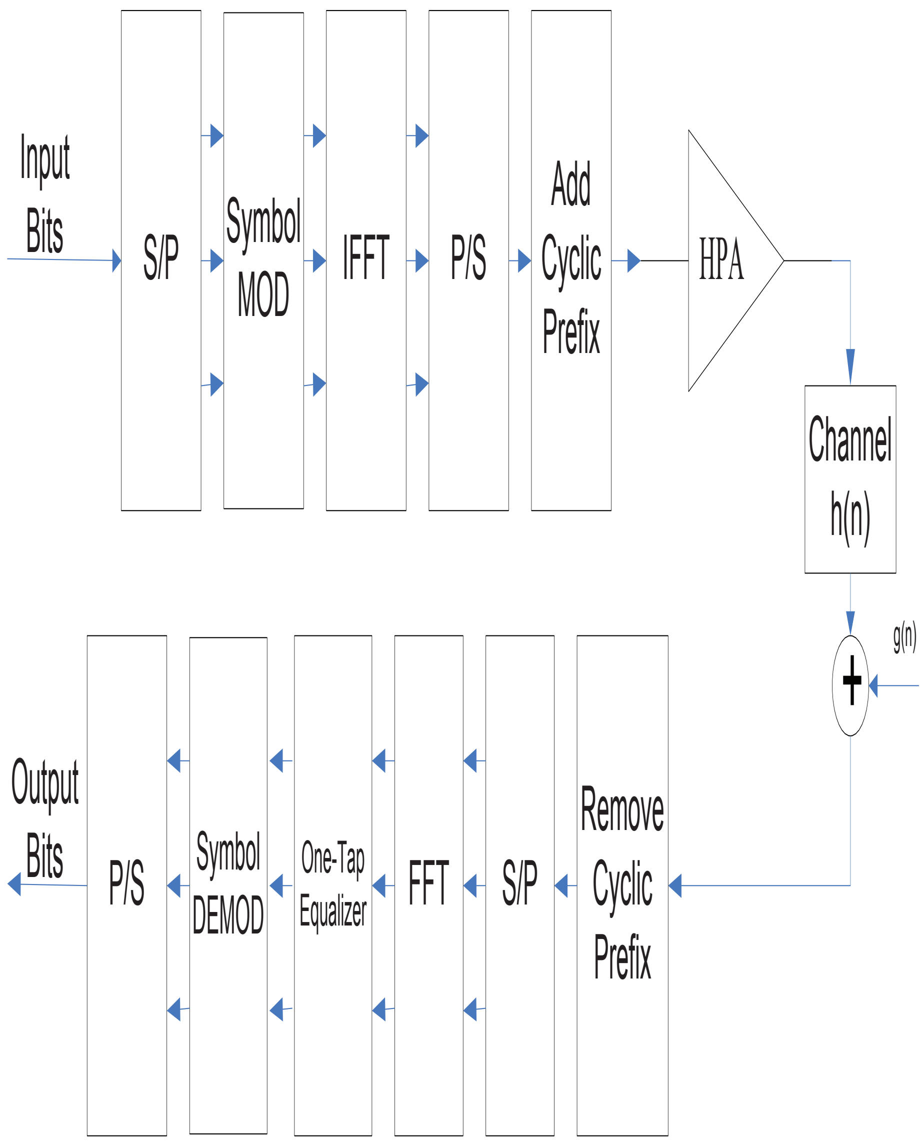

Figure 1. Block Diagram of FFT-based OFDM system

size assigned to each subcarrier, X_n. Each of these groups can be represented by a data symbol vector $\mathbf{X} = [X_0, X_1, \cdots, X_{N-1}]^T$.

To optimize the overall bit error rate over the whole data symbol vector, each subcarrier can be allocated with different modulation by adaptive modulation algorithms like bit loading where the constellation size is a function of the subchannel quality. The subcarriers with better quality, i.e. higher signal-to-noise ratio (SNR), use larger constellation size. In that scenario, channel state information (CSI) normally obtained at the receiver (RX) needs to be sent back to the transmitter (TX). Coding and interleaver can also be applied at TX in practical OFDM systems to improve the system performance. For keeping the model simple with focus on nonlinear PA effects, however, adaptive modulation, coding and interleaving are not considered in this research.

The OFDM symbol $\mathbf{X}$ is fed to IFFT and the discrete-time OFDM sequence is obtained. The time domain multicarrier signal $x_k, k = 0, 1, \cdots, N-1$ after the IFFT operation is given by

$$x_k = \frac{1}{\sqrt{N}} \sum_{n=0}^{N-1} X_n e^{j\frac{2\pi}{N}nk}, \quad k = 0, 1, \ldots, N-1 \tag{2.1}$$

where $\frac{1}{\sqrt{N}}$ is the normalization factor. The modulation process can also be represented in matrix form. Let $\mathbf{x} = [x_0, x_1, \cdots, x_{N-1}]^T$, then

$$\mathbf{x} = \mathbf{W_N X} \tag{2.2}$$

where

$$\mathbf{W}_N = \begin{bmatrix} W_{1,1} & W_{2,1} & \cdots & W_{N,1} \\ W_{1,2} & W_{2,2} & \cdots & W_{N,2} \\ \vdots & \vdots & \ddots & \vdots \\ W_{1,N} & W_{2,N} & \ldots & W_{N,N} \end{bmatrix} \quad (2.3)$$

and

$$W_{m,n} = \frac{1}{\sqrt{N}} e^{j2\pi(m-1)(n-1)/N} \quad (2.4)$$

$\mathbf{W}_N$ is a symmetric and orthonormal matrix. After the discrete coefficients x_k are converted into analog values by digital-to-analog converter (DAC), the values x_k can be deemed as samples of a continuous-time signal $x(t)$ taken at times $t = kTs/N$, where T_s is the symbol period.

$$x(t) = \frac{1}{\sqrt{N}} \sum_{n=0}^{N-1} X_n e^{j2\pi n t/T_s}, \quad 0 \leq t \leq T_s, \quad (2.5)$$

then $x(t)$ is upconverted to modulate the carrier and transmitted over the channel after being amplified by HPA.

The frequency spacing between two adjacent subcarriers is usually set as $1/T_s$, the subcarriers are specified as

$$f_k = k/T_s, \quad k = 0, 1, \cdots, N-1 \quad (2.6)$$

By selecting the bandwidth of $1/T_s$ for each subcarrier to be very small, the symbol time duration is large compared with channel time dispersion, which effectively avoids ISI. At the receiver, the signal is demodulated by FFT. The orthogonality of baseband subcarriers, that is,

$$\int_0^{T_s} \cos(2\pi f_i t + \theta_i)\cos(2\pi f_j t + \theta_j)\,dt = 0, i \neq j$$

guarantees the subcarriers can be easily separated at the receiver.

To mitigate ICI caused by multipath fading, a guard interval of size of ν modulated symbols in time domain is added. If the guard interval is chosen larger than the channel response duration L, ICI free reception can be obtained by discarding the extra symbols at the receiver. Two forms of guard intervals can be adopted, namely zero padding and cyclic prefix (CP). Cyclic prefix copies ν extra samples from the end of the OFDM symbol and then appends them to the beginning of the OFDM symbol while zero padding adds ν extra zeros there. Both ideas are motivated by simple equalization at the receiver. Cyclic prefix is generally used in the system since zero padding introduces slightly more nonlinear distortion in the presence of nonlinear PA clipping effects [27].

The signal is then converted into analog by DAC, amplified by a high power amplifier (HPA)and fed into the channel. The sequence is transmitted through a channel with frequency selective fading whose channel impulse response (CIR) has L non-zero taps denoted as $\mathbf{h} = [h_0, h_1, \ldots, h_{L-1}]^T$. Note $L < \nu$. Assuming that carrier-frequency offset and time offset estimations are perfect and compensated without any synchronization error, the received signal contaminated by channel noise is expressed as

$$\tilde{\mathbf{y}} = \mathbf{h} * \mathbf{x}_{cp} + \tilde{\mathbf{g}} \tag{2.7}$$

where $*$ denotes convolution operation, $\mathbf{x}_{cp}$ denotes the signal with cyclic prefix and $\tilde{\mathbf{g}}$ is the zero mean additive complex Gaussian channel noise. Note $\tilde{\mathbf{y}}$ is a vector with length $N+\nu+L-1$.

The receiver basically reverses the process at the transmitter. The receiver strips off the CP and then gathers N samples of the received signal, $\mathbf{y} = [y_0, y_1, \cdots, y_{N-1}]^T$ that satisfy

$$\mathbf{y} = \tilde{\mathbf{H}}\mathbf{x} + \mathbf{g} \tag{2.8}$$

where $\mathbf{g}$ is the additive zero mean circularly symmetric complex Gaussian noise vector with covariance matrix $N_0\mathbf{I_N}$, $\mathbf{H}$ is an $N \times N$ circulant Toeplitz matrix derived from the CIR $\mathbf{h}$ as

$$\tilde{\mathbf{H}} = \begin{bmatrix} h_0 & 0 & \cdots & 0 & 0 & h_{L-1} & \cdots & h_1 \\ h_1 & h_0 & 0 & \cdots & \cdots & 0 & \ddots & \vdots \\ \vdots & h_1 & h_0 & 0 & 0 & \ddots & 0 & h_{L-1} \\ h_{L-1} & \vdots & h_1 & \ddots & 0 & \ddots & 0 & 0 \\ 0 & h_{L-1} & \vdots & \ddots & h_0 & \ddots & \ddots & 0 \\ \vdots & 0 & h_{L-1} & \ddots & h_1 & h_0 & 0 & 0 \\ \vdots & \vdots & 0 & \ddots & \vdots & \vdots & \ddots & 0 \\ 0 & 0 & \cdots & 0 & h_{L-1} & \cdots & h_1 & h_0 \end{bmatrix} \tag{2.9}$$

The matrix $\tilde{\mathbf{H}}$ is circulant, the eigendecomposition of $\tilde{\mathbf{H}}$ with the maxtrix W_N^H is

$$\tilde{\mathbf{H}} = \mathbf{W_N}\,\mathbf{H}\,\mathbf{W_N^H} \tag{2.10}$$

where $\mathbf{H} = diag\{H_0, H_1, \cdots, H_{N-1}\}$ is a diagonal matrix with

$$H_k = \sum_{l=0}^{L-1} h_l e^{-\frac{j2\pi kl}{N}}, \quad k = 0, 1, \cdots, N-1 \tag{2.11}$$

H_k is the samples of frequency channel response.

The detection at the receiver simply applies FFT to get

$$\begin{aligned} \mathbf{Y} &= \mathbf{W_N^H}\,\mathbf{y} \\ &= \mathbf{W_N^H}\,\mathbf{W_N}\,\mathbf{H}\,\mathbf{W_N^H}\,\mathbf{x} + \mathbf{W_N^H}\,\mathbf{g} \end{aligned} \tag{2.12}$$

The CP insertion and removal combined with FFT render the channel time convolution operation to a circular convolution operation. Then in frequency domain, the convolution operation converts into a multiplication operation.

$$\mathbf{Y} = \mathbf{H}\,\mathbf{X} + \mathbf{G} \tag{2.13}$$

where $\mathbf{G}$ is the frequency domain channel noise. If the CSI is available, which implies that $H_k, k = 0, 1, \cdots, N-1$ are all known, the estimation of data symbol X can be simply obtained as

$$\hat{\mathbf{X}} = DecML\{\mathbf{H^H}\,\mathbf{Y}\} \tag{2.14}$$

where $DecML\{\cdot\}$ denotes the maximum likelihood symbol detection.

It can be seen from Equation 2.14 that the equivalent channel matrix is diagonal and the frequency selective channel is therefore decoupled into N flat fading channels in parallel. The equivalent flat channel coefficients are just the FFT of the L tap channel impulse response as Equation 2.11. Note that the CP is just a replica of part of the original block signal and it therefore does not change the power characteristics of the original signal. It is easy to implement.

2.2 PAPR in OFDM systems

The time-domain signal in Equation 2.5 is constituted by the superposition of N complex exponential subcarrier signals at every time instant. At the instants that subcarriers are all in phase, the instantaneous power of the signal can reach N times the value of the signal average power if uniform modulation is used for each subcarrier. These large fluctuations are the major drawback of multicarrier signals. HPAs are key components in communication systems. Owing to cost, design, and the most importantly, power efficiency, HPA cannot accommodate the large dynamic range in the transmitted signal. Clipping the signal at some point is inevitable, i.e. PA saturation. Consequently distortions are generated. In the meanwhile, large fluctuations in the signal also require large word length in DAC or ADC to diminish the precision cut-off errors, which increases the system complexity and cost.

To counteract the peak power problem inherent in multicarrier modulation, a large amount of research work has been done in exploiting signal transformation schemes to neutralize the PA nonlinearity. Most of the research focuses on reducing the Peak to Average Power Ratio (PAPR) of the signal. PAPR is defined in continuous-time domain as:

$$\text{PAPR} = \frac{\max\limits_{0 \leq t \leq T_s} |x(t)|^2}{\mathbf{E}(|x(t)|^2)} \tag{2.15}$$

In this dissertation, the PAPR of discrete-time sequences (the sampled sequence as in Equation 2.1) is of particular interest. So, PAPR defined for discrete-time samples is used to approximate the value in Equation 2.15 with x_k. However, it is noted that the Nyquist rate sampled discrete-time signal can not fully capture the actual peak values in the continuous domain. So, oversampling is needed for discrete-time signal to approximate the continuous PAPR. Accordingly, samples of $x(t)$ at $t = kT_s/NQ$ can be efficiently computed via IFFT as

$$\underline{x}_k = \frac{1}{\sqrt{N}} \sum_{n=-NQ/2}^{NQ/2-1} \underline{X}_n \, e^{j\frac{2\pi}{NQ}nk}, \;\; k = 0, 1, \ldots, NQ-1 \tag{2.16}$$

where $\underline{\mathbf{X}} = \{\underline{X}_n\}$ of size NQ is obtained by inserting $(Q-1)N$ zeros into the original OFDM symbol as $\underline{\mathbf{X}} = [X_0, \cdots, X_{N/2-1}, 0, \cdots, 0, X_{-N/2}, \cdots, X_{N-1}]$ and Q is the oversampling factor. Correspondingly the PAPR definition on the oversampled sequence is

$$\text{PAPR} = \frac{\max\limits_{0\le k\le(NQ-1)} |\underline{x}_k|^2}{E\left\{|\underline{x}_k|^2\right\}}. \tag{2.17}$$

Interpolating the discrete-time signal with an oversampling factor $Q = 4$ can generate an acceptable approximation of PAPR in Equation 2.15 [28].

Suppose the input symbols in Equation 2.5 are statistically independent and identically distributed (i.i.d.), when the number N is considerably large, based on central-limit theorem, the resulting signal $x(t)$ approximates a complex Gaussian random process with zero-mean and variance σ^2. Its envelope follows Rayleigh distribution while the power distribution becomes a central *chi-square* distribution with two degrees of freedom. The cumulative distribution function (CDF) of the power distribution is

$$F(u) = \int_0^u \frac{1}{2\sigma^2} e^{-\frac{s}{2\sigma^2}}\, ds \tag{2.18}$$

The probability that PAPR of an OFDM signal of size N exceeds a given level P_0, indicated by the complementary cumulative distribution function (CCDF), can be expressed as:

$$\text{CCDF} = \Pr\{\text{PAPR} > P_0\} = 1 - \left(1 - e^{-P_0}\right)^N. \tag{2.19}$$

CCDF is used to depict the effectiveness of PAPR reduction scheme in decreasing the probability of clipping, thus lowering possible nonlinear effects. After oversampling, the samples can not be approximated as uncorrelated random variables any more. To roughly evaluate the CCDF after oversampling, the oversampled sequence is deemed as composed of αN uncorrelated samples. Then CCDF becomes

$$\text{CCDF} = \Pr\{\text{PAPR} > P_0\} = 1 - \left(1 - e^{-P_0}\right)^{\alpha N}. \tag{2.20}$$

Simulations indicate a good approximation can be obtained by setting the value $\alpha = 2.8$ in case of oversampling [29]. As seen from Equation 2.20, when the number of subcarriers increases, the probability of large PAPR decreases very quickly.

2.3 Efficiency of Power Amplifiers

A perfectly linear ideal memoryless power amplifier produces an output signal that is a scalar multiple of the input signal. The scalar is referred as the gain of the power amplifier. In reality, no practical amplifier is able to provide unlimited output power. All power amplifiers have certain maximum output-power capacity, referred as saturation. It imposes a limitation for PA input signal amplitudes. When the envelope of the input signal exceeds the limitation, the corresponding output will not be amplified normally. Instead, the output signal is in effect “clipped off” bounded by the saturation. This is the major source of nonlinear distortions. In practical systems when DAC is applied, the cut-off of DAC on precision conversion also produces similar nonlinear distortions; but such distortion is relatively very small. Thus in this work, only PA nonlinear distortion is considered. Note that besides the saturation clipping, signal distortions can also be generated due to a loss of linearity in envelop amplification and nonlinear phase shift for different input power levels and different frequency components in the input signal. All factors result in the nonlinearity of the PA and cause intermodulation-distortion (IMD) especially when multicarrier signals are applied.

A typical class of memoryless power amplifiers is solid state power amplifiers (SSPA). The nonlinear curve to characterize SSPA input-output power relationship is shown as Figure 2. One way of avoiding nonlinear distortion is to offset the input average power away from the saturation so as to fit the whole dynamic range of input signals into the linear range of PA, which is referred as Input Back-Off (IBO). It is defined in decibels as:

$$\mathrm{IBO} = 10\log\frac{P_{insat}}{P_{in}} \tag{2.21}$$

where P_{insat} is the input saturation power which is the minimum power that drives output power to saturation, and P_{in} is the average power of the input signal. Accordingly, the Output Back-Off (OBO) is defined as:

$$OBO = 10\log\frac{P_{outsat}}{P_{out}} \tag{2.22}$$

where P_{outsat} is the output saturation power and P_{out} is the actual output power. Clearly, increasing IBO reduces input power and consequently reduces output power.

Power amplifier efficiency is a significant factor affecting the efficiency of most wireless communication systems. Poor efficiency at the PA stage leads to large energy consumption, not only lowering the system efficiency like reducing the battery lifetime of the devices, but also exacerbating thermal problems with the devices thus causing other issues like instability. Power efficiency is usually defined to measure what portion of the PA consumption power P_{DC} is delivered to the load.

$$\eta_{dc} = \frac{P_{out}}{P_{DC}} \tag{2.23}$$

Depending on the properties of linearity, gain and design, amplifiers can be assigned to a number of classes. The main types of amplifiers with good linearity are Class A, Class AB, and Class B. Other classes power amplifiers with relative large nonlinearity belong to Class C, D, E, F, G, H and S [30]. Power efficiency varies from the class of power amplifiers, but power efficiency is usually low. A typical Class A has efficiency around 50% even at 0 dB OBO, while Class B may reach around 80% at the same condition. A relation between the efficiency and the OBO is illustrated in Figure 3 [30]. So, it is critical to improve power efficiency to avoid energy loss. Reducing the input back-off or increasing the

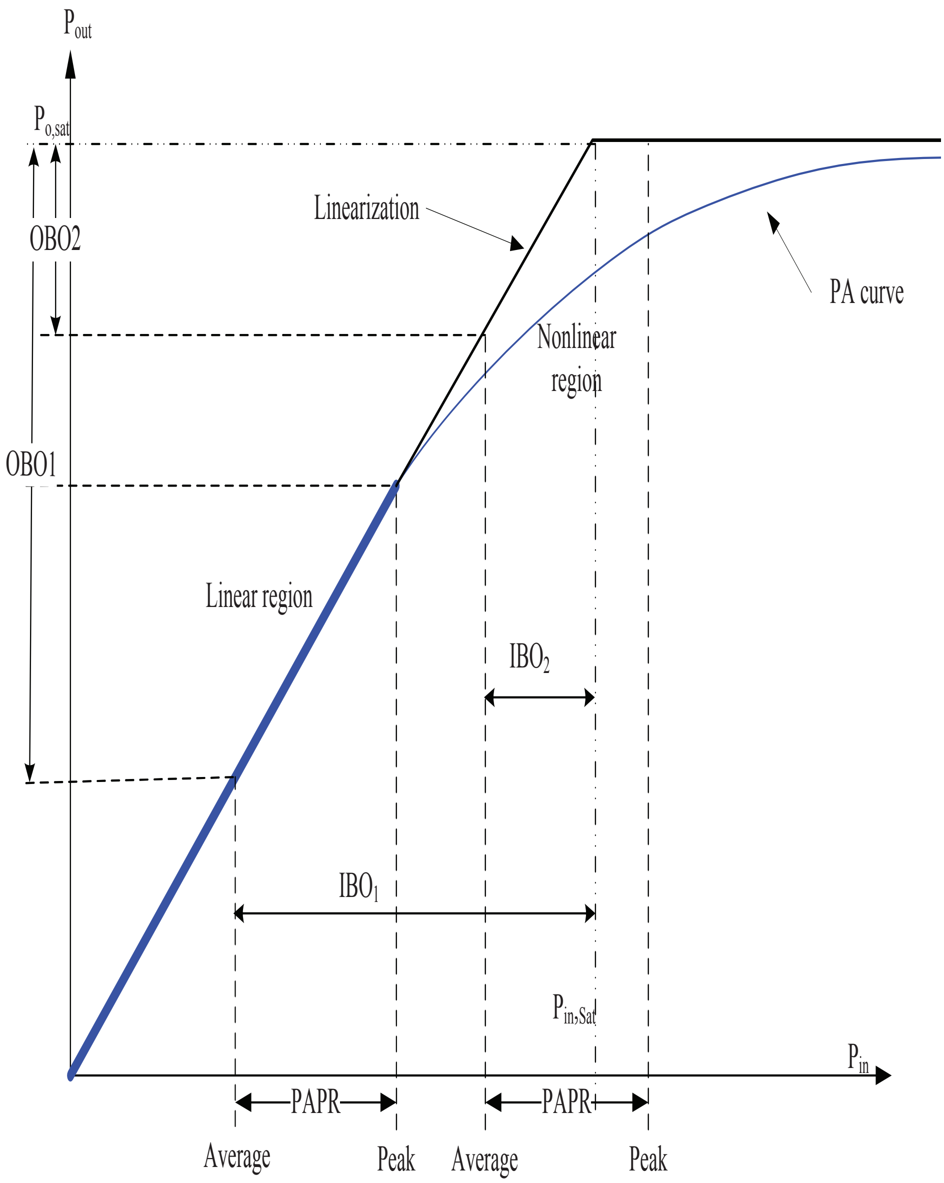

Figure 2. PA Nonlinear AM/AM curve of Rapp Model

average operating power of the PA increases the efficiency, on the hand, using large back-off degrades the efficiency of PA. For a Class A PA, every 3dB increase in IBO halves power efficiency.

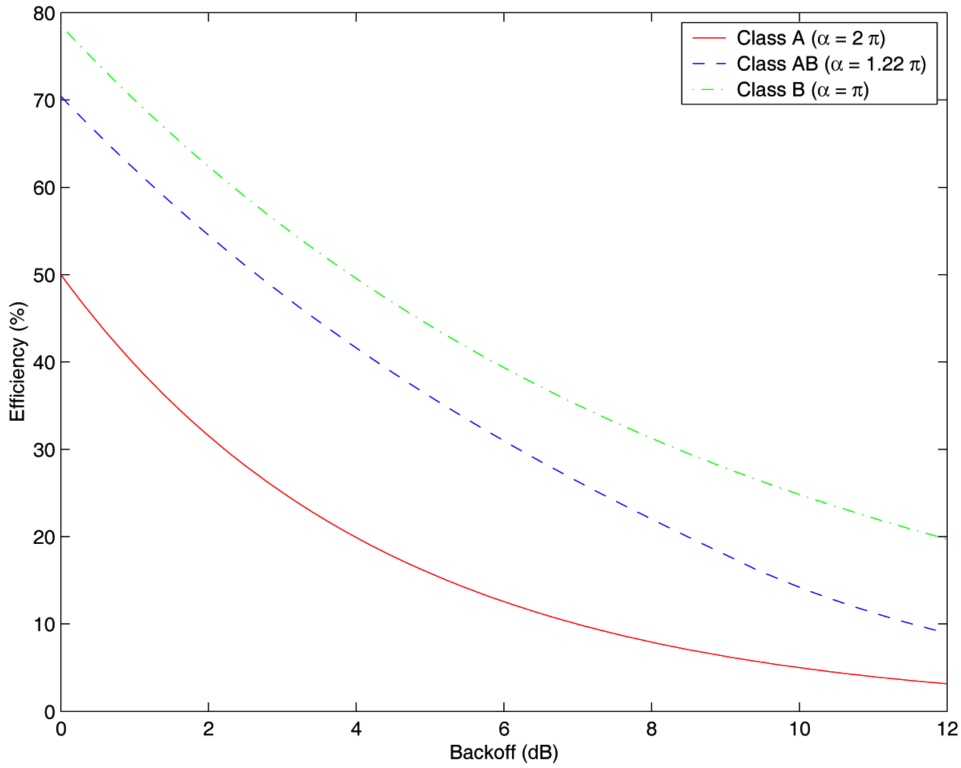

Figure 3. Efficiency versus OBO for various PA classes

One way to boost power efficiency while not incurring signal nonlinear distortions is to increase PA linear range by using digital pre-distorter (DPD) before feeding signals into PAs [31]. DPD rectifies nonlinear envelop amplification and nonlinear phase shift in real PA especially for the input range close to PA saturation. After DPD compensation, the combined nonlinearity is equivalent to a soft limiter as shown in Figure 2. In this work, a soft limiter is assumed in the performance comparison and phase nonlinearity is assumed to be very small and neglected which is essentially true for SSPA PA using Rapp model [32]. The input-output relation is

$$y(t) = A\left(|x(t)|\right)\, e^{(jx(t))}\, e^{(j\Phi(|x(t)|))} \tag{2.24}$$

where the AM-to-AM and AM-to-PM characteristics in Rapp model are

$$A(x) = \frac{x}{[1 + (\frac{x}{A_0})^{2p}]^{\frac{1}{2p}}} \tag{2.25}$$

$$\Phi\left(x\right) \approx 0 \tag{2.26}$$

Equation 2.26 means SSPA adds no phase distortion, $A_0 > 0$ is the saturating amplitude from PA, and $p > 0$ is the parameter which controls the smoothness of the transition from the linear region to the saturating region. Note that even if DPD is used, the linear range might be enlarged for input power, but output signal power is still bounded by the saturation, and the output signal still suffers from saturation clipping.

In order to obtain more output power from PA with high power efficiency, PA has to be driven to high input levels close to saturation (low IBO). In such a scenario complete linear amplification is difficult to fulfill. The nonlinear distortions are increased though power efficiency is boosted. Another alternative is to reduce PAPR to combat nonlinear effects while enhancing power efficiency. An approximate

PAPR	0	2	4	6	8	10	12	14
Class A Efficiency	58.7	45.75	35.66	27.79	21.66	16.89	13.16	10.26
Class B Efficiency	90.7	71.32	56.08	44.10	34.67	27.26	21.44	16.86

TABLE I

POWER EFFICIENCY (%) OF CLASS A AND CLASS B PA WITH INPUT SIGNAL AT DIFFERENT PAPR LEVELS

relationship of the power efficiency of class A and B PA and PAPR of a multicarrier signal **x** is given as [24] [33]:

$$\bar{\eta} = \alpha * e^{-\beta * \mathrm{PAPR}(\mathbf{x})} \tag{2.27}$$

where $\mathrm{PAPR}(\mathbf{x})$ indicates the PAPR of the input signal **x**, and α and β are coefficients depending on the PA class, e.g. $\alpha = 58.7$ and $\beta = 0.1246$ for Class A PA and $\alpha = 90.7$ and $\beta = 0.1202$ for Class B PA. The power efficiency of typical Class A and Class B PA's driven by an input signal with different PAPR is shown in Table I. The power efficiency increases monotonically as the PAPR decreases. So, it is desirable to boost power efficiency by reducing the PAPR of the input signal instead of improving PA linearity.

2.4 PAPR reduction schemes

A large effort has been devoted recently to address the high peak power issue in multicarrier systems [18, 19, 21]. Existing signal transformation schemes targeted at reducing PAPR can be divided into several categories: Clipping Based, Coding Based, Multiple Representation and Signal Adding Context.

2.4.1 Clipping-Based Schemes

The simplest way to avoid high peaks is clipping. Time-domain signals are clipped and the peak values are limited up to the clipping threshold before application to PA. By clipping the signals deliberately, peak values can be controlled thereby avoiding unmanageable nonlinear effects of PA.

To achieve better performance, the clipping threshold is usually preset lower than the saturation value of PA, due to which more distortion is expected to be generated. While the OOB distortion is critically limited in practical systems for the purpose of not interferencing adjacent channels, so filtering is usually followed the hard clipping to remove the OOB distortion. It has been argued [34] that filtering in frequency domain will regrow the time domain peaks in some way. A method of improvement is to iteratively do the clipping-filtering process to remove distortion [35].

Although distortion can be removed by filtering, it is not adequately controlled to meet the requirements of some specifications. Thus distortion controllable methods are developed. [36] introduced the distortion control schemes by setting a bound on modifications on frequency domain symbols after each recursive clipping-filtering process. In [37] similar distortion control is applied, using different bounds for in-band processing and out-of-band processing.

Clipping gives rise to out-of-band power by introducing sharp edges in the time domain signal. To mitigate the out-of-band frequency content, an alternative is to apply a companding transform to adjust the signal gradually instead of directly clipping it [38]. At the receiver, an inverse process is needed to recover the original signal.

A hybrid scheme of combining clipping and companding is proposed in [39]. The combination is targeted to reduce PAPR while not degrading BER performance compared to conventional μ-law companding scheme. The authors [39] proposed a concept of "proper" clipping ratio which limits the amplitude but does not degrade BER performance. The "proper" clipping ratio is identified through simulations according to different modulation sizes of QAM.

Peak Windowing is another method closely related to clipping [25,29,40,41]. Large peaks were multiplied by a window function, chosen to reduce out-of-band distortion by smoothing the sharp corners. The selection of different window functions and parameters enables designers to control the distortion level to comply with the regularities.

2.4.2 Coding-Based Schemes

This class of techniques limit PAPR by excluding codewords that generate large PAPR from the transmission codebook. Only those signals with a peak amplitude below the targeted level are chosen. This results in a complete elimination of the clipping noise.

Coding based scheme was first proposed in [42], in which an exhaustive search method is applied to produce a 3/4 rate block code, reducing the PAPR of a four-carrier signal from 6.02dB to 2.48dB. A general analysis reveals that only limited redundancy is needed to achieve the goal of reducing PAPR, however, no good codes for practical values of $N > 64$ are known. A simple strategy is to exhaustively check all possibilities and use a table lookup. Some codes are chosen based on the observation that an OFDM symbol with a small PAPR has an instantaneous power that is most of the time close to the average power. The symbol before the IFFT block therefore has a spectrum close to flat, or alternatively an impulse-like autocorrelation. Two codes based on this criterion are Golay sequences [43] and m-sequences [44].

All these block codes provide a low PAPR, typically below 3 dB for the small number of carriers considered, but suffer some serious drawbacks. They introduce significant overhead (25% to 50%) and are only available for a small number of carriers (4 to 16) and small constellation sizes (1 to 4 bits per carrier).

In theory, the error correcting capabilities of these codes can also be exploited, thus leading to codes to protect both BER and PAPR. However, finding a good code which is also good for PAPR reduction purposes is not an easy task, because if a codeword has good PAPR characteristics most likely its neighbors will too, but they cannot be chosen as codewords since adequate distance should be provided for good coding. Moreover, no efficient implementations are available yet. These drawbacks dramatically limit their usefulness with regard to real applications.

2.4.3 Multiple Signal Representation Schemes

The idea behind multiple signal representation is to generate multiple equivalent representations of the transmitted information block and choose the representation resulting in the lowest PAPR to transmit [45]. This approach does not remove the high PAPR completely, but lower the probability of occurrences of high peaks, and it requires less redundancy compared with coding based schemes.

Selective Mapping (SLM) [46] uses different phase vectors to rotate the pre-IFFT OFDM symbol to generate different representations, and side information indicating which phase vector being used is needed for the receiver to convert it back. The drawbacks of the schemes lies on high computational complexity in exhaustive search for the best representation out of the candidate pool, and side information needed to be transmitted to indicate which one being selected. Partial Transmit Sequences (PTS) [47] aiming to reduce the complexity of SLM, groups the subcarriers into sub blocks. For each block a rotation phase vector is applied. The complexity is reduced by eliminating the need to compute IFFT for every phase vector.

Although the partition can reduce complexity from SLM, PTS still needs to address the problem of how to obtain the optimal phase vector for each block. Exhaustive search is proven to be inefficient. A gradient descent search [48] accelerates the process and lowers the complexity. [49] addresses the issues in PTS of search complexity of high dimensional vector and optimal transmission of side information. It formulates the search process as a combinational optimization (CO) and develops simulated annealing to solve it. It concluded that random search can achieve better performance over sequence search. A scheme of embedded side information was also mentioned.

Since side information has to be transmitted, it causes some data rate loss. Some methods are proposed to transmit the side information implicitly, that is, no explicit side information is transmitted but it is suitably hidden in the data without sacrificing bandwidth [50]. However, this is achieved at some cost in power.

For PTS, it is common to use uniform rotation phase factors in $[0, 2\pi)$. Given a partition method (adjacent, interleave or random), after studying relative phase changes referenced to the phase of peak in the cluster, [51] concludes that such phase changes to optimize PTS can be approximated properly by a Gaussian-like curve. Then, it suggests the use of **non-uniform** phase factors in PTS which can be determined in advance according to the number of subcarriers and the number of PTS clusters and PTS partition. The non-uniform phase factors are obtained by optimizing a MMSE objective function which is similar to minimizing quantization errors, using discrete points to approximate a Gaussian-like curve.

Other methods can also be used to generate multiple representations, for example, different interleavers are used in [52]. Each interleaver generates one representation of the original information data. The advantages of interleaving is that it protects data transmission from the burst errors and increases the robustness of transmission thus lowering the bit error rate.

2.4.4 Signal Addition Schemes

Schemes in this category seek to reduce PAPR by adding property alteration signals in the OFDM system. In the adding context, the property alteration signal can be designed in the frequency domain and then inserted in null or data-bearing subcarriers; or designed in time domain and then directly imposed on the signal. Unlike removing the peaks by directly hard clipping, the alteration signal is designed with the interaction between time and frequency domain, with some iterative process involved in the schemes. Through the process, clipping noise is distributed accordingly under the criterion of not degrading the system performance.

The added signal is required not to affect the information transmitted. This can be done by either reserving peak cancellation carriers [53–55], or using pilot tones [56], or adjusting the constellation symbols [57–59].

Tone reservation (TR) [55] designs the alteration signal by projecting the clipping noise to reserved subcarriers, while data-bearing subcarriers are not affected. The cancellation signal can also be designed through convex programming [60, 61].

Active Constellation Extension (ACE) [58, 62] adds signals to data bearing or null subcarriers without degradation by adjusting the constellation points along some specific directions. Only the outer points of a constellation can be extended along the direction that increases their distances with all other points, thus not degrading BER performance at cost of large power consumption and increased complexity of iterative processing between frequency and time domain.

Yoo et al. [63] proposed a scheme named Selective Mapping of Partial Tones (SMOPT). It combines the ideas of TR and SLM. Instead of optimally searching dummy symbols added into all the unused subcarriers, it presets a finite set of PAPR Reduction Tones (PRT) vectors that contain symbols designed to reduce PAPR. Then only selecting the best vector out of the finite set given the number and positions of PRT. It reduces the time cost by avoiding TR search process, but as expected, its performance is not as good as TR and still side information of SLM needs to be transmitted.

The PAPR problem is formulated [64] as a two-stage optimization process of adjusting signs and amplitudes of subcarriers respectively. First the signs of values of different subcarriers are adjusted and then the problem is converted into a convex optimization problem to choose the amplitudes. Unlike [60] [61], it restricts the change of amplitudes to correspond to some search direction to guarantee the BER performance.

[65] deemed the out-of-band subcarriers after taking FFT back from oversampled time signal as "Ghost carriers" introduced in [66], values are set on those subcarriers under some spectrum constraint via convex optimization to minimize PAPR, simulations showed the scheme respects the spectrum mask even after average power was increased in this adding context, similar work was also reported in [67]. Similarly in the adding context, [68] borrows the idea from [69] to design an adding signal that only contains one or two extra subcarriers. The adding signal is calculated from time domain signal which exceeds the clipping threshold.

Some cost is still incurred in these schemes in transferring clipping noise effects. If the signal is added on reserved peak cancellation subcarriers, data transmission rate is correspondingly lost. Meanwhile, the average power of transmitted signal is increased after adding the alteration signals, equivalently, the power used for data transmission is decreased, which affects the system performance.

2.5 Analysis and Trade-off Considerations of PAPR Reduction

As shown before, many signal transformation schemes proposed to mitigate nonlinear effects adopt PAPR as the cost function and try to reduce nonlinear effects by achieving smaller PAPR. In order to improve the system performance, we expect that PAPR should predict the amount of distortion induced by nonlinear power amplifier. However, we note that PAPR itself is not enough to capture the statistical effects of PA nonlinearity.

Firstly, PAPR only indicates the maximal peaks in time domain as shown in Equation 2.17 while some secondary peaks beyond the clipping threshold also contribute to nonlinear distortions. But the PAPR value does not capture this situation especially in the high power efficiency region, where it is common to have more than one peak clipped by the PA saturation. Secondly, PAPR indicates the probability of clipping in conjunction with IBO and PA saturation from Equation 2.19; but it is not clear how the probability of clipping explicitly expresses the nonlinear impact, that is, given the same PAPR, different locations of clipping may produce different nonlinear effects. Therefore, only evaluating the capability of achieving smaller PAPR is inadequate to represent the overall link performance. Thirdly, It may be intuitive to think there is an explicit relationship between PAPR and BER in the presence of nonlinear PA. To some extent, PAPR should indicate or predict the distortions when nonlinear PA is present. However, the relationship is quite complicated. From Equation 2.19, PAPR can indicate the probability of clipping after a specific system configuration is given such as the number of subcarriers and PA saturation level above the average power, but it is not clear to estimate how the probability of clipping affects the amount of nonlinear distortions and degrades the system performance, since at the receiver clipping noise is spread by Fourier Transform to all subcarriers if clipping occurs. Further, we note that if signals have the same PAPR values, the distortions may still vary in different IBO configuration and PA saturation. So, we note that PAPR is, in this sense, not an appropriate measurement to show the potential nonlinear distortions.

To describe the system performance in case of nonlinear amplification, one should consider both in-band distortion and out-of-band distortion. We denote the frequency domain signal after nonlinear amplification as $\widetilde{X}_n^{(NQ)}$,that is,

$$\widetilde{X}_n^{(NQ)} = \mathrm{IFFT}^{(NQ)}(x_k) \tag{2.28}$$

where $\mathrm{IFFT}^{(NQ)}(\bullet)$ represents NQ point IFFT and $x_k,\ \ k = 0, 1, \ldots, NQ-1$ is obtained from Equation 2.16. We define $\widetilde{X}^{(NL)} = [\widetilde{X}^{(IB)}\ \ \widetilde{X}^{(OOB)}]$ where $\widetilde{X}^{(IB)}$ corresponds the in-band portion of PA output signal; and $\widetilde{X}^{(OOB)}$ is the out-of-band portion. By Bussgang theorem, the output signal of PA in time domain $\widetilde{x}_k$ can be decomposed as [70]:

$$\widetilde{x}_k = \alpha x_k + d_k \tag{2.29}$$

where d_k is the distortion generated by nonlinearity; and α is a complex factor chosen such that d_k is uncorrelated with x_k,

$$\alpha = \frac{E[\widetilde{x}_k x_k^*]}{E[|x_k|^2]} \tag{2.30}$$

Taking IFFT over distortion term d_k in Equation 2.29 and partitioning it into in-band and out-of-band frequency terms, equivalently we can express the distortion as $D = [D^{(IB)} \; D^{(OOB)}]$. Accordingly, we note that out-of-band distortion $D^{(OOB)}$ here is actually equal to $\widetilde{X}^{(OOB)}$. In this way, the in-band distortion and out-of-band distortion due to nonlinearity can be separately quantified.

$$\widetilde{X} = \alpha X + D^{(IB)} + D^{(OOB)} \tag{2.31}$$

When clipping occurs in PAPR-reduced signals, the distortions appear both in-band and out-of-band. It can be seen that the BER performance depends only on $D^{(IB)}$ after this decomposition. A common evaluation that limits consideration to PAPR and BER trade-off, takes into account just partial impact of PAPR reduction to the link performance, namely in-band distortion, while ignoring out-of-band distortion. Thus only PAPR or BER assessment is not sufficient to characterize the impact of PAPR reduction to system performance.

Therefore, it is natural to develop different schemes to address the preferences on OOB or IB or trade-off between both which are determined by system specifications and user demands. In this research, concerns on OOB or IB are addressed by the proposed methods applied at the transmitter or the receiver or both ends.

CHAPTER 3

TRANSMITTER-ORIENTED SCHEME: IMPROVED SIGNAL DESIGN IN PEAK WINDOWING

3.1 Introduction

Among the PAPR schemes described in the literature [18–21], the peak windowing method [71] [29] is widely used in practice as it does not require transmission of side information [46] [47] or receiver modification [38] [72]. It does not incur loss of data rate for coding or reserving tones [55] nor does it require extensive computational load for iteratively processing between frequency and time domain [35] [58]. Built on the idea of smooth attenuation of peaks to avoid sharp corners caused by direct clipping [34], peak windowing produces much smaller out-of-band (OOB) radiation than direct clipping with comparable complexity [40].

In conventional peak windowing [29] [40], each peak is treated by a common symmetric window function weighted with the amount of the peak above the clipping level and the overall window function is the superposition of the sequence of all window functions. However, excessive attenuation may occur due to the convolutional summation at all time instances. When consecutive peaks cluster together, neighboring peak window functions will overlap leading to over-attenuation from closely spaced windowed segments. An adaptive algorithm is applied in [73] to design the window coefficients obtained by minimizing the mean square error (MSE) between the peak windowing attenuated signal and the desired signal with reduced peaks. However, the weighting factors obtained by averaging errors do not guarantee the windowing attenuated signal to be below the targeted clipping level at all time instances. A finite impulse response (FIR) feedback-structure was proposed in [74] to replace negative values in the overall window function with zeros if necessary, but excessive clipping may still occur due to the convolution when peaks are close. In [41], the overall window function is taken as the maximal envelope of all single peak window functions to avoid over attenuation caused by the superposition, but new sharp corners appear at some conjunction points of adjacent peak window functions. In [25], a new procedure for calculating weighting coefficients is applied instead of the usual method using the exceeding amount of the peak over the clipping level in case that successive peaks appear within a half of the window length. The new weighting factors for each peak are obtained by solving matrix-based linear equations to control the attenuated peak amplitudes tightly bounded by the given threshold. However, the coefficient matrix, depending on the window shape, the window length and relative distances among neighboring peaks, may be subject to ill-conditioning and may produce undesirable results. In the aforementioned schemes, the extent of performance improvement is limited especially in the case of successive peaks. It should be noted that the window for treating each peak is symmetric with a fixed window length, and only the weighting factor for each peak window is altered to improve the performance. However, peaks are randomly distributed in the time signal, and a fixed-length symmetric peak window is not flexible enough.

3.2 Peak Windowed System Model

The most straightforward way to reduce PAPR is to cancel the peaks by clipping the signal over a threshold, but it generates sharp corners in the time domain thus increasing OOB radiation. An alternative is to employ some window function to smooth the corners to lower OOB radiation from direct

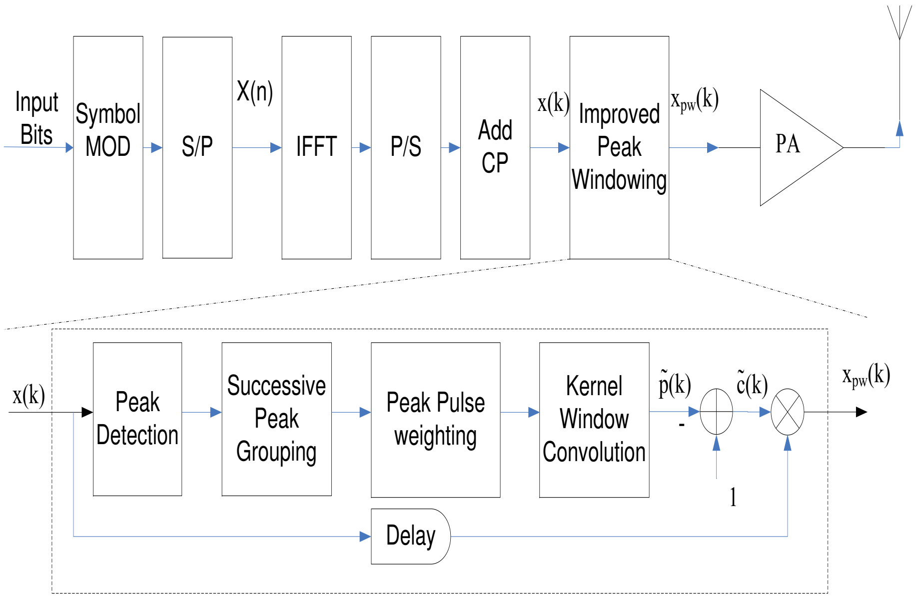

Figure 4. OFDM transmitter block diagram with peak windowing

clipping, as shown in Figure 5. A block diagram of the OFDM system by employing a block of peak windowing into Figure 1 under consideration is shown in Figure 4.

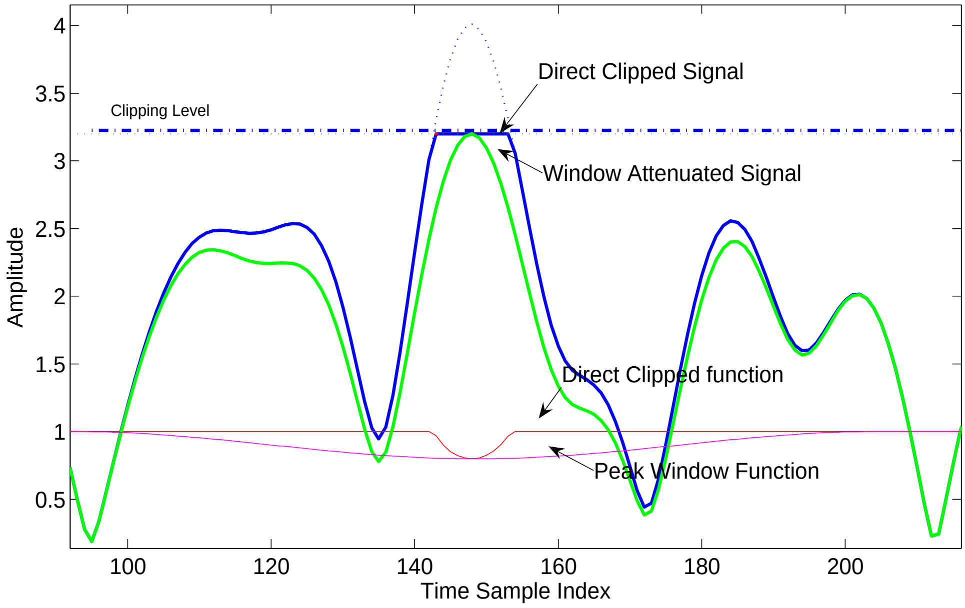

Figure 5. Peak windowing smooths signal from direct clipping.

3.3 Peak Windowing Algorithms

The direct clipping on the envelop of the complex baseband signal $x(n)$, can be expressed with a scale function $c(n)$ as

$$x_{pw}(n) = c(n)x(n) \tag{3.1}$$

$$c(n) = 1 - p(n) \tag{3.2}$$

$$p(n) = \begin{cases} 1 - \frac{A}{|x(n)|} & |x(n)| \geq A \\ 0 & |x(n)| < A \end{cases} \tag{3.3}$$

$p(n)$ is the peak pulse sequence above the clipping threshold A; $x_{pw}(n)$ is the output.

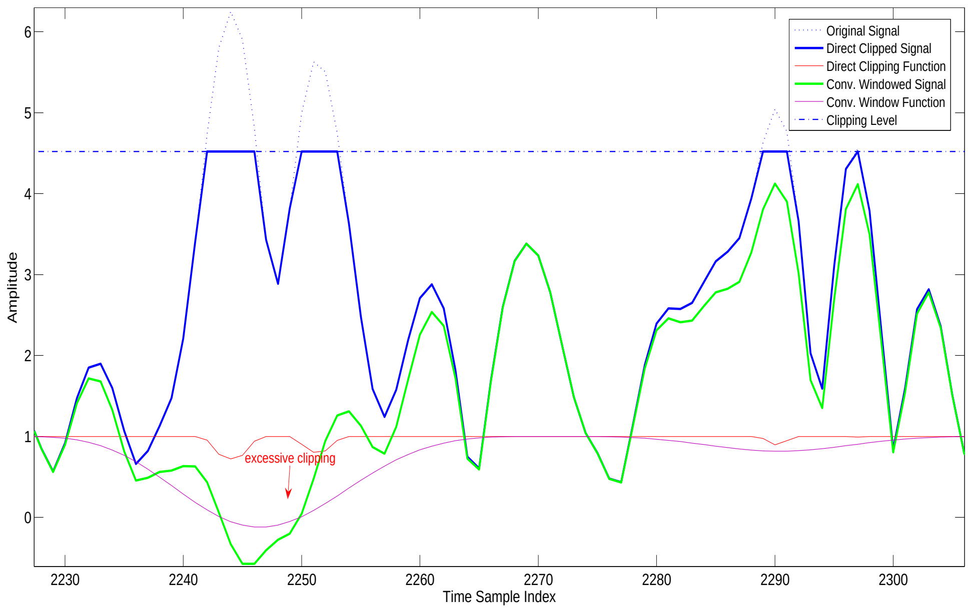

Figure 6. Excessive clipping appears due to convolution in conventional peak windowing.

Peak windowing smooths the sharp corners in the scale function $c(n)$ to generate a new function $\tilde{c}(n)$.

$$\tilde{c}(n) = 1 - \sum_{i=-\infty}^{\infty} a(i)w(n-n_i) \tag{3.4}$$

where $w(n)$ is a common symmetric window function with a length L. The criterion to choose the coefficients $a(n)$ is that the resultant envelope of $x_{pw}(n)$ never crosses the threshold A, which implies that at all time instances especially the peak locations $\tilde{c}(n)$ satisfies

$$\tilde{c}(n) \leq c(n) \tag{3.5}$$

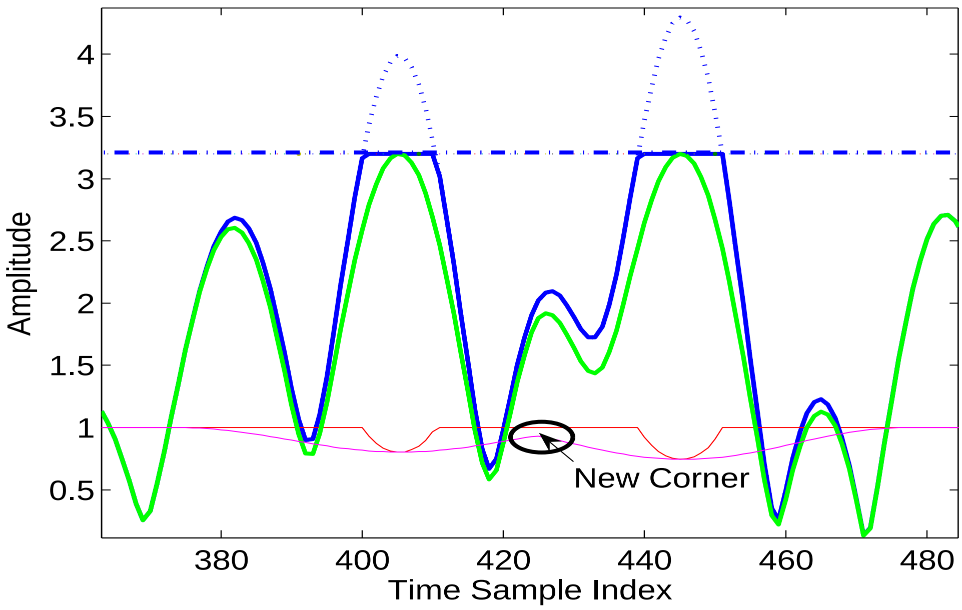

Figure 7. New corners emerge at the conjunction of adjacent peak windows in MES.

So all peaks should be clipped below the given threshold after peak windowing. To avoid large distortion, $\tilde{c}(n)$ should approximate $c(n)$ as closely as possible. Any window function with good spectral characteristics can be adopted in Equation 3.4, such as Hamming, Gaussian or Kaiser window. A Kaiser window with length L and attenuation factor β is expressed as:

$$w(n) = \frac{I_0\left(\beta\sqrt{1-(\frac{2n}{L+1}-1)^2}\right)}{I_0(\beta)} \tag{3.6}$$

where $I_0(\cdot)$ is the zeroth order modified Bessel function of the first kind. The kernel window function can easily be shaped by changing L and β, so the adjustable Kaiser window is used in general.

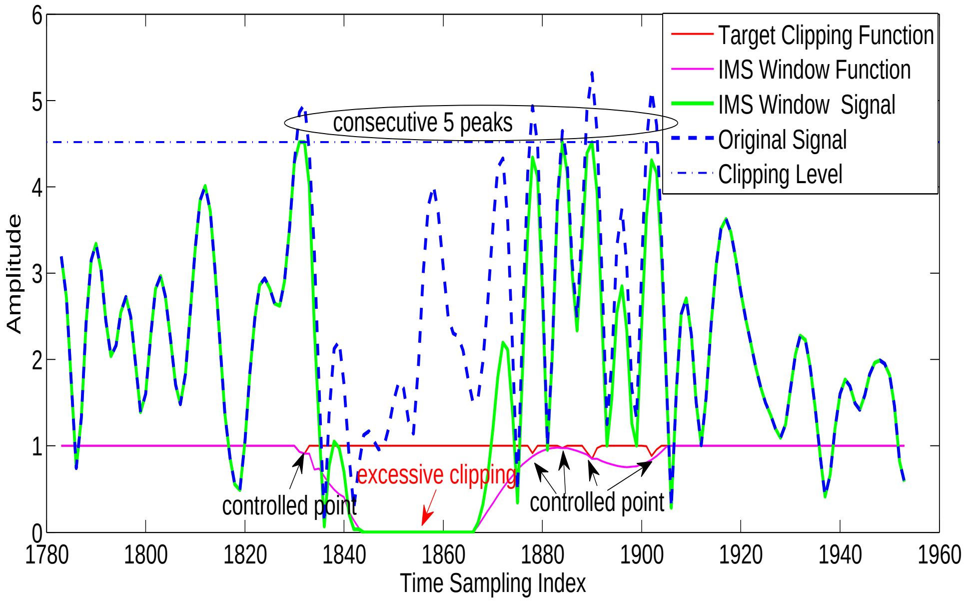

Figure 8. Excessive clipping occurs between the controlled points in IMS.

In conventional peak windowing, $a(n)$ is easily set as

$$a(n) = \sum_{m=-\infty}^{\infty} p(h_m)\delta(n-h_m) \tag{3.7}$$

$$h_m = \arg\{\max_{n_{m-} \leq n \leq n_{m+}} |p(n)|\} \tag{3.8}$$

where n_{m-} denotes the index of rising edge of the mth peak pulse and n_{m+} denotes the index of falling edge of the mth peak pulse, $\delta(\cdot)$ is the unit impulse. Then $\tilde{c}(n)$ in Equation 3.4 is a convolutional summation of all peak windows. The superposition may generate values greater than 1 resulting in negative values of $\tilde{c}(n)$ [74]. The signal is over-attenuated thus increasing IB distortion as shown in Figure 6. The situation is further aggravated in the presence of closely spaced peaks when a large window length is applied. This problem is addressed in the maximal envelop scheme (MES) [41] and the inversion matrix scheme (IMS) [25], but their performance improvement is limited. At every time instance, instead of summation, MES takes the maximal envelope of all neighboring peak windows to establish the overall window function. The over-attenuation is therefore avoided, however, the resultant window function may not be smooth at the conjunction points of two adjacent peak windows shown in Figure 7. Such inflexions increase the out-of-band radiation. IMS computes new weighting values $a'(n)$ for each peak window instead of $a(n)$ when peaks are closely spaced within half of the applied window length. A coefficient matrix is first formed according to the relative distances between the neighboring peaks, then new weighting factors of neighboring peak windows are acquired by multiplying the inverse coefficient matrix with the targeted weighting values at peak locations in $p(n)$. The weighting factors $a'(n)$ make the values at peak locations of clipped signal tightly equal to the targeted clipping threshold, however, for other points away from peak locations, the overall window function may be severely attenuated due to improper weight factors $a'(n)$ shown as Figure 8. The coefficient matrix only depending on the peak locations and the kernel window shape, may be ill-conditioned so as to produce bad weighting factors.

3.4 Improved Peak Windowing Schemes

As discussed before, if peaks are spaced with large distances, i.e. greater than the window length, the neighboring peak windows will not overlap, then IMS degrades with one peak and MES has only one entry in the inverse matrix. In this case, either IMS and MES has the same performance as the conventional peak windowing. However, when peaks are closely spaced with respect to the window length, adjacent peak windows will overlap and the performance of peak windowing will be deteriorated if all peak windows are added unrestrictedly.

MES completely replaces the summation with taking the maximal values of the window terms to reduce distortion, but it incurs discontinuity at the conjunction points of adjacent peak windows. Note that such discontinuities can be effectively smoothed or canceled by partial summation to reduce OOB radiation. So, the combination of partial summation and maximization helps to smooth the re-emergent sharp corners while maintaining the advantages of MES.

IMS computes the coefficients by taking all peaks in the vicinity under consideration. If two peaks are very close in distance, they may result in two very similar columns in the coefficient matrix which makes the coefficient matrix close to ill-conditioning. After the matrix inversion, the resultant new coefficients may be extremely large positive or negative values which cause undesired scaling despite that the scaling function is well controlled at peak locations.

However, if the two peaks vary a lot in height, the lower peak may be masked by the window of the other higher peak, then it is not necessary to compute the coefficient for the lower peak, where the ill-conditioning column in the matrix thus is removed. So, identifying the relative height differences between peaks helps to determine the actual effective peaks in constructing the overall window function while mitigating the influence of the small peaks.

The distance between peaks determines the effect of superposition of peak windows. While peaks are randomly distributed with varying distances, the symmetric window with a fixed length for each peak is not suitable for reducing distortion whens canceling peaks. As in Equation 3.5, peaks should be canceled with the smallest possible distortions. Variable window length and asymmetric window shape is expected to better satisfy the condition in Equation 3.5.

Thus we propose two new peak windowing schemes [75], called Sequential Asymmetric Superposition (SAS) and Optimally Weighted Windowing (OWW) respectively, to overcome the disadvantages in previous schemes and improve the peak window schemes.

3.4.1 Sequential Asymmetric Superposition

The key idea in SAS is to exploit the benefits of large window lengths and smooth conjunction points while limiting performance loss caused by over-attenuation and discontinuity. The overall window function is constructed in an adaptive way that the window length on the side of a closely-spaced neighboring peak is reduced and the function is smoothed by summing the adjacent asymmetric peak windows.

Peaks in the time signal are first detected to get the location indices h_m and then grouped into blocks if their locations h_m are within half of a predefined window length, as in IMS [25]. However, unlike IMS [25], we further sequentially aggregate successive peaks to isolate those peaks with large heights and construct asymmetric windows for them to form the scaling function.

SAS relies on adaptively varying window length based on the proximity of successive peaks to form asymmetric windows for each peak. The overall scaling function is smoothed by summing the adjacent asymmetric peak windows. The procedure of SAS is as follows:

(i) sort all peaks in the block by height and label them all as 'unprocessed';

(ii) starting from the highest peak, check the labeling;

(iii) if the peak is 'unprocessed', apply single peak windowing with a predefined window length and add it to the aggregated window function;

(iv) if the current peak is ‘uncovered’, use the distance to the closest preceding peak labeled ‘survivor’ as the half of the window length and use the exceeding amount of the current peak over the aggregated window function as the weighting factor to construct a window function; Add the left side of the window function to the aggregated window function; then do the similar operation to update the aggregated window function with the right side of the current peak window;

(v) label the current maximal peak as ‘survivor’;

(vi) check if remaining peaks are covered by the current aggregated window function; label those covered as ‘purged’ peaks and those uncovered but in the range of the current aggregated window function as ‘uncovered’; keep those peaks out of the range of the aggregated window function still as ‘unprocessed’;

(vii) back to (ii), till all peaks are labeled either as ‘survivor’ or ‘purged’.

(viii) adopt the aggregated window function as part of the scaling function for the current block of successive peaks.

In this way, small peaks, similar in MES [41], are concealed under large neighboring peaks by the aggregation and purged from further processing. Only those peaks with large heights will contribute to constructing the scaling function. The new scaling function is:

$$c_{sas}(n) = 1 - \sum_{i=-\infty}^{\infty} a_s(i)[w_{sl}(n-n_i) + w_{sr}(n-n_i)] \tag{3.9}$$

where $w_{sl}(n)$ and $w_{sr}(n)$ are the left side and the right side half of the window function respectively which have different window lengths; $a_s(i)$ is the new weighting factors, for those concealed peaks indexed by j, $a_s(j) = 0$.

For each unconcealed peak, we design an asymmetric window as in step (iv), and then superpose all peak windows to build up the overall window function for the block. The distance between the current peak and the adjacent preceding peak defines the left-side window length, the window coefficient at the current peak is one, while zero is at the preceding peak. The right side of the peak window is obtained similarly. Each peak window is made of two asymmetric segments in general. For the first and last peaks at both ends of the block, the predefined window length is used as the window length.

The weighting factor for each asymmetric window is adaptively updated in step (iv). They are actually set as the corresponding value in $p(n)$, which guarantees that the peak is tightly bounded below the threshold, thus avoiding over-attenuation. Note that the superposition of asymmetric peak windows occurs only between adjacent unconcealed peaks, so the overall window function is smoothed without new corners.

3.4.2 Optimally Weighted Windowing

The strategy underlying OWW is to take the advantages of the inverse matrix approach with limited attenuation at peak locations but impose constraints on coefficients to avoid ill-conditioning.

In this scheme, similar to the first stage shown in Figure 4, peaks in the input signal are detected and grouped into blocks which contain consecutive peaks captured by the half of the given window length, and then peaks are sequentially ordered according to their heights.

After that, instead of constructing asymmetric windows for peaks, a symmetric window with the predefined window length is still used for each peak, so we establish a coefficient matrix from the predefined common window function according to the relative distances among those peaks. Instead of using the procedure in IMS [25] of calculating the weighting factors by multiplying the inverse coefficient matrix with the target peak pulse values in $p(n)$, we formulate a constrained optimization problem and solve it to get the optimal weighting factors for peaks.

The optimization is performed with U peaks in one block. It is formulated as follows:

$$\begin{aligned} minimize \quad & \|\alpha\| \\ subject\ to: \quad & W_h \alpha \geq P \end{aligned} \tag{3.10}$$

where $\alpha = [\alpha_1, \alpha_1, \cdots, \alpha_K]$ that contains K weighting factors for peaks grouped in one block; W_h is a $K \times K$ symmetric matrix with entry values from the predefined common window function according to the relative distances among peaks in the block; $P = [p_{h_1}, \cdots, p_{h_K}]$ contains the desired peak pulse heights at the peak locations in $p(n)$.

In this way, the window attenuated signal can be tightly limited up to the threshold at peak locations so that over-attenuation is avoided. In the meanwhile, the constraint in Equation 3.10 guarantees that Equation 3.5 is satisfied. The new scaling function can be expressed as:

$$c_{oww}(n) = 1 - \sum_{m=-\infty}^{\infty} \alpha'_{oww}(h_m) w(n - h_m) \tag{3.11}$$

where α'_{oww} denotes the new weighting factors on all peaks and h_m indicates the peak locations.

Equation 3.10 is a general Quadratic Programming (QP) problem. It is easy to solve and implement using some standard algorithm [76]. Depending on the clipping level and the predefined window length, the peaks may be grouped in different ways, consequently the formation of coefficient matrix is also varying. However, large PAPR ratios only occur very infrequently and very large window length should be avoided as it increases the IB distortion [29]. So with moderate window lengths and clipping levels, usually only several peaks are grouped in one block, which do not impose heavy computational burden to solve this optimization problem. And the number of unconcealed peaks in one block is usually small after the aggregation process in the first stage, so only slight computation load is incurred to solve this optimization problem.

3.5 Simulation Results and Discussion

Simulation results and comparison analysis are presented in this section. As discussed in [29], the performance of peak windowing schemes relies on the common window waveform and the window length. The shape of the window function affects the spectral properties of the window clipped signal. Given that the window shape is fixed, a larger window length is expected to produce smaller OOB radiation but larger IB distortion. To some extent, the choice of of window shape and window length should be factored in for evaluating the performance. So, to fairly compare the performance of proposed schemes with others, we only fix the window shape in our simulation using a Kaiser window with $\beta = 12$ while the window length is varied to observe the capabilities of each scheme.

When the window length is being changed, IB distortion and OOB radiation are two competing factors. The trade-off between them must be considered in the performance evaluation. In our simulation, Relative Constellation Error (RCE) and Adjacent Channel Power Ratio (ACPR) are computed to characterize the IB distortion and the OOB distortion respectively [7].

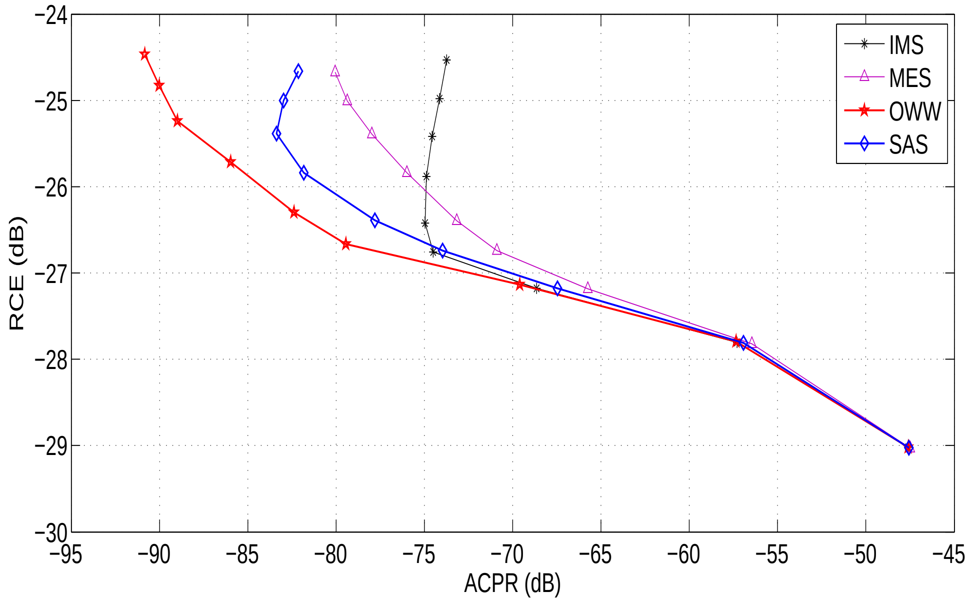

Figure 9. RCE versus ACPR curve for peak windowing schemes with different window length at a fixed output power level

To fairly assess different peak windowing schemes, our simulation focuses on power efficiency that measures how much PA output signal power is delivered to the communication channel. This output power is tightly connected with SNR which in turn impacts the receiver BER. So, RCE and ACPR are evaluated with different window lengths given that the output signal power after power amplifier (PA) is normalized among all schemes. In the meanwhile, the nonlinearity of PA is the main source of distortions, but here we focus on evaluating peak windowing schemes, so, an ideal linearized PA up to its saturation is assumed.

In our simulation, OFDM signal is modulated with 16QAM and has 256 subcarriers, and an oversampling factor of 8 is used. The window length is defined as the number of time samples after oversampling varying from 17 to 225.

schemes	IMS	MES	SAS	OWW
Window Length	97	193	161	179
RCE	-26.41	-25.00	-25.38	-25.00
$ACPR$	-76.93	-81.34	-85.34	-91.58

TABLE II

ACHIEVABLE MINIMAL ACPR FOR DIFFERENCE PEAK WINDOWING SCHEMES UNDER A CONSTRAINT($RCE \leq -25DB$)

Given a required PA output power level of output backoff 2.47dB, the RCE and ACPR trade-off curves of all peak windowing schemes are shown as in Figure 9.

For each scheme, RCE increases with increasing the window length, while ACPR decreases, as expected. When the window length is short, the improvement of the new proposed schemes is not obvious because all peaks are treated as individual peaks and no clustered peaks are detected. With the window length increasing, correspondingly more consecutive peaks appear. As a result, the advantages of proposed SAS and OWW schemes become larger compared with MES and IMS.

Considering the trade-off between RCE and ACPR, the SAS and OWW methods both achieve smaller ACPR given the same RCE constraint compared with existing MES and IMS. For example, given a requirement that RCE is below -25dB as in the WiMax standard [7], the minimal ACPR that can be achieved by different schemes with different window length are listed in Table II. When RCE is limited under the condition that the output power level is fixed, the window length can not be increased indefinitely to decrease the ACPR. But we do not set any constraint on window length, so we assume as long as RCE is under the RCE requirement, any window length can be used.

It can be seen that SAS has ACPR approximately 8dB lower than that of IMS and ACPR 4dB lower than that of MES when the constraint of RCE is applied. OWW even achieve 6dB lower OOB radiation than that SAS. So, given the RCE constraint, the proposed schemes outperform the existing schemes in obtaining smaller OOB radiation. OWW even exhibits the best performance among these schemes.

CHAPTER 4

RECEIVER-ORIENTED SCHEME: CLIPPING NOISE ESTIMATION AND COMPENSATION

4.1 Introduction

With the increasing demand for high speed data transmission, more bandwidth is employed in the physical layer techniques in wireless communications systems, e.g. bandwidth in mobile wireless systems increases from 5MHz in 3G WCDMA to 20MHz 4G LTE systems. This trend of employing larger bandwidth to provide higher data rate extends to on-going standardization activities in LTE-A systems and even to future 5G systems. The use of OFDMA in those systems therefore demands high order OFDM with a large number of subcarriers being adopted.

In recent years various methods have been proposed to address the PAPR issue at the receiver side [77], aiming to lighten the computational burden at the transmitter. Receiver-oriented methods are highly desirable when limitations on power consumption, implementation cost or computational complexity exist at the transmitter depending on system specifications or user applications. However, receiver-oriented reconstruction methods face new challenges in OFDMA systems. The envelope variations of the multicarrier signal become even more severe due to significantly large number of subcarriers being used in OFDMA.

Conventional receiver-oriented methods require all subcarriers in one OFDM symbol to be demodulated in order to perform decision-aided iterative estimation and compensation [78–80]; however in

OFDMA each user only knows his/her own modulation while modulations of other users are generally unknown, which precludes these methods from being deployed. Unlike the approach of performing iterative reconstruction on the entire signal in [81], the clipped signal in OFDMA is compensated in [82] with iterative band-limited signal recovery over reserved subcarriers after applying simple clip localization on signal samples at Nyquist rate.

In this research, we propose a novel method of estimating clip locations with spectrogram analysis on oversampled signal sequences and reformulating the signal reconstruction with frame theory to develop an iterative algorithm of alternating projection over convex sets to tackle the problem of clipping noise mitigation in OFDMA [83, 84]. As discussed in [82], the accuracy of clip locations in the recovery process is a key factor that dictates the selection of the coefficient sub-matrix out of the full-size Discrete Fourier Transform (DFT) matrix in the inverse problem, and thus it significantly impacts the system performance.

We explore three factors to identify the clip candidates in the time domain: the closeness of signal level to the clipping threshold, the time distance of neighboring samples that exceed the clipping threshold, and the out-of-band power in local windowed spectrogram based on time-frequency structure extracted from Short Time Fourier Transform (STFT). After clip locations are extracted from the received signal, the iterative projection method is adopted to recover the clipped signal. Extensive simulations are conducted to show that our proposed method significantly outperforms the method in [82] especially in high SNR regime.

4.2 Transceiver Model in OFDMA

Unlike the general case of OFDM in Equation 2.5, OFDMA signals under investigation here include multiple users and guard subcarriers reserved to protect signals from ISI of other bands. Let us consider a complex baseband representation of an OFDMA signal with N subcarriers and P users,

$$\begin{aligned} x(t) &= \frac{1}{\sqrt{N}}\sum_{p=1}^{P}\sum_{m\in\mathscr{U}_p} X_m e^{j2\pi mt/T_s} \\ &\quad + \frac{1}{\sqrt{N}}\sum_{r\in\mathscr{R}} X_r e^{j2\pi rt/T_s}, \quad 0 \le t \le T_s \end{aligned} \tag{4.1}$$

where $\mathscr{U}_p$ is the index set of subcarriers allocated to the pth user; $\mathscr{R}$ is the index set of pilot and guard band subcarriers as non-data-bearing tones; X_m is a data symbol on the mth subcarrier modulated from a given QAM constellation for data-bearing tones or known values or zeros on non-data-bearing tones. The union of all index sets covers all subcarriers, i.e. $\{\bigcup_{p=1}^{P}\mathscr{U}_p\}\bigcup\mathscr{R} = \{0, 1, \dots, N-1\}$. In this research, all subcarriers in $\mathscr{R}$ are used for signal recovery at the receiver. When clipping occurs at the transmitter due to nonlinear PA effects, the output signal $x_c(t)$ of the PA is bounded by a predefined clipping threshold V_s, similar to Equation 3.3, assuming the phase is unchanged.

$$x_c(t) = \begin{cases} \frac{V_s}{|x(t)|}x(t), & |x(t)| > V_s \\ x(t), & |x(t)| \le V_s \end{cases} \tag{4.2}$$

The clipping ratio is defined as

$$\gamma = V_s/\sigma. \tag{4.3}$$

Generally V_s is either close or identical to the actual PA saturation level, while the signal power σ^2 is adjusted by input back off (IBO) to PA saturation. It is obvious that the selection of a proper clipping ratio γ highly depends on $PAPR$ in Equation 2.15.

Normally N-point Inverse Discrete Fourier Transform (IDFT) is applied at the transmitter to obtain the discrete time signal sampled as $x(n) = x(t)|_{t=nT_s/N}$ in Equation 4.1. Briefly its vector form with $\mathbf{x} = \{x(n)\}$ is the same as Equation 2.2, $\mathbf{x} = \mathbf{W_N}\,\mathbf{X}$, with $\mathbf{X} = \{X(m)\}$ and $\mathbf{W_N}$ is the N-IDFT matrix.

The clipped signal is expressed as $\mathbf{x_c} = \{x_c(n)\} = \{x_c(t)|_{t=nT_s/N}\}$ and the clipping noise is given by

$$e_c(n) = x_c(n) - x(n) \tag{4.4}$$

In OFDMA receiver, assuming that the frequency channel response $\mathbf{H}$ is known, the received frequency domain signal, similar to Equation 2.13, at subcarrier m is

$$Y(m) = H(m)X_c(m) + G(m), m \in [0, N-1]. \tag{4.5}$$

After zero-forcing (ZF) channel equalization [85], the output signal in frequency domain is

$$\begin{aligned} Y(m) &= X_c(m) + G(m)/H(m) \\ &= X(m) + E_c(m) + G(m)/H(m), m \in [0, N-1]. \end{aligned} \tag{4.6}$$

where $\mathbf{X_c} = \{X_c(m)\}$ is the DFT of $\mathbf{x_c} = \{x_c(n)\}$, $G(m)$ is the Gaussian channel noise in frequency domain with zero mean and variance σ_w^2, and $E_c(m)$ is the distortion due to clipping. The demodulated signal of the pth user is estimated with maximal likelihood as

$$\hat{X}(m) = \arg\min_{\chi_p} |Y(m) - \chi_p|^2, \; m \in U_p \tag{4.7}$$

where χ_p denotes the constellation points of the modulation scheme of user p.

Clearly if the clipping distortion $E_c(m)$ in Equation 4.6 is compensated, better results are obtained by replacing $Y(m)$ with $\tilde{Y}(m) = Y(m) - E_c(m)$ in Equation 4.7. Note that in the absence of other users' modulation information, the pth user cannot utilize the difference between $\hat{X}(m)$ and $Y(m)$ of the whole symbol $X(m), 0 \leq m \leq (N-1)$ to iteratively cancel $e_c(n)$ which invalidates the conventional schemes [78] [80].

4.3 Recovery of Clipped Signal

With a normal clipping ratio, it is easily seen from Equation 4.2 that the clipping noise in Equation 4.4 consists of a sequence of pulses in time domain. Given one symbol period of the input signal $x(t), t \in [0, T_s]$, each pulse in the clipping noise sequence $e_c(t)$ characterized by its location, duration, magnitude, shape and phase is determined by the clipping ratio γ. The original signal $x(t)$ is approximately a Gaussian random process following the central limit theorem. Therefore, the pulse characteristics are completely random from symbol to symbol.

As widely known, the magnitude of $x(n)$ in Equation 5.1 is approximately Rayleigh distributed [86]. The average up level-crossing rate depends on the clipping ratio γ as [87],

$$\overline{N_p} = N\sqrt{\frac{\pi}{6}} * \gamma * e^{-\frac{\gamma^2}{2}} \tag{4.8}$$

where $\overline{N_p}$ denotes the average number of samples out of N with magnitudes exceeding the threshold V_s. For instance, for a practical clipping ratio of 4dB, the average number of clipping pulses in one OFDM symbol period is about $0.0775 * N$.

For the discrete samples $e_c(n)$, it is necessary to specify the location, magnitude and phase of each pulse to fully determine the clipping noise sequence. However, it is very difficult to determine the characteristics of the clipping noise directly from equalized frequency samples in Equation 4.6 without knowing clip locations, because known variables on pilots, guard band subcarriers and target user data subcarriers are far fewer than all unknown variables that characterize the pulses in the clipping noise. As in [82], we recover the clipped signal in two major steps, namely, peak localization and magnitude estimation, as shown in Figure 10.

Firstly the locations of clip candidates are estimated through peak processing and corresponding phases of clips are predicted, and secondly magnitudes of clips are obtained by iteratively solving equations established with the estimated clip locations and the difference between $Y(m)$ and $X(m)$ on reserved subcarriers in set $\mathscr{R}$.

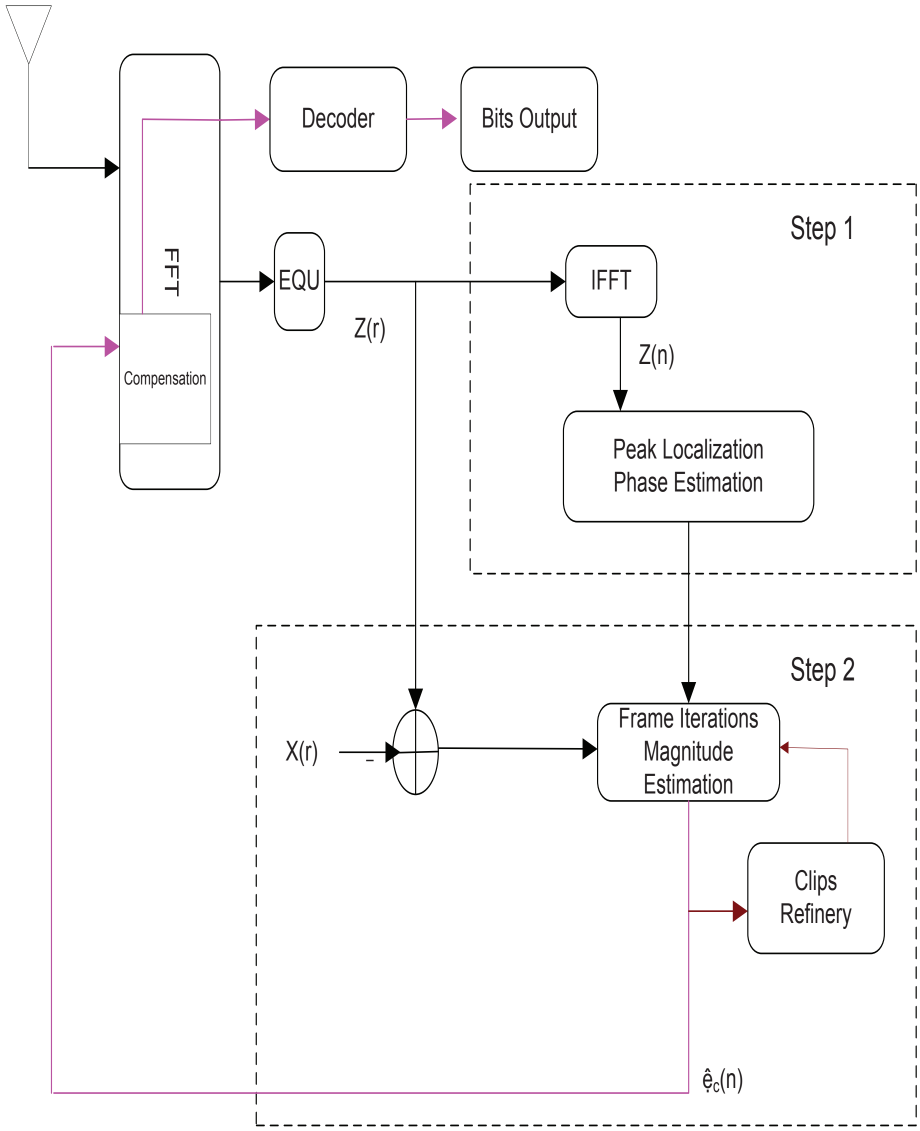

Figure 10. Block Diagram of FAP Recevier

By utilizing all known values $X(r), r \in \mathscr{R}$ on frequency reserved subcarriers, the differences between received samples and prior known values are obtained as known variables to guide the calculation of the unknown magnitudes of clips.

$$E_{c0}(r) = Y(r) - X(r), r \in \mathscr{R} \tag{4.9}$$

The difference $E_{c0}(r)$ contains the equalized channel noise and clipping noise as indicated in Equation 4.6. From Equation 4.4, $\mathbf{e_c}$ has non-zero values only at the clip locations while being zeros at other locations, so there exists

$$\mathbf{E_c} = \mathbf{W_{r,c}}^H \mathbf{e_c} + \xi \tag{4.10}$$

where $\mathbf{W_{r,c}}^H$ is the $L_r \times L_c$ sub matrix taken L_r rows and L_c columns from N-DFT matrix $\mathbf{W}^H$, $(\cdot)^H$ denotes Hermitian transpose, and ξ denotes the channel noise. The index set of L_c columns is determined by clip locations. The clipping noise $e_c(n)$ can be calculated with Least-Square (LS) projection when $L_c < L_r$ as

$$\hat{\mathbf{e_c}} = (\mathbf{W_{r,c}}\mathbf{W_{r,c}}^H)^{-1}\mathbf{W_{r,c}}\mathbf{E_{c0}} \tag{4.11}$$

If the number of possible clips $L_c > L_r$ the cardinality of set $\mathscr{R}$, Equation 4.10 becomes under-determined. The results obtained from Equation 4.11 can be ill-conditioned. The clip candidates are refined or the recovery process for this OFDM symbol is skipped. Therefore the accuracy of estimating the number and locations of clips significantly impacts the performance of clipped signal recovery.

4.3.1 Clip Localization through peak filtering

PA clipping in Equation 4.2 affects the entire continuous-time signal. Unlike [82] where clips are estimated with samples at Nyquist rate, our clip localization samples the received signal with an up-sampling factor $J > 4$, which facilitates the localization of all the peak pulse candidates in Equation 4.4. The discrete JN samples of the input signal are given as $\bar{\mathbf{x}} = \{\bar{x}(n)\} = \{x(t)|_{t=nT_s/JN}\}, n \in [0, JN-1]$ from Equation 4.1, that is,

$$\begin{aligned}\bar{x}(n) &= \frac{1}{\sqrt{JN}} \sum_{k=1}^{K} \sum_{m \in \mathscr{U}_k} \bar{X_k}(m) e^{j2\pi mn/JN} \\ &+ \frac{1}{\sqrt{JN}} \sum_{r \in \mathscr{R}} \bar{X}(r) e^{j2\pi rn/JN}, n \in [0, JN-1]\end{aligned} \tag{4.12}$$

where $\{\bar{X}(n)\}$ of size JN can be seen as zero-padding the original OFDM block $\{X(n)\}$ of size N. Thus the corresponding received signal in time domain is

$$\bar{y}(n) = \bar{x}(n) + \bar{e}_c(n) + \bar{\eta}(n) \tag{4.13}$$

where $\bar{\eta}(n)$ is up-sampled equalized noise. Deep frequency fading in **H** may boost noise severely in frequency domain but $\bar{\eta}(n)$ in time domain is smoothed due to IDFT averaging effects. Further, we employ median filtering with size $J/2+1$ over $\bar{y}(n)$ to remove the disturbance from large impulse values in noise $\bar{\eta}(n)$ to clip location estimation.

Under normal circumstances for reliable communications the signal power is much larger than the noise power and thus the magnitude of the signal is much larger than the noise at the time instances where clipping occurs. The equalized signal magnitude satisfies [82]

$$|\bar{y}(n)| \gg |\bar{\eta}(n)| \tag{4.14}$$

which is exploited to identify the potential clip locations. So the equalized time samples with magnitudes close to V_s are selected as clip candidates. Assuming the clipping threshold V_s is known at the receiver, samples in $\bar{y}(n)$ with the magnitude greater than $V_s - \mu\sigma_w$ are selected, where μ is a factor chosen to adjust the number and locations of clip candidates and σ_w is standard deviation of noise power. Depending on the system configuration, μ can be chosen offline to avoid clips being missed due to small μ values or being falsely reported due to large μ values.

The clipping pulse duration is a Rayleigh random variable depending on the clipping ratio γ [87] which is also exploited to identify the potential clip locations. So we use run-length analysis over the sequence of clip candidates identified according to Equation 4.14. Clip candidates are filtered out if the number of consecutive samples spanned by the clip candidates is less than a threshold $\bar{\tau}$ determined in [87]. The L_r known variables are usually insufficient to recover all unknown magnitudes of up-sampled clip candidates obtained from $\bar{y}(n)$. So we have to find the clipped sample locations at Nyquist rate to establish the equations as Equation 4.10. Clip candidates that span multiple consecutive samples are consolidated and represented by the close sample location in Equation 4.4 which reduces the number of unknowns.

From Equation 4.2 the clipped time signal exhibits a flattened top shape where clipping occurs and the instantaneous frequency components contain larger out-of-band power at clipped samples than that at non-clipped samples, which is another factor exploited to estimate clip locations. We introduce STFT based spectrogram to examine local time-frequency structures of the up-sampled sequence. The sequences used to calculate the spectrogram are constructed as follows: (1) select the local short window length as $2J - 1$; (2) apply a rectangular window with that length centered at each sample obtained at the Nyquist rate, thus the up sampled sequence is divided into N sub sequence with 50% overlapped between adjacent windows; (3) inside each windowed sub sequence, subtract from the samples with the line determined by the start and end samples of the window; (4) append to each resultant sub sequence with a negative duplicate of itself; (5) cyclically extend the sub sequence to length $2N$; (6) take 2N-DFT over the extended sequence to get spectrogram. A threshold P_o of measuring out-of-band power of instantaneous frequency components for each time sample at Nyquist rate is used to further filter out the clip candidates with small out-of-band power in the previous steps.

Our peak filtering procedure to locate clips is summarized in Table III.

TABLE III

PEAK FILTERING PROCEDURE FOR CLIP LOCALIZATION
1) up sample the sequence and apply median filtering
2) label all samples as clips;
3) filter out clips with magnitude $\lvert\bar{y}(n)\rvert < V_s - \mu\sigma_w$;
4) filter out clips with number of consecutive samples less than $\bar{\tau}$;
5) calculate spectrogram and out-of-band power at each time sample;
6) filter out clips with out-of-band power less than a threshold P_o;
7) obtain the clip candidate set **C**

It is noted that peak filtering detects and locates almost all the actually clipped samples but it reports some false peaks as well, which can be refined during the iteration steps.

As the clipping model in Equation 4.2 indicates, the clipping noise maintains the phase as the time domain signal. So the phases of located clips are chosen identical to the equalized signal at the receiver.

$$\angle(e_c(n)) = \angle(x_c(n)) \cong \angle(y(n)), \text{ for } n \in \mathbf{C} \tag{4.15}$$

where **C** denotes the index set of peak locations obtained from Table III.

Although the noise item introduces some disturbance in the received signal, the phase changes are ignored due to noise magnitude being far smaller than the signal strength in Equation 4.14.

4.3.2 Frame-based Alternating Projection for Magnitude Estimation

To avoid matrix inversion and possible ill-conditioned calculation that may cause large estimation errors in Equation 4.11, an iterative algorithm based on the band-limited signal recovery is adopted in [82] to resolve Equation 4.10. The iterative process in [82] is

$$\begin{aligned} \mathbf{e}_i &= \mathbf{I_c W I_r W}^H \mathbf{I_c e}_{i-1} + \mathbf{e}_0, i > 1 \\ \mathbf{e}_0 &= \mathbf{I_c W}^H \mathbf{E_{c0}} \end{aligned} \tag{4.16}$$

where $\mathbf{I_c}$ is a diagonal $N \times N$ matrix with diagonal elements equal to 1 only corresponding to clipping locations and 0 otherwise. $\mathbf{I_r}$ is also a diagonal $N \times N$ matrix with 1's corresponding to user data subcarriers and 0's corresponding to reserved subcarriers.

Studying Equation 4.16, the iterative process is implemented over the signal of full size N. It updates the potential clips and forces other non-clip samples to be zeros in time domain, while updating samples on user data carriers and keeping reserved subcarriers unchanged in the frequency domain.

When errors still exist in ith iteration e_i, the error disperses into user data subcarriers [82], which may degrade the performance especially when channel noise power is small and clipping noise makes the major contribution.

As the simulation results in [82] reveal, the performance of the iterative process Equation 4.16, however, is not as good as the direct least square (LS) solution when SNR is high ($> 25dB$). In the high SNR regime, the iterative process Equation 4.16 is deficient. When SNR is high, the noise power is relatively small; estimation of clip locations is more accurate for using the LS method since ill-conditioned matrix inversion is less likely to happen.

Revisiting Equation 4.10, the matrix $\mathbf{W_{r,c}}^H$ has $L_r > L_c$ as the clip location estimation determines. Then the rows of matrix $\mathbf{W_{r,c}}^H$ can form a finite frame [88]. A set of vectors $\Phi = \{\phi_p\}_{p=1}^P$ in $\mathbb{C}^K$ is a *frame* if there exist $A, B \in \mathfrak{R}$, and $0 < A \leq B$ such that

$$A \|\mathbf{x}\|^2 \leq \sum_{p=1}^{P} |\langle \mathbf{x}, \phi_p \rangle|^2 \leq B \|\mathbf{x}\|^2, \quad \forall \mathbf{x} \in \mathbb{C}^K, \tag{4.17}$$

where $\|\cdot\|$ and $\langle\cdot\rangle$ denote norm and inner product in Euclidean space respectively. A and B are called lower and upper frame bounds. Clearly, $\mathbf{W_{r,c}}^H$ has upper and lower bounds because it is a sub matrix from DFT matrix $\mathbf{W}^H$. According to frame theory, the finite frame Φ can be associated with a matrix $\mathbf{Q}$ by setting the rows of $\mathbf{Q}$ as the elements of the frame, the bounds A and B are actually determined by the minimal and maximal eigenvalues of the square matrix $\mathbf{Q}^H\mathbf{Q}$. Considering the dual frame operator with $\mathbf{W_{r,c}}^H$

$$\mathbf{W_{r,c}}\mathbf{W_{r,c}}^H\mathbf{x} = \sum_{r=1}^{L_r} \langle \mathbf{x}, \mathbf{w}_r \rangle \mathbf{w}_r \tag{4.18}$$

where $\mathbf{w}_r$ is the rth row of $\mathbf{W_{r,c}}$. Define $T = I - \frac{2}{B+A}\mathbf{W_{r,c}}\mathbf{W_{r,c}}^H$. Since A and B are the bounds of the frame, then,

$$||T|| \leq \frac{B-A}{B+A} \leq 1 \tag{4.19}$$

Then,

$$(\mathbf{W_{r,c}}\mathbf{W_{r,c}}^H)^{-1} = \frac{2}{B+A}(I-T)^{-1} = \frac{2}{B+A}\sum_{i=1}^{\infty} T^i \tag{4.20}$$

When truncating the infinite series to different values, different levels of approximation to the matrix inversion are obtained. Then the iterative inverse construction is formulated as

$$\mathbf{x}_k = \mathbf{x}_{k-1} + \frac{2}{B+A}\sum_{r=1}^{L_r}(\langle \mathbf{x}_0, \mathbf{w}_r\rangle - \langle \mathbf{x}_{k-1}, \mathbf{w}_r\rangle)\mathbf{w}_r \tag{4.21}$$

As Equation 4.20 indicates, the iteration in Equation 4.21 is guaranteed to converge to the LS solution. Meanwhile, the iteration in Equation 4.21 performs only on the sub space of $\mathbf{W}^H$ with size L_r and L_c.

The band limited recovery formulation is actually a projection over convex set (POCS). The set of vectors with $\Psi = \{\mathbf{e_c} | e_c(j) = 0, j \notin \mathbf{C}, 0 \leq j \leq N\}$ is convex.

Proof. $\forall 0 \leq \alpha \leq 1$, $\alpha \in \mathfrak{R}$, let $\mathbf{s} = (1-\alpha)\mathbf{e_{c1}} + \alpha\mathbf{e_{c2}}$ where $\mathbf{e_{c1}} \in \Psi$, $\mathbf{e_{c2}} \in \Psi$.

Consider all $j \notin \mathbf{C}$, $s(j) = (1-\alpha)e_{c1}(j) + \alpha e_{c2}(j) = (1-\alpha)*0 + \alpha * 0 = 0$.

So, $\mathbf{s} \in \Psi$. Therefore, Ψ is convex.

□

The same argument applies to the set Ω in frequency domain, $\Omega = \{\mathbf{E_c} | E_c(m) = E_{c0}(m), m \in \mathscr{R}, 0 \leq m \leq N\}$. So the projection with DFT matrix $\mathbf{W}^H$ is over the two convex sets.

Our new frame-based alternating projection scheme seeks to find another alternating projection path between the two convex sets Ψ and Ω to tackle the performance degradation in high SNR regime. We concatenate the iterative process in Equation 4.21 and Equation 4.16, to make use of the upper bound of frame to narrow down the candidates in the sub space in Equation 4.21 and speed up the convergence process. The new iterative process is

$$\begin{aligned} \mathbf{e}_i &= (\frac{B-1}{B}\mathbf{I} + \frac{1}{B}\mathbf{I_c W I_r W}^H)\mathbf{I_c W I_r W}^H\mathbf{I_c e}_{i-1} + \mathbf{e}_0, i > 1 \\ \mathbf{e}_0 &= (I + \frac{1}{B}\mathbf{I_c W I_r W}^H)\mathbf{I_c W E_{c0}} \end{aligned} \tag{4.22}$$

The coefficient $2/(A+B)$ in Equation 4.21 adjusts the convergence rate in the frame-based iterative process. As $\mathbf{W_{r,c}}^H$ takes a sub matrix of N-DFT matrix, it has spectral norm $||\mathbf{W_{r,c}}^H|| < 1$ [89], that is, the largest eigenvalue B is bounded, so $1/B$ is used instead of $2/(A+B)$ to accelerate the convergence linearly.

As discussed, both iterative processes converge to the LS's solution if the noise is zero. Comparing Equation 4.23 and Equation 4.16, the complexity of both schemes is the same. The coefficient matrix can be pre-caculated and stored before each iteration. The stop condition is simply selected as $||\mathbf{e}_i - \mathbf{e}_{(i-1)}|| < \epsilon$ where ϵ is a predefined threshold. Extensive simulations are conducted to verify the performance and simulation results validate the performance of the new proposed frame-based alternating projection scheme.

4.4 Simulation Results and Discussion

The performance of the proposed scheme is examined through simulations. The OFDMA system is set up according to the IEEE802.16 2004 WiMAX standard [6]. The system takes total $N = 2048$ subcarriers out of which are 192 pilot and 319 guard band carriers used as reserved carriers for clipping noise recovery. A total of 8 users equally share the remaining data subcarriers in an interleaved pattern. The target user uses 64QAM modulation, and other users randomly select modulation schemes from BPSK, QPSK, 16QAM and 64QAM, which is unknown to the target user. The additive white Gaussian noise (AWGN) channel is used to simulate flat fading case. The WiMAX SUI3 channel model is used to represent the frequency selective fading channel [90]. Uncoded OFDM without bit loading is assumed at the transmitter. A typical clipping ratio $\gamma = 4\mathrm{dB}$ is used in the simulation. The performance of different schemes is studied in terms of BER versus SNR curves with normal practical range of SNR that is normally up to 32dB.

The effect of the proposed clip localization through peak filtering is compared with the existing simple clip location estimation adopted in [82]. Using clip locations known at the transmitter as the reference, the ratio of correctly located clips to the reference clips at difference SNR level is shown in Figure 11. It is seen that peak filtering can locate many more actual clips compare with the simple localization method, above 99.8% clips at the transmitter are located correctly at the receiver. The level is lower than 97.6% in simple localization by which some real peaks are missed in detection. And the ratio of falsely reported clips to the reference clips at difference SNR level is shown in Figure 12. With SNR increasing, the amount of false clips are reduced since the noise power is much smaller compared to the signal power, the interference to detecting the clips is also reduced. Compared with

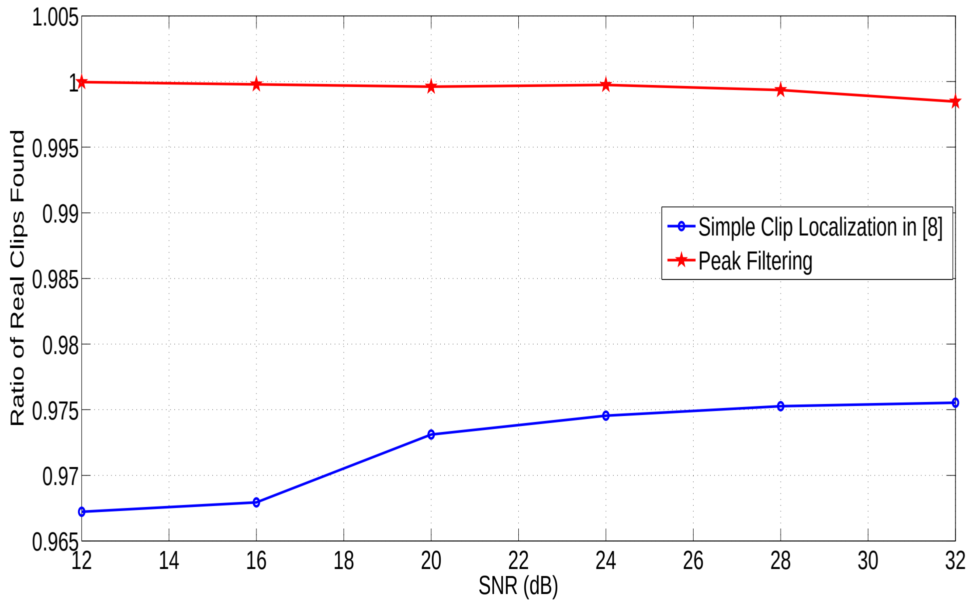

Figure 11. Real Clips Found by Peak Filtering versus Simple Clip Localization

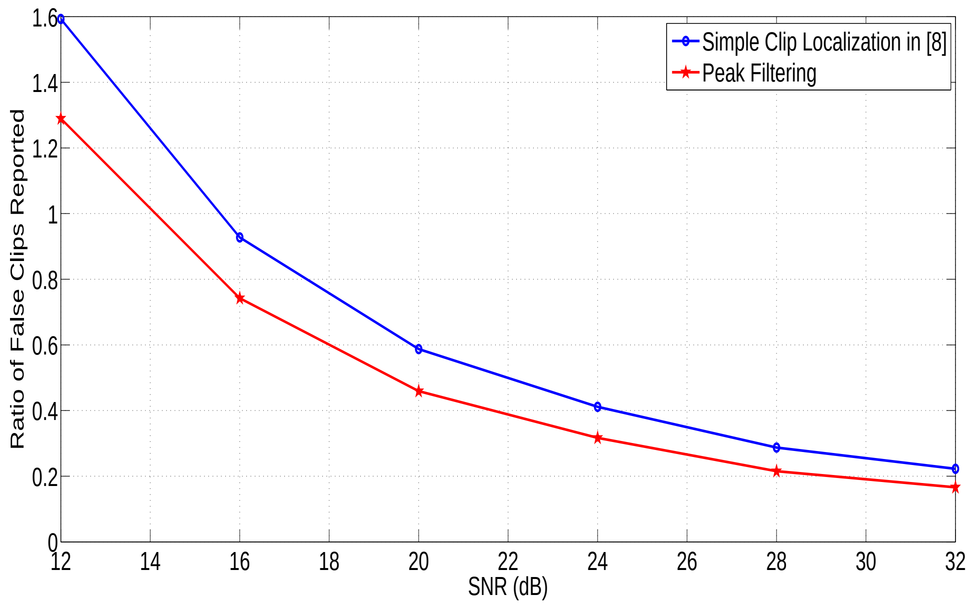

Figure 12. False Clips Reported by Peak Filtering versus Simple Clip Localization

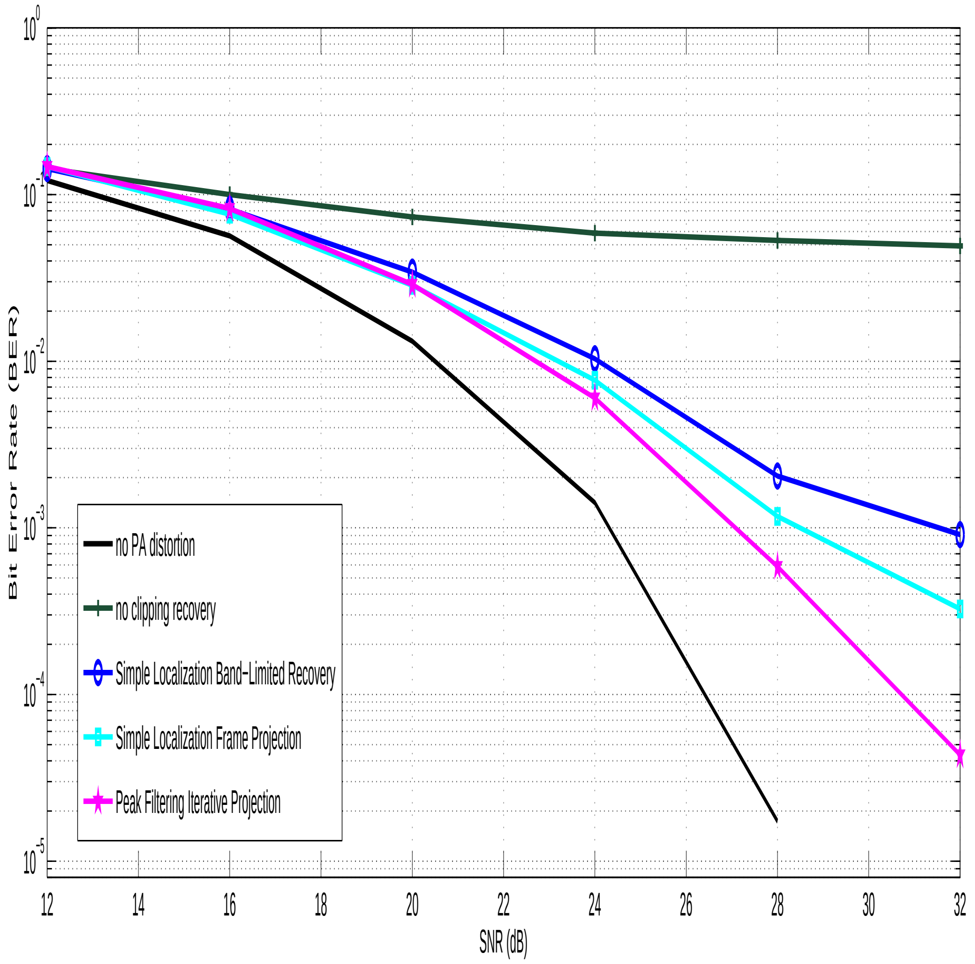

Figure 13. Clipping Recovery with peak filtering localization and iterative projection in OFDMA

simple localization that locates extra 23% false clips, peak filtering reduces the false clips to lower than 17% at a SNR at 32dB.

The BER curves at different SNR levels in different cases are shown in Figure 13. With no clipping noise compensation at the receiver, it is obvious that a BER floor exists even if the SNR is as high as over 30dB, which deteriorates the system performance. With increased accuracy in locating clips by peak filtering, the performance of the magnitude estimation of clipping noise is also improved which leads to BER enhancement over the method in [82]. After combining peak filtering for clip localization with frame-based iterative projection for clip magnitude estimation, our proposed method outperforms the reference method of simple clip localization and band limited signal recovery algorithm in [82], especially in high SNR regimes. At $\mathrm{SNR} = 32\mathrm{dB}$, around 14% information bits are wrong if no noise suppression is applied; and [82] improves the error rate to below 0.1%. With our proposed scheme, the BER is further reduced to below 0.04%.

When SNR is low, the interference from channel noise is so strong that the number of falsely reported clips exceeds the number of the actual clips by a factor greater than one, which may lead to a longer convergence time. It is noted that oversampling is adopted in peak filtering to extract the clip characteristics inherent in the time sequence. Oversampling used in the proposed method is uniform, some detailed information around clips or samples close to the clipping threshold may be lost due to the uniform sample. Considering this, level-crossing based non-uniform sampling [91] in analog-to-digital converter may retrieve more detailed information to further improve the performance, which we will investigate in future work.

CHAPTER 5

JOINT DESIGN OF TRANSMITTER AND RECEIVER SCHEMES

5.1 Introduction

The PAPR issue has been addressed in various solutions [19–21]. The solutions either reduce PAPR to avoid nonlinear clipping on the transmitter (TX) side, such as multiple representations [92], tone reservation (TR) [55] and constellation extension [93], or reconstruct nonlinear distorted or clipped signal on the receiver (RX) side [72, 82, 94]. Receiver-oriented methods are highly desirable when limitations on power consumption, implementation cost or computational complexity exist at TX. Conventional RX-oriented methods like [72], [94] require modulation information of all subcarriers at RX in order to perform decision-aided iterative estimation. However, in OFDMA, modulation information of other users is generally unknown to any individual user which invalidates schemes based on frequency domain reconstruction over the entire symbol block. Most recent approaches [95], [96] utilize Compressed Sensing (CS) framework to estimate and compensate the time-domain clipping noise as a sparse signal with partial frequency-domain information on reserved or reliable subcarriers in OFDM. An approach of combining TR and CS is reported in [97]. However, the sparsity level in CS framework imposes constraints on the number of clipping samples allowed at TX and the recovery algorithms do not show adequate performance when measurements are corrupted by severe noise [20], thus the performance of [97] is limited when high power efficiency is demanded with severe clipping scenario.

In this research we propose a novel method of jointly designing TR at TX and frame-based alternating projections (FAP) at RX to improve the performance in presence of severe clipping. The non-data-bearing tones in one OFDM symbol, normally available in practical systems [7], are partitioned into two disjoint sets, one set used for TR at TX to reduce peak values, the other set used for FAP at RX to recover the clipped signal. The hybrid PAPR reduction at TX is designed with a clipping step that follows with TR at TX to satisfy the required output power level and boost power efficiency. The clipping step cancels residual peaks after TR step of peak reduction. Only a few subcarriers are needed in TR and thus the complexity in resolving TR at TX can be reduced to the minimal acceptable level. On the other hand, the combination of TR with clipping reduces the out-of-band emission with lower PAPR compared with directly clipping case. Unlike CS recovery [97] in which the number of clipping samples is picked due to the necessity of maintaining sparsity for CS recovery at RX, FAP tolerates more clipping samples and therefore a smaller clipping ratio can be adopted at TX to further increase power efficiency. The overall system complexity is well balanced with the freedom in choosing clipping ratio and the flexibility of allocating subset of non-data-bearing tones between TR and FAP. Numerical results are presented to show the proposed method significantly improves BER performance compared with that of the existing method when the clipping ratio is low.

5.2 System Model

In OFDMA transmission with P users, a complex symbol block $\mathbf{X} = \{X_n | n = 0, \ldots, N-1\}$ is passed to an N-point inverse fast Fourier transform (IFFT) to obtain the discrete time-domain samples to be transmitted. The complex baseband representation of an OFDMA signal is

$$
\begin{aligned}
x_k &= \frac{1}{\sqrt{N}} \sum_{p=1}^{P} \sum_{m \in \mathscr{U}_p} X_m e^{j2\pi mk/N} \\
&\quad + \frac{1}{\sqrt{N}} \sum_{r \in \mathscr{R}} X_r e^{j2\pi rk/N}, k = 0, \ldots, N-1
\end{aligned}
\tag{5.1}
$$

where $\mathscr{U}_p$ is the index set of subcarriers allocated to the pth user; $\mathscr{R}$ is the index set of pilot and guard band subcarriers as non-data-bearing tones; X_m is a data symbol on the mth subcarrier modulated from a given QAM constellation for data-bearing tones or known values or zeros on reserved tones. Briefly its vector form with $\mathbf{x} = \{x_k\}$ is

$$\mathbf{x} = \mathbf{W}\,\mathbf{X} \tag{5.2}$$

where $\mathbf{W}$ is the N-IDFT matrix.

To characterize the dynamic range of the OFDM signal in time domain, PAPR is defined as the maximal power of the transmitted signal divided by its average power σ^2 in the continuous time domain. An estimate with discrete samples $\mathbf{x}$ can be obtained as

$$\mathrm{PAPR}(\mathbf{x}) = \frac{\max\limits_{k=0,\ldots,N-1} |x_k|^2}{\sigma^2} = \frac{\|x_k\|_\infty^2}{\frac{1}{N}\|x_k\|_2^2} \tag{5.3}$$

where $\|\cdot\|_2$ is the 2-norm and $\|\cdot\|_\infty$ stands for the ∞-norm.

5.2.1 Tone Reservation

As described in 2.4.4, Tone Reservation (TR) is a distortionless method that adds a peak canceling signal onto the original signal and the resultant signal has a lower PAPR. The peak canceling signal is designed over a subset of tones in frequency domain which carry no information data, i.e.,

$$\tilde{\mathbf{x}}_\mathbf{T} = \mathbf{x} + \mathbf{x}_\mathbf{T} = \mathrm{IDFT}(\mathbf{X} + \mathbf{X}_\mathbf{T}) \tag{5.4}$$

where $\mathbf{X}_\mathbf{T} = \{X_{T,k}, k = 0, 1, \cdots, N-1\}$ and $\mathbf{X}$ have non-zero values on disjoint frequency subspaces. So $\mathbf{X}_\mathbf{T}$, the signal added, does not impact the information data bearing subcarriers. The target in this formulation is then to find $\mathbf{x}_\mathbf{T}$ that minimizes the maximum peak value of the new signal $\tilde{\mathbf{x}}_\mathbf{T}$, i.e.

$$\mathbf{x}_\mathbf{T} = \arg\min_{\mathbf{x}_\mathbf{T}} \|\mathbf{x} + \mathbf{x}_\mathbf{T}\|_\infty = \mathrm{IDFT}(\arg\min_{\mathbf{X}_\mathbf{T}} \|\mathbf{x} + \mathrm{IDFT}(\mathbf{X}_\mathbf{T})\|_\infty) \tag{5.5}$$

The values of $X_{T,k}, k \in \mathscr{R}_T$ are obtained by resolving Equation 5.5 through a convex optimization, which can be cast into a Linear Programming (LP) problem of complexity $O(|\mathscr{R}_T|N^2)$, where $\mathscr{R}_T$ is the index set of non-zero values of $\mathbf{X}_\mathbf{T}$ and $|\cdot|$ denotes the cardinality of a set. The complexity tightly depends on the number of reserved tones as $|\mathscr{R}_T|$. Some simplification [98] is introduced to reduce the complexity while comprising the capability of PAPR reduction. The locations of those reserved tones have significant impact on the capability of PAPR reduction as well. Without restriction, all tones could be reserved for this purpose, but in this research, only pilots and guard band subcarriers are reserved.

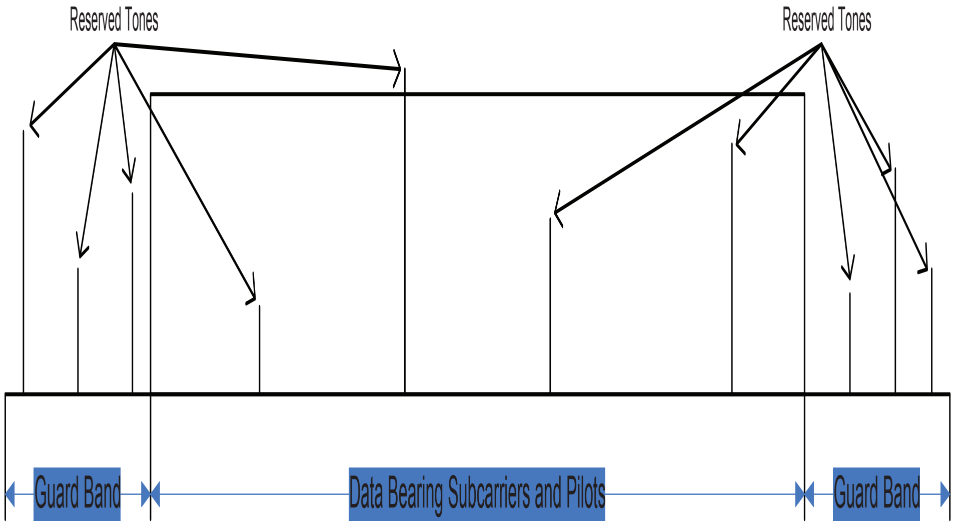

Figure 14. Sparsity of TR Peak Canceling Signal in Frequency Domain

Actually it is noted [99] that only using a few subcarriers can achieve reasonable level of PAPR reduction and render a good balance between the complexity and PAPR reduction. A few subcarriers in guard bands and pilots are reserved to contain the adding signal in the frequency domain. Thus, the signal $\mathbf{X_T}$ is "sparse" in frequency domain as Figure 14 illustrates.

5.2.2 Direct peak clipping

When clipping occurs at TX, the output signal $\tilde{x}_k$ of PA is bounded by a predefined clipping threshold A_s assuming the phase is unchanged from the input signal x_k.

$$\tilde{x}_k = \begin{cases} \frac{A_s}{|x_k|} x_k, & |x_k| > A_s \\ x_k, & |x_k| \leq A_s \end{cases} \tag{5.6}$$

The clipping ratio is defined as $\gamma = A_s/\sigma$. Generally A_s is either close or identical to the actual PA saturation level, while the signal power $\tilde{\sigma}^2$ is adjusted by IBO to PA saturation. The clipping noise is

$$e_k = \tilde{x}_k - x_k, k = 0, \ldots, N-1 \tag{5.7}$$

In OFDMA receiver, assuming that a guard interval of sufficient length is used at TX and the frequency channel response $\mathbf{H} = \text{diag}\{H_m, m = 0, \ldots, N-1\}$ is obtained using other methods like preamble training, the end-to-end equivalent received symbol in frequency domain is

$$Y_m = H_m \tilde{X}_m + G_m, m = 0, \ldots, N-1. \tag{5.8}$$

where G_m are complex white Gaussian noise samples with zero mean and variance σ_g^2. After zero-forcing channel equalization, the output signal in frequency domain is

$$\begin{aligned} \tilde{Z}_m &= Y_m/H_m = \tilde{X}_m + G_m/H_m \\ &= X_m + E_m + G_m/H_m, m = 0, \ldots, N-1 \end{aligned} \tag{5.9}$$

where $\tilde{\mathbf{X}} = \{\tilde{X}_m\}$ is the DFT of $\tilde{\mathbf{x}} = \{\tilde{x}_k\}$ and $\mathbf{E} = \{E_m\}$ is the DFT of $\mathbf{e} = \{e_k\}$ which indicates the distortion in frequency domain due to clipping. The demodulated signal of the pth user is estimated with maximal likelihood as

$$\hat{X}_m = \arg\min_{\chi_p} \left|\tilde{Z}_m - \chi_p\right|^2, \ m \in \mathscr{U}_p \tag{5.10}$$

where χ_p denotes the constellation points of user p. It is noted that $\tilde{Z}_m$ contains clipping noise E_m. Clearly better estimates are acquired by substituting $\tilde{Z}_m$ with $Z_m = \tilde{Z}_m - E_m$ in Equation 5.10. Note that distortion **E** due to time-domain clipping noise **e** spreads to all subcarriers. In the absence of other users' modulation information, user p can not estimate the whole symbol $\{\hat{X}_m, m = 0, \ldots, N-1\}$ to iteratively recover $\tilde{\mathbf{x}}$ so as to cancel $\{E_m, m \in \mathscr{U}_p\}$ from $\tilde{Z}_m$.

5.3 Hybrid Design of Tone Reservation and Clipping at Transmitter and Signal Recovery at Receiver

From Equation 5.3 and Equation 5.6, we observe that for a fixed PA saturation, a lower PAPR of **x** allows smaller IBO and thus achieves larger power efficiency. Directly clipping like Equation 5.6 reduces PAPR of $\tilde{\mathbf{x}}$, however it incurs not only in-band distortion spread as **E** but also out-of-band emission which needs to be controlled under the standard spectral mask [7]. So it is desirable to introduce other schemes at TX to reduce PAPR first and thus lower out-of-band emission to some extent; and then combine a sequential clipping step to further enhance the power efficiency. The in-band distortion due to clipping is left to compensate through signal recovery at RX. Non-data-bearing subcarriers inherent in the system can be divided into two portions, one portion for TX use, the other for RX use. A joint TX and RX scheme is thereby proposed to mitigate the PA nonlinear effects by judiciously allocating reserve tones for TR at TX and adequately controlling the clipping ratio to expose the number of clipped samples for FAP at RX. The sparsity in the frequency domain is explored through reserving a few tones to suppress OOB emission with acceptable complexity, while the sparsity in the time domain is controlled by only clipping a few peaks and thus utilized to make signal recovery feasible at RX.

5.3.1 Hybrid Tone Reservation and Clipping at TX

Tone Reservation [55] partitions all subcarriers in two separate sets: data-bearing set $\mathscr{D}$ and reserved set $\mathscr{R}_T$ with $|\mathscr{D}|+|\mathscr{R}_T| = N$ where $|\cdot|$ denotes the cardinality of a set. Some dummy signals $\mathbf{X}_T = \{X_q|X_q \neq 0, q \in \mathscr{R}_T; X_q = 0, q \in \mathscr{D}\}$ are inserted in the frequency domain thereby adding $\mathbf{x}_T$ to alter the waveform in the time domain so that peak values are optimized at TX. While the peak values are optimized as Equation 5.5, the signal average power is also changed, which affects the PAPR of the signal. Alternatively, PAPR can be directly optimized as the objective function,

$$\min_{\mathbf{X}_T} \mathrm{PAPR}(\tilde{\mathbf{x}}_T), \text{ with } \tilde{\mathbf{x}}_T = \mathbf{x}+\mathbf{x}_T \tag{5.11}$$

Those dummy signals are ignored at RX and BER is not affected because of the orthogonality between $\mathscr{D}$ and $\mathscr{R}_T$. The achievable PAPR in Equation 5.11 depends on the degree of freedom in $\mathscr{R}_T$ as $|\mathscr{R}_T|$ and the indices. When the set $\mathscr{R}_T$ is not determined the optimization in Equation 5.11 is NP-hard.

Reexamining Equation 5.1, note that part of non-data-bearing subcarriers $\mathscr{R}$ in practical systems can be used as the reserved tones in TR. With narrowing the searching range from N to $|\mathscr{R}|$ for candidate PAPR reduction tones (PRT), the complexity in resolving Equation 5.4 is decreased. Depending on limitations on TX, finding the optimal solution in Equation 5.4 may still be undesirable. Usually some iterative algorithm is employed to acquire the near-optimal solution. The algorithm iterates between frequency domain by adjusting $\mathbf{X}_T$ and time domain by searching $\mathbf{x}_T$ to make PAPR within a preset error tolerance with respect to the target PAPR. Empirically using only a few reserved tones reduces

PAPR significantly, such that $|\mathscr{D}| \gg |\mathscr{R}_\mathrm{T}|$. $\mathbf{X}_\mathrm{T}$ exhibits a sparse signal in frequency domain which is utilized to design $\mathbf{x}_\mathrm{T}$.

When high power efficiency is demanded with less stress on distortion, a clipping step is further incorporated after TR to bound peak values to PA saturation.

$$\tilde{\mathbf{x}}_{\mathrm{T,E}} = \tilde{\mathbf{x}}_\mathrm{T} + \mathbf{e} = \mathbf{x} + \mathbf{x}_\mathrm{T} + \mathbf{e}, \quad \|\tilde{\mathbf{x}}_{\mathrm{T,E}}\|_\infty \leq A_s \tag{5.12}$$

where $\mathbf{e}$ is the clipping noise between the signal output from TR and the signal output from PA. Naturally $\mathbf{e}$ consists of a sequence of pulses in time domain according to Equation 5.6. The degraded system performance due to $\mathbf{e}$ at TX is neutralized after estimating and compensating the clipping noise at RX. As $\mathscr{R}_\mathrm{T} \subset \mathscr{R}$, frequency distortion due to $\mathbf{e}$ that spans over the set $\mathscr{R}_\mathrm{F} = \{\mathscr{R} \setminus \mathscr{R}_\mathrm{T}\}$ is only introduced by clipping so it is utilized as known information to infer $\mathbf{e}$. The size of $\mathscr{R}_\mathrm{F}$ is much smaller than the dimension of $\mathbf{e}$, which makes the problem under-determined. However, the sequence $\mathbf{e}$ contains a lot of zeros, which appears to be a "sparse" signal in time domain. The sparsity in time domain makes solving the under-determined problem more "feasible" and then it is utilized to recover the signal at RX.

Therefore, the combination of TR and clipping at TX generates a very effective PAPR reduction approach in terms of controlling out-of-band distortion and boosting power efficiency. The in-band distortion reduced by TR is shifted to be further compensated at RX as in [95, 96] where CS framework is applied to recover the clipping noise. However, in order to guarantee the sparsity, CS framework only allows the s-maximal samples to be clipped at TX, which implies a relatively high clipping ratio and limits the space for power efficiency enhancement. When clipping ratio is low, more samples are clipped, the sparsity in $\mathbf{e}$ is not maintained which makes CS algorithms less effective in finding the good estimation of clipping noise.

5.3.2 Signal Recovery through Frame-based Alternating Projection at RX

Compressed Sensing [100, 101] tends to minimize the number of samples or measurements $\mathbf{E}_c$ (less than Nyquist rate), which are acquired through the sensing matrix $\mathbf{W}_\Phi$, to retain the information necessary to recover the original signal $\mathbf{e}$, that is, $\mathbf{E}_c = \mathbf{W}_\Phi\ \mathbf{e}$ with $|\mathbf{E}_c| \ll |\mathbf{e}|$. Normally it is impossible to recover the unknown original signal from the measurements of deducted dimension. However, if the sensing matrix $\mathbf{W}_\Phi$ satisfies the Restricted Isometry Property (RIP), that is, with $\delta \in (0,1)$,

$$(1-\delta)\,\|\mathbf{e}\|_2^2 \leq \|\mathbf{W}_\Phi \mathbf{e}\|_2^2 \leq (1+\delta)\,\|\mathbf{e}\|_2^2 \tag{5.13}$$

holds for all *s-sparse* vectors $\mathbf{e}$ that have at most s non-zeros, the recovery is feasible.

In OFDMA, the estimation of $\{E_m, m \in \mathscr{U}_p\}$ for user p relies on recovery of the entire clipping noise $\mathbf{e}$ in time domain. Taking the measurements Ec_r as the differences between received equalized samples $\tilde{Z}_r$ and a prior known values X_r in $\mathscr{R}_F$ ($|\mathscr{R}_F| < N$), that is,

$$Ec_r = \tilde{Z}_r - X_r, r \in \mathscr{R}_F \tag{5.14}$$

and taking the sensing matrix $\mathbf{W}_\Phi$ as the sub-matrix $\mathbf{W_F}^H$ selected rows in $\mathscr{R}_F$ from N-DFT matrix $\mathbf{W}^H$, the CS formulation [97] reaches

$$\mathbf{E}c = \mathbf{W_F}^H\ \mathbf{e} + \mathbf{G}c \tag{5.15}$$

where $\mathbf{E}c = \{Ec_r, r \in \mathscr{R}_F\}$ and $\mathbf{G}c$ represents the unrecoverable channel noise with $\|\mathbf{G}c\|_2 < \xi$. Then under CS framework the estimation of clipping noise $\mathbf{e}$ is transformed into an l_1-minimization problem.

$$\min_{\hat{\mathbf{e}}} \|\hat{\mathbf{e}}\|_1^2, \text{ subject to } \left\|\mathbf{E}c - \mathbf{W_F}^H \hat{\mathbf{e}}\right\|_2 < \xi \tag{5.16}$$

Standard convex optimization algorithms can be applied to solve Equation 5.16, but in the context of CS, signal recovery algorithms that utilize *a prior* knowledge of the sparsity level of s are normally employed such as regularized optimization algorithm like least absolute shrinkage and selection operator(LASSO) [102] or greedy algorithm as ROMP [103]. Note that in those algorithms the information of locations of non-zeros (clips) is not pre-determined before the iterative searching process. Revisiting Equation 5.6, given a targeted PA output power level, the clipping threshold is known or derived at RX, however such information is not utilized in the CS formation for signal recovery in [97].

The noise level of the recovery algorithms is related to the sparsity level s and the channel noise level ξ, e.g. for ROMP it is proportional to $\sqrt{\log(s)}\xi$ [103]. In order to reduce the noise level of the recovery, small s is preferred. The sparsity level is controlled at TX by only selecting a small number of s maximal values in $\mathbf{e}$ to be clipped [97], which normally leads to high clipping ratio and thus low power efficiency. When clipping ratio is high, the CS recovery algorithms become less efficient.

As widely known, the magnitude of x_k in Equation 5.1 is approximately Rayleigh distributed. The average up level-crossing rate above some threshold A_s depends on the clipping ratio approximately as [87]

$$\overline{N_c} = N\sqrt{\frac{\pi}{3}}\,\gamma\, e^{-\gamma^2} \tag{5.17}$$

And it requires $|\mathscr{R}_F| \sim \mathscr{O}(\overline{N_c} * \log N)$ measurements in frequency domain to recover the original clipping noise [104]. For instance, for a typical clipping ratio of 2dB, the average number of clipping pulses in one OFDM symbol period is about $0.1316 * N$ and it needs $|\mathscr{R}_F| > 892$ measurements out of $N = 2048$ subcarriers which incurs large data rate loss ($>$ 43% reserved tones needed). So when severe clipping occurs, the sparsity level is not guaranteed and thus CS recovery is not sufficiently effective.

At the receiver, we design Frame-based Alternating Projections (FAP) to recover the clipping noise in two steps . Firstly the locations of clip candidates are estimated with help of *a prior* knowledge of the clipping threshold and corresponding phases of clips are predicted according to Equation 5.6, and secondly we cast the problem Equation 5.15 with frame theory instead of CS optimization formulation in Equation 5.16, and then magnitudes of clips are obtained by alternating projections established on frame iterations between the complimentary part of reserved tones and clip candidates.

Under normal circumstances for reliable communications the signal power is much larger than the noise power and thus the magnitude of the signal is much larger than the noise g_k at the time instances where clipping occurs [82]; and the clipping noise e_k is also much lower than the in-band OFDM signal, for a typical value of 2dB clipping ratio, the clipping noise is -18dB lower than the in-band OFDM signal (c.f. (27) in [87]). The equalized signal magnitude satisfies from Equation 5.9

$$|\tilde{z}_k| \gg |g_k| \quad \text{and} \quad |\tilde{z}_k| \gg |e_k|. \tag{5.18}$$

These conditions are exploited to identify the potential clip locations. So the equalized time samples with magnitudes close to A_s are selected as clip candidates, that is, samples in $\tilde{z}_k$ with the magnitude greater than $A_s - \mu\sigma_g$ are selected in the set of clip candidates C, where μ is a factor chosen to adjust the number and locations of clip candidates and σ_g is standard deviation of noise power.

It is noted that μ tends to be selected to make the signal contain as many as possible potential clips while tolerating some falsely reported locations. During the iterative projections in the next step to refine the magnitudes at all possible clip locations, the estimated clipping noise is most likely confined to the actually clipped locations, while the values at falsely reported locations reduce to zero which do not significantly affect the final estimate. Depending on system configurations, μ can be trained offline to avoid increasing the complexity of iterations because of including too many false locations.

As clipping in Equation 5.6 indicates, the clipping noise maintains the phase as the time domain signal. Although the noise item g_k introduces some disturbance in the received signal, the phase changes are ignored due to noise magnitude being far smaller than the signal strength in Equation 5.18. So the phases of located clips are chosen identical to the equalized signal at the receiver.

$$\angle(e_k) = \angle(x_k) \cong \angle(\tilde{z}_k), \text{ for } k \in C \tag{5.19}$$

From Equation 5.15 after locations of clip candidates are identified, e_k has non-zero values only at the clip locations $k \in C$ while being zeros at other locations, so

$$\mathbf{E}_c = \mathbf{W_{F,c}}^H \, \mathbf{e}_c + \mathbf{G_c} \tag{5.20}$$

where $\mathbf{W_{F,c}}^H$ is the $|\mathscr{R}_F| \times |C|$ sub-matrix taken $|\mathscr{R}_F|$ rows and $|C|$ columns from N-DFT matrix $\mathbf{W}^H$. Note that the matrix $\mathbf{W_{F,c}}^H$ actually represents a frame matrix that means the rows of $\mathbf{W_{F,c}}^H$ are elements of a finite frame [88]. Recall the definition of frame, a set of vectors $\Phi = \{\phi_\nu\}_{\nu=1}^{V}$in $\mathbb{C}^K$ is a *frame* if there exist $A, B \in \mathfrak{R}$, and $0 < A \leq B$ such that

$$A\,\|\mathbf{e}\|^2 \leq \sum_{\nu=1}^{V} |\langle \mathbf{e}, \phi_\nu \rangle|^2 \leq B\,\|\mathbf{e}\|^2, \quad \forall \mathbf{e} \in \mathbb{C}^K, \tag{5.21}$$

where $\langle \cdot \rangle$ denotes inner product in Euclidean space. A and B are called lower and upper frame bounds. Clearly, ${\mathbf{W_{F,c}}}^H$ has upper and lower bounds because it is a sub-matrix from N-DFT matrix W, the bounds A and B are actually determined by the minimal and maximal eigenvalues of the square matrix $\mathbf{W_{F,c}}{\mathbf{W_{F,c}}}^H$.

Revisiting Equation 5.13 and Equation 5.21, the frame formulation does not impose the s-sparsity requirements on the unknown signal $\mathbf{e}$ which is more suitable in presence of severe clipping scenario when sparsity level is difficult to be maintained due to the requirement of high power efficiency at TX.

Following the frame-based alternating projection, the iterative process is

$$\begin{aligned} &\mathbf{e}_i = (\tfrac{B-1}{B}\mathbf{I} + \tfrac{1}{B}\mathbf{I_c}\mathbf{W}\mathbf{I_r}\mathbf{W}^H)\mathbf{I_c}\mathbf{W}\mathbf{I_r}\mathbf{W}^H\mathbf{I_c}\mathbf{e}_{i-1} + \mathbf{e}_0, i > 1 \\ &\mathbf{e}_0 = (\mathbf{I} + \tfrac{1}{B}\mathbf{I_c}\mathbf{W}\mathbf{I_r}\mathbf{W}^H)\mathbf{I_c}\mathbf{W}E_{c0} \end{aligned} \tag{5.22}$$

where $\mathbf{I_c}$ denotes a diagonal $N \times N$ matrix with diagonal elements equal to 1 only corresponding to clipping locations and 0 otherwise; $\mathbf{I_r}$ is also a diagonal $N \times N$ matrix with 1's corresponding to user data subcarriers and 0's corresponding to reserved subcarriers in $\mathscr{R}_F$.

The stopping condition is simply selected as $||\mathbf{e}_i - \mathbf{e}_{(i-1)}|| < \epsilon$ where ϵ is a predefined threshold. The iterative process converges to the Least Square solution if the noise $\mathbf{G}_c$ is ignored in Equation 5.20. The

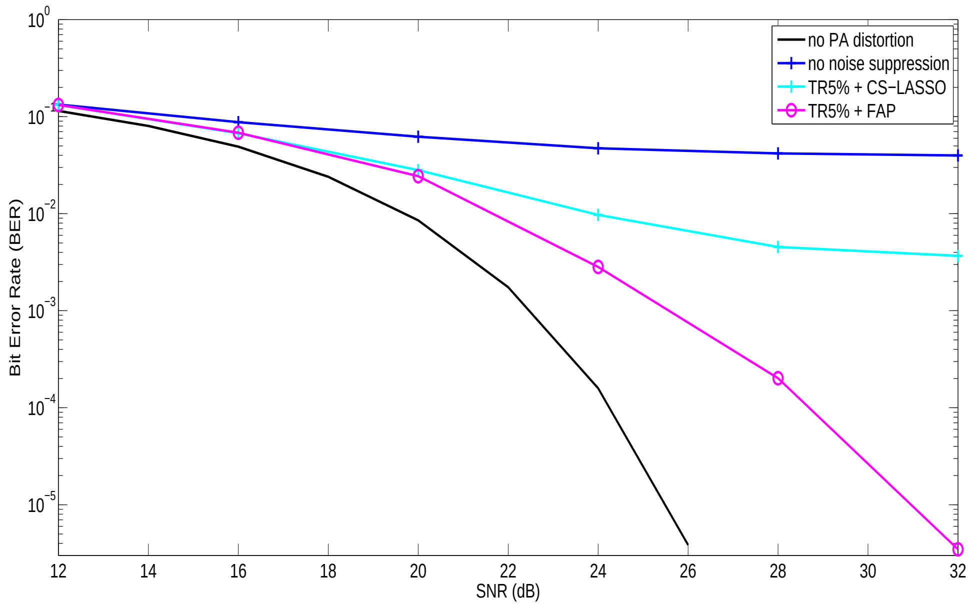

Figure 15. Recovery of clipping noise with TR at TX and CS and FAP at RX in OFDMA (CR=2dB)

energy dispersed on reserved subcarriers in frequency domain tends to be confined to actual clips in time domain in each iteration to solve Equation 5.20. Although there exist falsely reported clip candidates, the values at those false clips gradually diminish in each iteration. After the clip locations are determined, the coefficient projection matrix in Equation 5.22 can be pre-calculated and stored before iterations, and thus the actual iterative process only involves matrix multiplication which lowers the implementation complexity.

The load balance between TX and RX can be jointly designed by selecting tones dedicated to TR in $|\mathscr{R}_{\mathrm{T}}|$ and tones used to recovery in $|\mathscr{R}_{\mathrm{F}}|$. For systems with constraints on out-of-band emission, it is preferable to allocate more tones to TR, while for those with demands of high power efficiency and constraints on TX complexity, simply clipping tends to be used at TX, then the complexity is shifted to RX with a larger number of subcarriers being in $\mathscr{R}_F$.

Extensive simulations are conducted to verify the performance and simulation results validate the performance of the new proposed method in obtaining more accurate clip locations and the BER performance is therefore significantly improved.

5.4 Simulation Results and Discussion

The OFDMA system is set up according to the IEEE802.16 WiMAX standard [7]. The reserved subcarriers are 192 pilot and 319 guard band carriers $|\mathscr{R}| = 512$ out of the total $N = 2048$ subcarriers. Total 8 users equally share the other data subcarriers in an interleaved pattern. The target user uses 64QAM modulation, and other users randomly select modulation schemes from BPSK, QPSK, 16QAM and 64QAM, which is unknown to the target user. Some percentage of the subcarriers are used for TR, e.g. 5%*$|\mathscr{R}|$. Uncoded OFDM without bit loading is assumed at the transmitter.

As shown in Figure 16, TR at TX reduces PAPR and thus lower out-of-band emission while boosting PA output power level. The larger number of reserved tones dedicated to TR, the larger is the achieved reduction in PAPR. But the complexity of calculating the additive signal $\mathbf{x}_T$ also increases and the PAPR level with TR only is still high. So clipping is combined with TR to reduce the computational load and cancel residual peaks. More PAPR reduction is acquired by combining TR with CS type of clipping (only the s-maximal values being clipped). The sparsity level s is limited by the number of available measurements $s < |\mathscr{R}_F|/\log(N)$, thus it does not reach the target PAPR level if high power efficiency is demanded with a low clipping ratio $\gamma = 2\mathrm{dB}$, that is, if more clips are generated due to severe clipping, CS recovery becomes invalid because the number of measurements used is insufficient.

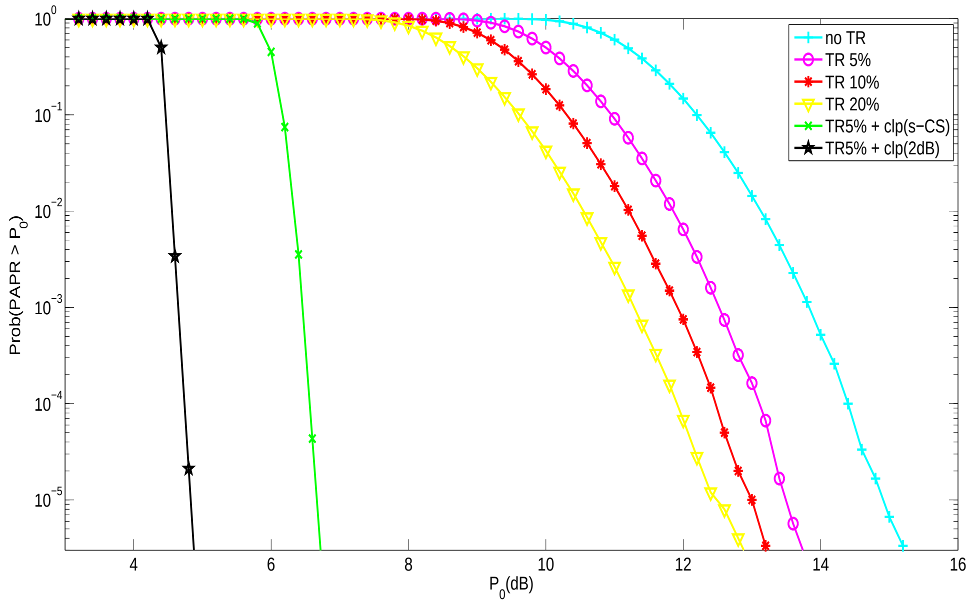

Figure 16. CCDF with different schemes (only s-maximal samples clipped in CS)

The performance of different schemes are studied in terms of BER versus SNR curves with practical range of SNR that is normally up to 32dB. Similar to [97], the CS recovery scheme uses 5% tones in the set of reserved subcarriers to perform TR, and the remaining reserved subcarriers are used to provide measurements for CS recovery in which LASSO algorithm is used. To maintain the fairness of the comparison, same allocations of subcarriers for TR are also applied in the scheme of FAP recovery proposed in this section. Meanwhile, a typical clipping ratio $\gamma = 2\text{dB}$ is applied at TX in both schemes to ensure that the identical TX power efficiency is achieved. The BER performance of CS recovery and FAP recovery is compared in Figure 15. It is obvious that FAP recovery outperforms CS recovery especially in the high SNR regime. When the clipping ratio is low, the insufficient compensation of clipping noise in CS recovery attributes to the limitation of the sparsity level that CS framework can handle when the available number of measurements is limited.

CHAPTER 6

PAPR REDUCTION IN MIMO-OFDM

6.1 Introduction

Multiple Input Multiple Output (MIMO) systems, employing Space Time Coding (STC) [105] [106], enable high capacities for wireless links both in theory and in practice. However, for broadband frequency-selective fading channels, conventional space-time decoding requires very complex equalization at the receiver. This drawback can be overcome by using MIMO systems in conjunction with OFDM, which significantly reduces the complexity of equalizing delay spread at the receiver by partitioning the broadband frequency-selective channel into parallel narrow-band frequency-flat subchannels [26]. MIMO-OFDM is widely accepted in standards as a technology for the broadband wireless communication systems that provide the high performance needed to meet the increasing demand of Internet and multimedia services. However, high PAPR of transmitter signals still remains an issue in MIMO-OFDM systems [21].

As discussed in section 2.4.3, multiple representation schemes are coarse control schemes in reducing PAPR, that is, they lower the probability of occurrences of large peaks, while not guaranteeing the peak level is below the PA saturation. Erasure Pattern Selection [107, 108] belongs to this category. EPS scheme introduces redundancy into the transmission by frame expansion, and this redundancy is used not only for PAPR reduction but also for error correction. Active Channel Extension (ACE) [58] is a different approach which lowers PAPR by modifying signals in the active channels, while a dual approach namely Fourier Projection Algorithm (FPA) inserts dummy signals on null channels to mitigate PAPR [53]. FPA designs the dummy signals by projecting hard clipping noise onto null subcarriers, while not affecting data bearing subcarriers. The redundant subcarriers introduced by EPS can be utilized for FPA purpose. A hybrid scheme of combining both achieve better performance compared with either of them being used separately, since EPS provides error protection while FPA provides fine control on PAPR reduction.

We examine the use of the EPS scheme developed for SISO for application to MIMO systems. Some recent work has addressed PAPR reduction in MIMO signal transmission via MIMO-SLM [109] and MIMO-ACE [110]. High peaks can appear on any antenna. Direct application of PAPR reduction schemes for SISO to each antenna individually in MIMO requires extensive computations to reach a final solution for all antennas, thus causing undesirable increase in complexity and redundancy. MIMO introduces additional spatial operations into systems besides the usual time frequency operations in SISO. We develop an EPS-based method to reduce the maximal peak power simultaneously over all antennas and utilize spatial diversity from STC [111]. We show that the scheme is advantageous in reducing redundancy when compared with directly applying it to individual antennas and it provides reliable transmission.

6.2 PAPR in MIMO-OFDM SYSTEM

We consider MIMO-OFDM system with M_t transmit antennas and M_r receive antennas which uses N subcarriers. A block diagram of MIMO-OFDM systems that uses Space Time Block Coding (STBC) is shown as in Figure 17.

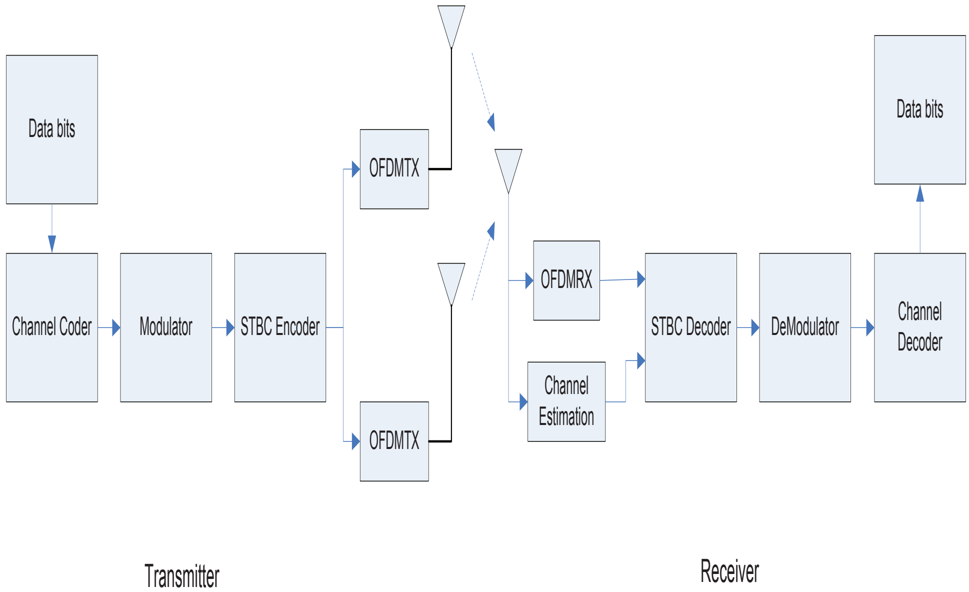

Figure 17. Overall MIMO-OFDM system model

Consider a MIMO frequency-selective Rayleigh fading channel with L independent propagation delays between each pair of transmit and receive antennas. The channel impulse response between the jth transmit antenna (j=1,...,M_t) and the ith receive antenna (i=1,...,M_r) is given by $g_{i,j}(l)(l$=0,...,$L-1)$. Let $M_t \times N$ data symbols be transmitted over the channel. Denote the sequence on the jth transmit antenna to be $\mathbf{X}_j = [X_j(0), X_j(1), ..., X_j(N-1)]$. Then the sequence is first subjected to IFFT operation following by appending a cyclic prefix (CP) at the transmitter. At the receiver the CP is removed and then an FFT operation is performed. The signal received at the ith antenna over the nth subcarrier is:

$$Y_i(n) = \sqrt{\frac{\rho}{M_t}} \sum_{j=1}^{M_t} H_{i,j}(n) X_j(n) + U_i(n) \tag{6.1}$$

where $\sqrt{\rho/M_t}$ is the factor that normalizes the power of the received signal; $U_i(n)$ is the additive white Gaussian noise at the nth subcarrier with variance $\sigma_n^2 = 1$; $H_{i,j}(n)$ is the channel frequency response for the nth OFDM subcarrier which is given by

$$H_{i,j}(n) = \sum_{l=0}^{L-1} g_{i,j}(l) exp\left(-j\frac{2\pi nl}{N}\right), \quad n = 0, 1, ..., N-1, \tag{6.2}$$

where l denotes the propagation delay, l=0,1,...,$L-1$. For Rayleigh fading channel, the coefficient $g_{i,j}(l)$ is a zero-mean complex Gaussian random variable with variance σ_l^2. It is assumed that $g_{i,j}(l)$ for any i,j,l are i.i.d random variables. And the variances σ_l^2 are normalized and set to equal power profile for multipath, i.e. $\sum_{l=0}^{L-1} \sigma_l^2 = \sum_{l=0}^{L-1} 1/L = 1$. The signals in Equation 6.1 can be rewritten in the vector form as

$$\mathbf{Y}(n) = \sqrt{\frac{\rho}{M_t}} \mathbf{H}(n) \mathbf{X}(n) + \mathbf{U}(n) \tag{6.3}$$

where $\mathbf{Y}$(n) is a column vector with $(\mathbf{Y}(n))_i$=Y_i(n), $\mathbf{U}$(n) is also a column vector with $(\mathbf{U}(n))_i$=U_i(n), and $\mathbf{H}$(n) is an $M_r \times M_t$ matrix with $(\mathbf{H}(n))_{i,j}$=$H_{i,j}$(n), $(i = 1, ..., M_r)$. For simplicity, an Orthogonal STBC (OSTBC) is employed in our approach, e.g. Alamouti scheme with $M_t = 2$ [112]. During the first OFDM symbol period, two OFDM symbols $\mathbf{X}_1$ and $\mathbf{X}_2$ are transmitted from antenna 1 and 2 respectively; during the next OFDM symbol period, $-\mathbf{X}_2^*$ and $\mathbf{X}_1^*$ are transmitted from antenna 1 and 2, where $(\cdot)^*$ denote element wise conjugate transpose. At the receiver, the Alamouti detection technique extracts $2M_r$ order diversity, which may give an effective input-output relation for symbols as:

$$\mathbf{Y}_i = \sqrt{\frac{\rho}{2}} \|\mathbf{H}\|_F^2 \mathbf{X}_i + \mathbf{U}_i, \quad i = 1, 2 \tag{6.4}$$

where $\|\cdot\|_F$ denotes the Frobenius norm and $(\mathbf{Y}_i)_n$=Y_i(n). With the help of OSTBC, ST decoding can be simplified into a symbol-to-symbol decision. Since MIMO-OFDM channel is decomposed into N parallel flat MIMO channels over each tone, the index n of each tone is dropped in Equation 6.4. Note that the channel needs to remain stable over at least two OFDM symbol periods in the above scheme.

Another point to be noted is that X_i and $\pm X_i^*(i = 1,2)$ have the same PAPR properties. PAPR reduction can therefore be considered only for the first symbol period, while the same performance can be achieved in the second period owing to the orthogonality. For OSTBC with $M_t > 2$, PAPR reduction needs to be applied to some consecutive symbol periods, but it lends itself to some simplification. For example, an OSTBC for 3 antennas can be constructed as:

$$S = \begin{pmatrix} s_1 & -s_2 & -s_3 & -s_4 & s_1^* & -s_2^* & -s_3^* & -s_4^* \\ s_2 & s_1 & s_4 & -s_3 & s_2^* & s_1^* & s_4^* & -s_3^* \\ s_3 & -s_4 & s_1 & s_2 & s_3^* & -s_4^* & s_1^* & s_2^* \end{pmatrix} \tag{6.5}$$

For this code, the PAPR reduction operations vary from the first to the fourth symbol period, whereas they remain the same for the first and the fifth symbol periods since symbols there exhibit similar PAPR properties. Consequently, the PAPR relationship over these two periods may be exploited to reduce the complexity.

6.3 Frame Expansion based Erasure Pattern Selection (EPS)

A detailed description of frame expansion theory can be found in [113]. Here we briefly introduce the major properties that are used in the PAPR reduction framework, and discuss the use of DFT frames in our approach.

A set of vectors $\Phi = \{g_n\}_{n=1}^{N}$ in $\mathbb{C}^K$ is a *frame* if there exist $A, B \in \mathbb{R}$,and $0 < A \leq B$ such that

$$A\|x\|^2 \leq \sum_{n=1}^{N} |\langle x, g_n \rangle|^2 \leq B\|x\|^2, \quad \forall x \in \mathbb{C}^K, \tag{6.6}$$

where $\|\cdot\|$ and $\langle \cdot \rangle$ denote norm and inner product in Euclidean space respectively. A and B are called lower and upper frame bounds; when $A = B$, the frame is called *tight.* The definition implies a necessary condition for a frame is $K \leq N$, and the ratio $r = N/K$ is defined as the redundancy of the frame. Note that any finite set of vectors that spans $\mathbb{C}^K$ constitutes a frame.

The frame Φ can be associated with a matrix G by setting the rows of G as the elements of the frame. A frame operator G is defined to extract the frame coefficients of a given K-dimensional vector x as:

$$x_n = (Gx)_n = \langle g_n, x \rangle, \quad n = 1, 2, ..., N \tag{6.7}$$

For tight frame,$G^*G = AI_K$. So, an overdetermined representation of a K-dimensional vector is obtained as N frame coefficients by expansion. Corresponding to the frame Φ, the canonical dual frame $\tilde{\Phi}$ can be used to recover the vector from the expansion coefficients. The dual frame operator is given as the conjugate transpose of the pseudo-inverse of the original frame, $\tilde{G} = \left((G^*G)^{-1} G^*\right)^* = G(G^*G)^{-1}$. It minimizes the reconstruction error.

Consider the case that the expanded vector goes through a white noise channel. The received vector is denoted as $\tilde{y} = y + \eta$, where $y = Gx$ is the expanded vector, and η is the noise vector with $E[\eta_i] = 0$

and $E[\eta_i^* \eta_j] = \delta_{i,j}\sigma^2$, where $\delta_{i,j}$ is Kronecker's delta. When the dual frame is used to recover the original vector x, the mean square error(*MSE*) per element is [114]

$$\mathrm{MSE} = \frac{1}{K} E[\|x - \hat{x}\|^2] = \frac{\sigma^2}{K} \sum_{k=1}^{K} \frac{1}{\lambda_k}, \tag{6.8}$$

where $\{\lambda_k\}_{k=1}^{K}$ is the set of eigenvalues of the matrix G^*G. It is easy to show that when all eigenvalues are equal, *MSE* is minimized as $MSE_0 = \frac{\sigma^2}{r}$. In this case, the frame G is tight. Among all frames, tight frames give the best performance in terms of reconstruction error in the presence of noise.

Overcomplete expansion through frame operation leads to redundancy, which makes the reconstruction feasible even if some coefficients are erased or missing during transmission. Vector y, expanded from vector x, is split into two parts, y_R and y_E, such that $y_R = G_R x$, $y_E = G_E x$. When sub vector y_E is erased, only R coefficients are received. Then x can still be reconstructed from y_R and G_R. It can be shown that if G_R forms a tight frame ($R \geq K$), the reconstruction MSE is minimized. MSE is affected by not only the number of erased samples but also their locations.

DFT frame is widely studied due to its good properties in conjunction with DFT codes and also fast computation using FFT. The DFT frame used in our approach is in $\mathbb{C}^K$ with an operator matrix:

$$G = \sqrt{\frac{N}{K}} W_N^h \Sigma, \tag{6.9}$$

where W_N is an $(N \times N)$ DFT matrix, namely $(W_N)_{nk} = \frac{1}{\sqrt{N}} e^{-j\frac{2\pi}{N}nk}$ and Σ is an $(N \times K)$ matrix, obtained by selecting from an identity matrix of order N the K columns corresponding to the indices of the used subcarriers. The factor N/K is used to normalize the power. Intuitively the DFT frame given in Equation 6.9 is tight, with $G^*G = \frac{K}{N} I_K$. As is shown in [114], *syndrome decoding* is equivalent to signal space projection reconstruction. The decoding process first recovers the erased samples y_E from the received vector y_R depicted as:

$$y_E = -\left(W^h_{E\times(N-K)} W_{(N-K)\times E}\right)^{-1} W^h_{E\times(N-K)} W_{(N-K)\times R}\, y_R \tag{6.10}$$

where $W_{(N-K)\times E}$ is the matrix obtained by selecting the $N-K$ rows from the DFT matrix W_N corresponding to the unused subcarriers and the E columns corresponding to the erased samples. As is shown in [114], when $E < K$, the sub frame G_R is not tight; but there are suboptimal sub frames that minimize MSE which satisfy

$$W^h_{E\times K} W_{K\times E} = \frac{K}{N} I_E. \tag{6.11}$$

This shows that MSE is minimized when the spacing between any pair of erasures is an integer multiple of N/K given N is a multiple of K. Accordingly, this selection of erasures simplifies significantly the syndrome decoding process by avoiding time-consuming matrix inversion due to the fact that:

$$W^h_{E\times(N-K)} W_{(N-K)\times E} = I_E - W^h_{E\times K} W_{K\times E} = \frac{N-K}{N} I_E, \tag{6.12}$$

so

$$y_E = -\frac{N}{N-K} I_E W^h_{E\times(N-K)} W_{(N-K)\times R}\, y_R. \tag{6.13}$$

Erasure Pattern Selection [107] utilizes frame expansion to introduce redundancy. The redundancy can be used not only for PAPR reduction but also for error correction. A K-dimensional data block is expanded to a N-dimensional data block by inserting zeros at the unused subcarrier locations followed by IFFT. Part of the redundancy introduced by frame expansion is removed by erasures. When the spacing between two adjacent erasures is fixed, all the erasure patterns are equivalent in terms of minimizing the reconstruction error. So, multiple representations are generated from different equivalent erasures on the expanded signal. The representation with lowest PAPR is chosen. Since the erasure patterns cover all elements in the expanded signal, peak values in the signal can be eliminated by erasure, thus PAPR is reduced significantly without degrading BER performance. In fact, the remained redundancy introduced by frame expansion can be exploited to provide error protection, or further reduce PAPR by incorporating FPA [53]. FPA adopts a certain projection over convex set (POCS) algorithm to insert some dummy symbols at the unused subcarrier locations while not changing data symbols at used subcarriers to decrease the PAPR. A faster algorithm for FPA is available to avoid time-consuming DFT and IDFT iterations, which reduces the complexity dramatically. In particular, complexity of the EPS scheme is less than SLM scheme with comparable configurations. In that approach, a shaping function is defined as the IDFT of a vector with zeros in the used subcarrier locations and ones in the unused subcarrier locations; one iteration of FPA is then simplified as finding clips then multiplying and adding a shifted clip-centered shaping function element-wise onto the time domain signal. In the frequency domain, only unused subcarrier values are changed, while they are ignored at the receiver. Hence, FPA does not affect BER performance.

6.4 Algorithm for EPS-FPA in MIMO systems

PAPR reduction in MIMO systems involves many additional considerations compared with SISO systems. Most schemes developed for SISO systems modify the input symbol in the frequency domain and then eliminate the peak in the time domain. For MIMO case, besides the time-frequency transformation, some spatial freedom is included into the framework by employing multiple antennas. Hence it is very advantageous to consider PAPR reduction over all transmit antennas together by utilizing spatial diversity. A precoding transform [106] is widely used in MIMO systems to combat channel fluctuation and thus increase channel capacity. In this paper, a so called frame precoding module is introduced into the system to reduce PAPR based on frame expansion. Unlike the common linear precoding for MIMO, the precoding introduced here focuses on reducing PAPR. Through frame expansion and proper spatial transform, it provides both error protection and PAPR reduction for MIMO-OFDM systems. To balance the total redundancy used in the system, the conventional channel coder can be ignored due to the properties of frame expansion, which reduces the complexity of the whole system again. Figure Figure 18 shows the block diagram of the scheme:

The frame precoding module basically consists of transforming the signal in frequency-space domain by evaluating PAPR in the time-space domain given a maximum peak constraint. Such transform operations may include scrambling, permutation or expansion. Unlike ACE [93], FPA needs some unused subbands in an OFDM symbol to reduce PAPR. Frame expansion exactly provides a way of identifying those unused subcarriers to facilitate FPA. By combining all transmitting antennas, more unused subcarriers can be utilized to reduce PAPR thereby outperforming a single antenna since more spatial freedom is available in the MIMO case. The EPS scheme provides multiple representations of the same information data by selecting different erasure patterns. In MIMO, a better solution to utilize the spatial freedom is to apply a common erasure pattern over all antennas. The EPS-FPA algorithm in MIMO is derived from the corresponding SISO algorithm , and it consists of the following steps:

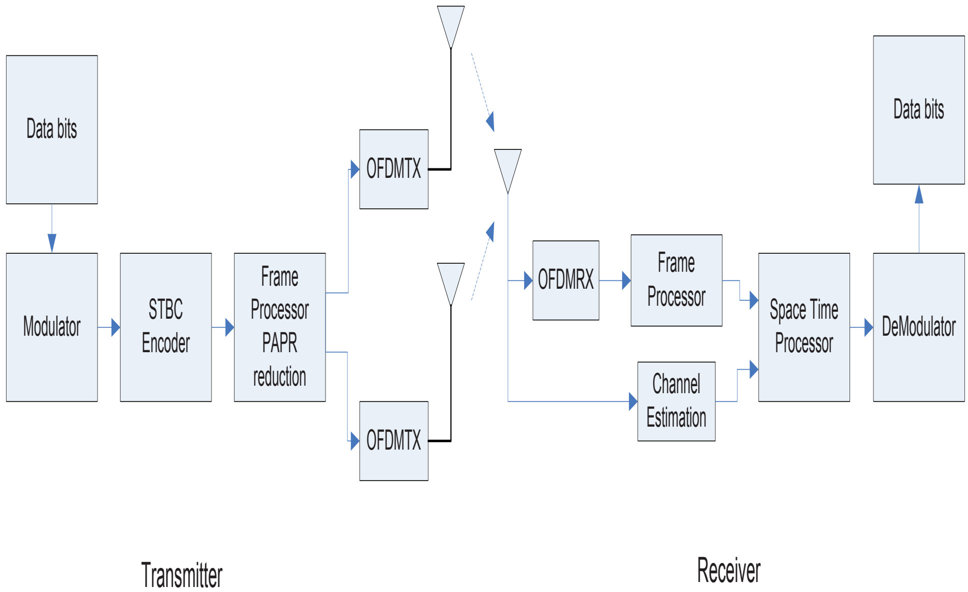

Figure 18. MIMO OFDM with frame expansion

1. Compute constellation symbols $X_1, X_2, ..., X_{M_t}$ each with size K for all antennas by mapping input binary digits to used carriers.
2. Code all $X_i, i = 1, 2, ..., M_t$ by OSTBC encoder, get a block code $\mathbf{X}_K$ of size $M_t K \times T$ in frequency-spatial domain (T is the time dimension of STBC); Map $\mathbf{X}_K$ into $\mathbf{X}_N$ by frame expansion.
3. Apply one erasure pattern from a total of P possible erasure patterns on all antennas, and record the values at the erasure pattern locations as used subcarriers.
4. Calculate IFFT for all antennas, then clip the magnitude of all time samples exceeding a constraint Th.
5. Reconstruct the signal in frequency-spatial domain by FFT and spatial transform.

6. Reset the values at used subcarrier locations and the corresponding erasure pattern locations, while preserving values at other locations.

7. Return to step 4 and iterate until the time-domain constraint is satisfied for all samples or the maximum allowed number of iterations is attained.

8. Return to step 3, apply another erasure pattern, repeat the whole process until exhausting all possible patterns.

9. Select the pattern satisfying the optimal criterion as the one used to reduce PAPR.

Since there is an equivalent and fast algorithm for FPA, IFFT and FFT operations above may be simplified significantly. Here instead of employing the optimal criterion stated in [46], a criterion namely minimax is used, which selects the erasure pattern to minimize the maximal PAPR values over all antennas.

$$\hat{p} = \arg\min_{p \in \mathbf{P}} \left(\arg\max_{1 \leq i \leq M_t} \left(\mathrm{PAPR}\left(\mathbf{X}_{N_i}\right)\right)\right) \tag{6.14}$$

where $\mathbf{P}$ is the predefined set of possible erasure patterns. At the receiver, the inverse process is employed to recover the original data symbols. As discussed, either construction method for frame can be used in presence of erasures. In the simulation, syndrome decoding is adopted and a similar simplified receiver structure is used as in [108].

As argued in [109], the side information to specify which erasure pattern is used in EPS can be protected more with STBC utilizing spatial diversity since all antennas share one common pattern. Actually, a better alternative is to use Erasure Pattern Identification (EPI) stated in [107], where the erasure pattern is detected by evaluating the power present in all possible erasures set. The one with lowest power will be selected as the actual pattern. Thus no side information is needed at the receiver, which is similar to blind identification, thus avoiding the potential errors of side information due to the transmission. Note that the side information is critical since any error in it might cause a burst of bit errors. Thanks to spatial-temporal diversity in MIMO again, estimation of the erasure pattern from EPI is similarly more robust since the common pattern is used over all antennas. Note that if OSTBC is employed, as pointed out before, the same erasure pattern can be used in different symbol periods in one block code, that increases the reliability of EPI again by using temporal diversity.

6.5 Simulation Results and Discussion

Simulation results are now presented along with a discussion of the proposed scheme. In our simulation, QPSK modulation is used and the channel is assumed to be frequency selective Rayleigh fading with AWGN. Here $M_r = M_t = 2, N = 128$ OFDM subcarriers per antenna. Alamouti orthogonal space time code is used in the simulation.

Simulation is run to compare the performance with (1) the conventional MIMO-OFDM system without PAPR reduction; (2) the MIMO-OFDM system using SLM to suppress the PAPR. For fairness in comparison, redundancy for different schemes is required to be equivalent; the complexity in different schemes is comparable. With these constraints, a rate of 1/2 convolutional channel coder is used to add redundancy in both cases which is slightly more than the redundancy introduced in the EPS-FPA scheme. Since *K* symbols are expanded to *N* which is twice of K, E erasures $(E < K)$ are applied to reduce the redundancy rate to $(N - E)/K$ which is less than 2. In our simulation, E=9 erasures are used, thus the redundancy introduced in EPS-FPA is slightly less. In SLM, a rate $1/2$ convolutional coder is applied before feeding the data stream into the space time encoder, and U=2 rotation vectors

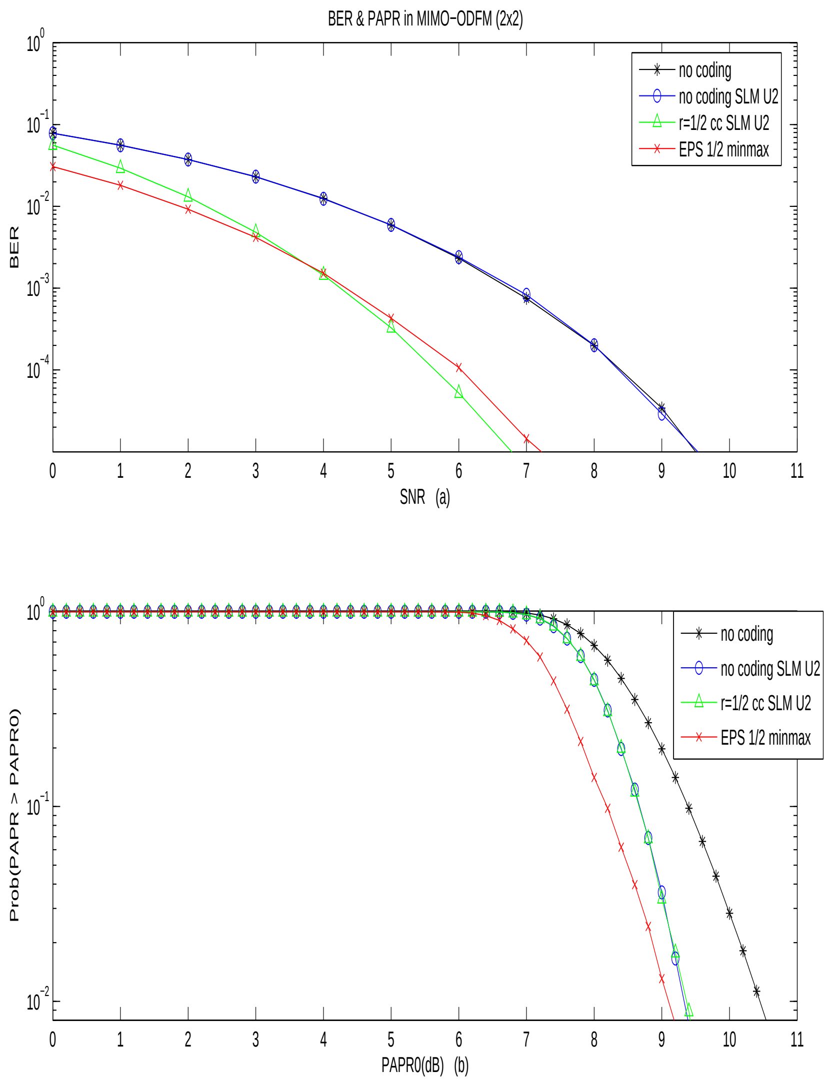

Figure 19. BER and PAPR in MIMO-OFDM

are used to produce multiple representations of OFDM symbols, as is shown in [108]. Complexities of this configuration and the EPS scheme are comparable. The simulation results are shown as Figure 19.

Figure 19 shows that EPS provides not only PAPR reduction but also BER protection. Compared to conventional MIMO-OFDM systems without error protection and PAPR reduction, EPS reduces BER and achieves around 1.5dB PAPR reduction gain with the same clipping probability. Given a bit error rate of 10^{-4}, EPS requires around 2.5dB less SNR than SLM scheme without channel coder. When a channel coder is applied in SLM, EPS has as good performance as SLM in BER; furthermore, it outperforms SLM in PAPR reduction by around 0.4dB for the practical value of clipping probability of 10^{-2}. Considering the complexity for each branch, which is mainly determined by vector multiplications, EPS needs total around 1664 operations in our configuration, while SLM needs around 1930. After adding complexity of channel coder, SLM requires extra complexity to achieve a performance comparable to EPS. Hence EPS performs better than SLM with channel coder in PAPR reduction while with similar redundancy and less computational complexity.

CHAPTER 7

CONCLUSION AND FUTURE WORK

7.1 Conclusion

In this research PAPR reduction schemes on OFDM link performance were investigated in the presence of nonlinear amplification. The emphasis was on power efficiency and cross-channel interference. We evaluated the performance regarding the cost introduced by signal transformations at the transmitter, and we also examined the computational cost of scheme implementation at the transmitter of both SISO and MIMO systems. We simplified the complexity of the transmitter and thus shifted the load to the receiver or jointly designed schemes to balance the load between the transmitter and the receiver. The performance of bit error rate of data transmission of evaluation is improved with our proposed algorithms.

In Chapter 3, two novel peak windowing schemes called sequential asymmetric suppression peak windowing and optimally weighted windowing were presented. Both schemes are focused on handling consecutive peaks that may cause excessive attenuation or spectral regrowth thus degrading the system performance in existing peak windowing schemes. Their RCE and ACPR performance is compared with existing schemes. Extensive simulations show that the proposed schemes outperforms existing schemes in terms of RCE-ACPR trade-off, and in particular, better performance is achieved when a larger window length is applied.

In Chapter 4, a novel and efficient algorithm based on improved clipping localization through peak filtering and frame-based alternating projection is proposed to recover signals nonlinearly distorted at the transmitter due to high PAPR in OFDMA systems. The clipping distorting is compensated and rectified in a way that does not require all subcarriers to be demodulated. With identifying key factors characterizing clips with oversampling the time signal sequence, clip location estimation through peak filtering is more accurate and thus in turn facilitate the recovery of clipping signal. Frame-based alternating projection exploits the iterative processing with the help of projection over convex sets which promotes its convergence and reliability. Simulation results show that the new proposed scheme outperforms existing schemes without increasing the complexity, and in particular, the system performance is improved significantly when SNR is high.

in Chapter 5, a hybrid scheme of joint designing tone reservation with clipping at TX and exploiting recovery of clipped signal at RX with frame-based alternating projection is presented to mitigate the PA nonlinear effects in OFDMA systems. Only a few tones are needed in TR with the help of clipping to suppress residual peaks, and complexity at TX is therefore reduced while power efficiency is boost. The clipping distortion is further estimated and compensated through FAP at RX which does not impose any restrictions on the number of clipped samples at TX. So the proposed method improves BER performance significantly compared with the existing CS recovery scheme [97] when high power efficiency is demanded with severe clipping at TX. The freedom of partitioning the non-data-bearing subcarriers available in practical systems promotes the flexibility of shearing computational load between TX and RX to meet different system requirements.

In Chapter 6, a method of combining frame-based EPS method with FPA is proposed to tackle the high PAPR problem in MIMO-OFDM systems. The extension utilizes the new variables introduced by multiple antennas to provide not only PAPR reduction but also error protection for MIMO-OFDM systems. Thanks to space time diversity, the side information for selected erasure pattern gets more protection, and its transmission may even be avoided. The complexity is thus reduced and robustness of transmission is increased. Simulation results show the advantage of the new approach which outperforms the existing SLM method [109] by providing more PAPR reduction with reduced complexity.

7.2 Future Work

In future work, we propose to investigate the following tasks related to our work in signal design and processing to combat the PA nonlinear effects in multicarrier systems:

- Integrate the PAPR reduction schemes along with predistortion methods as the basis of a joint design methodology to improve the PA efficiency. The easy adaptability of peak windowing facilitates the joint design to compensate the nonlinearity of PA. And also investigate hybrid schemes of combining multiple representations schemes such as interleaver with clipping based schemes such as peak windowing. The combination can utilize the distortionless feature of interleaver to improve the RCE performance of peak windowing, while using the fine tuning controllability of peak windowing to improve the ACPR performance thus boosting power efficiency.
- Investigate allocation schemes of non-data-bearing subcarriers shared by schemes between TX and RX, which provides flexibility and space to optmize system performance. And also explore reliable data-bearing subcarriers according to channel conditions to recover the clipping noise

through which less loss of data rate can be achieved because of reducing reserved subcarriers and thus spectrum efficiency is increased.

- Explore the impact of nonlinear PAs on the system performance in generalized multicarrier systems. It is expected similar nonlinear distortions would affect multicarrier modulation. However, with the specific formulation of the multi-bands multi-standards signals, new signal transformations needs to be investigated to counteract the nonlinear effects in such systems.

APPENDIX

IEEE PERMISSION FOR THESIS/DISSERTATION REUSE

IEEE says: “ The IEEE does not require individuals working on a thesis to obtain a formal reuse license, however, you may print out this statement to be used as a permission grant:

Requirements to be followed when using any portion (e.g., figure, graph, table, or textual material) of an IEEE copyrighted paper in a thesis:

1) In the case of textual material (e.g., using short quotes or referring to the work within these papers) users must give full credit to the original source (author, paper, publication) followed by the IEEE copyright line 2011 IEEE. 2) In the case of illustrations or tabular material, we require that the copyright line [Year of original publication] IEEE appear prominently with each reprinted figure and/or table. 3) If a substantial portion of the original paper is to be used, and if you are not the senior author, also obtain the senior authors approval.

Requirements to be followed when using an entire IEEE copyrighted paper in a thesis:

1) The following IEEE copyright/ credit notice should be placed prominently in the references: [year of original publication] IEEE. Reprinted, with permission, from [author names, paper title, IEEE publication title, and month/year of publication] 2) Only the accepted version of an IEEE copyrighted paper can be used when posting the paper or your thesis on-line. 3) In placing the thesis on the author’s university website, please display the following message in a prominent place on the website: In reference to IEEE copyrighted material which is used with permission in this thesis, the IEEE does not endorse any of [university/educational entity’s name goes here]’s products or services. Internal or per-

APPENDIX (Continued)

sonal use of this material is permitted. If interested in reprinting/republishing IEEE copyrighted material for advertising or promotional purposes or for creating new collective works for resale or redistribution, please go to `http://www.ieee.org/publications_standards/publications/rights/rights_link.html` to learn how to obtain a License from RightsLink.

If applicable, University Microfilms and/or ProQuest Library, or the Archives of Canada may supply single copies of the dissertation."

The reference link is: `http://www.ieee.org/publications_standards/publications/rights/permissions_faq.pdf`

CITED LITERATURE

1. Chang, R. W.: Synthesis of band-limited orthogonal signals for multichannel data transmission. Bell Sys. Tech. J., 46(12):1775–1196, Dec 1966.

2. Saltzberg, B. R.: Performance of an efficient parallel data transmission system. IEEE Trans. Commun., 15(6):805–811, Dec 1967.

3. Bingham, J.: Multicarrier modulation for data transmission: an idea whose time has come. Communications Magazine, IEEE, 28(5):5–14, May 1990.

4. IEEE Std. 802.11a-1999: Wireless LAN Medium Access control (MAC) and physical layer (PHY) specifications: High Speed Physical Layer in the 5Ghz Band, 1999.

5. IEEE Std. 802.11g-2003: Wireless LAN Medium Access control (MAC) and physical layer (PHY) specifications: Further Higher Speed Physical Layer Extension in the 2.4Ghz Band, 2003.

6. IEEE Std. 802.16-2004: IEEE Standard for Local and Metropolitan Area Networks Part 16: Air Interface for Fixed Broadband Wireless Access Systems, 2004.

7. IEEE Std. 802.16e-2005: IEEE Standard for Local and Metropolitan Area Networks Part 16: Air Interface for Fixed Broadband Wireless Access Systems, 2005.

8. IEEE Std. 802.11n-2009: Wireless LAN Medium Access control (MAC) and physical layer (PHY) specifications: Enhancements for Higher Throughput, 2009.

9. IEEE Std. 802.11ac-2014: Wireless LAN Medium Access control (MAC) and physical layer (PHY) specifications: Enhancements for Very High Throughput for Operation in Bands below 6 GHz, 2014.

10. 3GPP TS 36.211-2008: Evolved Universal Terrestrial Radio Access (E-UTRA); Physical channels and modulation, 2008.

11. 3GPP TS 36.201-2010: Evolved Universal Terrestrial Radio Access (E-UTRA); LTE physical layer; General description, 2010.

CITED LITERATURE (Continued)

12. Farhang-Boroujeny, B. and Kempter, R.: Multicarrier communication techniques for spectrum sensing and communication in cognitive radios. Communications Magazine, IEEE, 46(4):80–85, 2008.

13. Akansu, A., Duhamel, P., Lin, X., and de Courville, M.: Orthogonal transmultiplexers in communications: a review. IEEE Transactions on Signal Processing, 46(4):979–995, April 1998.

14. Batra, A., Balakrishnan, J., Aiello, G., Foerster, J., and Dabak, A.: Design of a multiband OFDM system for realistic UWB channel environments. IEEE Trans. Microw. Theory Tech., 52(9):2123–2138, September 2004.

15. Mitola, J.: The software radio architecture. Communications Magazine, IEEE, 33(5):26–38, May 1995.

16. A.R.S. Bahai, B. R. S. and Ergen, M.: Multi-carrier Digital Communications Theory and Applications of OFDM. New York, NY, USA, Springer Science Business Media, Inc, 2004.

17. van Nee, R. and Prasad, R.: OFDM for Wireless Multimedia Communications. Boston, London, Arteh House, 2000.

18. Wang, L. and Tellambura, C.: An overview of peak-to-average power ratio reduction techniques for ofdm systems. Signal Processing and Information Technology, 2006 IEEE International Symposium on, pages 840–845, Aug. 2006.

19. Jiang, T. and Wu, Y.: An overview: Peak-to-average power ratio reduction techniques for ofdm signals. IEEE Trans. Broadcast., 54(2):257–268, Jun. 2008.

20. Wunder, G., Fischer, R., Boche, H., Litsyn, S., and No, J.-S.: The papr problem in ofdm transmission: New directions for a long-lasting problem. Signal Processing Magazine, IEEE, 30(6):130–144, 2013.

21. Han, S. H. and Lee, J. H.: An Overview of Peak-To-Average Power Ratio Reduction Techniques for Multicarrier Transmission. IEEE Wireless Commun., 12(2):56–65, April 2005.

22. Ochiai, H.: Performance Analysis of Peak Power and Band-Limited OFDM System With Linear Scaling. IEEE Trans. Commun., 2(5):1055–1065, September 2003.

CITED LITERATURE (Continued)

23. Kubo, A., Tomisato, S., Hata, M., and Yoshino, H.: Transmission performance evaluation for designing an ofdm transmitter that offers iterative peak reduction. IEICE Trans. Fundam. Electron. Commun. Comput. Sci., E89-A(7):1968–1971, 2006.

24. Wulich, D.: Definition of Efficient PAPR in OFDM. IEEE Commun. Lett., 9(9):832–834, September 2005.

25. Cha, S., Park, M., Lee, S., Bang, K.-J., and Hong, D.: A new papr reduction technique for ofdm systems using advanced peak windowing method. IEEE Trans. Consum. Electron., 54(2):405–410, May 2008.

26. Stuber, G. L., Barry, J. R., McLaughlin, S. W., Li, Y. G., Ingram, M. A., and Pratt, T. G.: Broadband MIMO-OFDM wireless communications. In Proc. of the IEEE, volume 92, pages 271–294, February 2004.

27. Muquet, B., Wang, Z., Giannakis, G., Courtville, M., and P.Duhamel: Cyclic prefixing or zero padding for wireless multicarrier transmission? IEEE Trans. Comm., 50(12):2136–2148, December 2002.

28. Ochiai, H. and Imai, H.: Performance Analysis of Deliberately Clipped OFDM Signals. IEEE Trans. Commun., 50(1):89–101, January 2002.

29. van Nee, R. and de Wild, A.: Reducing the Peak-to-Average Power Ratio of OFDM. In Proc. of Vehicular Technology Conference, 1998. 48th IEEE, volume 3, pages 2072–2076, 18-21 May 1998.

30. Kennington, P.: High-linearity RF Amplifier Design. Artech House, 2000.

31. Katz, A.: Linearization: reducing distortion in power amplifiers. Microwave Magazine, IEEE, 2(4):37–49, Dec 2001.

32. Rapp, C.: Effect of hpa-nonlinearity on 4-dpsk/ofdm-signal for a digital sound broadcasting system. In Proceedings of the second European conference on satellite communications, pages 179–184, Oct. 1991.

33. Miller, S. and O'Dea, R.: Peak power and bandwidth efficient linear modulation. Communications, IEEE Transactions on, 46(12):1639–1648, Dec 1998.

34. Li, X. and Jr., L. C.: Effects of clipping and filtering on the performance of ofdm. In IEEE Comm. Lett., volume 2, pages 131–133, May 1998.

CITED LITERATURE (Continued)

35. Armstrong, J.: Peak-to-average power reduction for ofdm by repeated clipping and frequency domain filtering. Electronic Lett. IEEE, 38:246–247, Feb. 2002.

36. Deng, S.-K. and Lin, M.-C.: OFDM PAPR reduction using clipping with distortion control. In Proc. of the IEEE Intl. Conf. on Comm., volume 4, pages 2563–2567, May 2005.

37. Baxley, R., Zhao, C., and Zhou, G.: Constrained clipping for crest factor reduction in ofdm. IEEE Trans. Broadcast., 52(4):570–575, DEC 2006.

38. Jiang, T., Yang, Y., and Song, Y.-H.: Exponential Companding Technique for PAPR Reduction in OFDM Systems. IEEE Trans. Broadcast., 51(2):244–248, June 2005.

39. Kim, J. and Shin, Y.: An effective clipped companding scheme for papr reduction of ofdm signals. Communications, 2008. ICC ’08. IEEE International Conference on, pages 668–672, May 2008.

40. Pauli, M. and Kuchenbecker, H.-P.: On the reduction of the out-of-band radiation of ofdm-signals. Proc. IEEE Int. Conf. on Communications, 3:1304–1308, 1998.

41. Kuo, H. and Cheung, S.: Optimization of windowing and peak-windowing techniques for wcdma systems. In Proc. IEEE ICASSP 2006, volume 4, pages IV 313–IV–316, 14-19 May 2006.

42. Jones, A., T.A.Wilkinson, and Barton, S.: Block coding scheme for reduction of peak to mean envelope power ratio of multicarrier transmission schemes. Electronics Letters, 20(25):2098–2099, December 1994.

43. Sathananthan, K. and Tellambura, C.: Coding to reduce both par and picr of an ofdm signal. Communications Letters, IEEE, 6(8):316–318, Aug 2002.

44. Li, X. and Ritcey, J.: M-sequences for ofdm peak-to-average power ratio reduction and error correction. Electronics Letters, 33(7):554–555, Mar 1997.

45. Jayalath, A. and Athaudage, C.: On the par reduction of ofdm signals using multiple signal representation. Personal, Indoor and Mobile Radio Communications, 2003. PIMRC 2003. 14th IEEE Proceedings on, 1:799–803 Vol.1, Sept. 2003.

46. Bauml, R. W., Fischer, R. F. H., and Huber, J. B.: Reducing the peak-to-average power ratio of multicarrier modulation by selected mapping. IEEE Elec. Lett., 32(22):2056–2057, October 1996.

CITED LITERATURE (Continued)

47. Müller, S. H. and Huber, J. B.: OFDM with Reduced Peak-to-Average Power Ratio by Optimum Combination of Partial Transmit Sequences. IEEE Elec. Lett., 33:368–369, February 1997.

48. Han, S. H. and Lee, J. H.: Papr reduction of ofdm signals using a reduced complexity pts technique. Signal Processing Letters, IEEE, 11(11):887–890, Nov. 2004.

49. Nguyen, T. T. and Lampe, L.: On Partial Transmit Sequences for PAR Reduction in OFDM Systems. Wireless Communications, IEEE Transactions on, 7:746–755, February 2008.

50. Jayalath, A. and Tellambura, C.: Slm and pts peak-power reduction of ofdm signals without side information. Wireless Communications, IEEE Transactions on, 4(5):2006–2013, Sept. 2005.

51. Tsai, Y.-R. and Huang, S.-J.: Pts with non-uniform phase factors for papr reduction in ofdm systems. Communications Letters, IEEE, 12(1):20–22, January 2008.

52. Jayalath, A. and Tellambura, C.: Use of data permutation to reduce the peak-to-average power ratio of an ofdm signal. Wireless Communications and Mobile Computing, 2(2):187–203, Mar. 2002.

53. Gatherer, A. and Polley, M.: Controlling clipping probability in dmt transmission. In Proc. Asilomar Conf. Signals, Systems, and Computers, volume 1, pages 578–584, November 1997.

54. Lawrey, E. and Kikkert, C.: Peak to average power ratio reduction of ofdm signals using peak reduction carriers. Signal Processing and Its Applications, 1999. ISSPA '99. Proceedings of the Fifth International Symposium on, 2:737–740 vol.2, 1999.

55. Tellado, J.: Peak to Average Power Reduction for Multicarrier Modulation. Doctoral dissertation, Stanford Univ., 2000.

56. Devlin, C., Zhu, A., and Brazil, T.: Peak to average power ratio reduction technique for ofdm using pilot tones and unused carriers. Radio and Wireless Symposium, 2008 IEEE, pages 33–36, Jan. 2008.

57. Tan, C. and Wassell, I.: Data bearing peak reduction carriers for ofdm systems. Information, Communications and Signal Processing, 2003 and the Fourth Pacific Rim Conference on Multimedia. Proceedings of the 2003 Joint Conference of the Fourth International Conference on, 2:854–858 vol.2, Dec. 2003.

CITED LITERATURE (Continued)

58. Krongold, B. S. and Jones, D. L.: PAR Reduction in OFDM via Active Constellation Extension. In Proc. IEEE Int. Conf. Acoustics, Speech,and Signal Processing, volume 4, pages IV–525–IV–528, April 2003.

59. Sezginer, S. and Sari, H.: Metric-based symbol predistortion techniques for peak power reduction in ofdm systems. Wireless Communications, IEEE Transactions on, 6(7):2622–2629, July 2007.

60. Aggarwal, A. and Meng, T. H.: Minimizing the peak-to-average power ratio of OFDM signals via convex optimization. In Proceedings of IEEE Globecom Conference 2003, pages 2385–2389, December 2003.

61. Aggarwal, A. and Meng, T. H.: A convex interior-point method for optimal OFDM PAR reduction. In Proceedings of IEEE International Conference on Communications 2005, volume 3, pages 1985–1990, Seoul, South Korea, May 2005.

62. Kou, Y., Lu, W.-S., and Antoniou, A.: A new peak-to-average power-ratio reduction algorithm for ofdm systems via constellation extension. Wireless Communications, IEEE Transactions on, 6(5):1823–1832, May 2007.

63. Yoo, S., Yoon, S., Kim, S., and Song, I.: A Novel PAPR Reduction Scheme for OFDM Systems: Selective Mapping of Partial Tones (SMOPT). IEEE Trans. Comsumer Electronics, 52(1):40–43, February 2006.

64. Sharif, M., Florens, C., Fazel, M., and Hassibi, B.: Amplitude and sign adjustment for peak-to-average-power reduction. IEEE TRANSACTIONS ON COMMUNICATIONS, 53:1243–1247, August 2005.

65. Zabre, S., Palicot, J., Louet, Y., and Lereau, C.: Reduction of OFDM Peak to Mean Envelope Power Ratio Using Ghost Carriers. In Proceedings of Wireless and Mobile Communications, 2007. ICWMC '07. Third International Conference on, pages 37–41, March 2007.

66. de Courville, M., Duhamel, P., Madec, P., and Palicot, J.: Blind equalization of OFDM systems based on the minimization of a quadratic criterion. In Proceedings of Communications, 1996. ICC 96, Conference Record, Converging Technologies for Tomorrow's Applications. 1996 IEEE International Conference on, volume 3, pages 1318–1322, June 1996.

CITED LITERATURE (Continued)

67. Zabre, S., Palicot, J., Louet, Y., and Lereau, C.: SOCP Approach for OFDM Peak-to-Average Power Ratio Reduction in the Signal Adding Context. In Proceedings of IEEE Symposium on Signal Processing and Information Technology (ISSPIT'06), pages 834–839, Vancouver,Canada, August 2006.

68. Guel, D., Louet, Y., and Palicot, J.: A geometric method for papr reduction in a signal adding context for ofdm signals. Digital Signal Processing, 2007 15th International Conference on, pages 347–350, July 2007.

69. Jun, Y., Jiawei, Y., and Jiandong, L.: Reduction of the peak-to-average power ratio of the multicarrier signal via artificial signals. Communication Technology Proceedings, 2000. WCC - ICCT 2000. International Conference on, 1:581–585 vol.1, 2000.

70. Dardari, D., Tralli, V., and Vaccari, A.: A theoretical characterization of nonlinear distortion effects in OFDM systems. IEEE Commun. Lett., 48(10):1755–1764, October 2000.

71. Pauli, M. and Kuchenbecker, H.-P.: Minimization of the intermodulation distortion of a nonlinearly amplified ofdm signal. Wirel. Pers. Commun., 4(1):93–101, 1997.

72. Chen, H. and Haimovich, A.: Iterative estimation and cancellation of clipping noise for ofdm signals. In IEEE Comm. Lett., volume 7, pages 305–307, July 2003.

73. Sano, H., Kubo, H., and Murakami, K.: Adaptive peak power reduction scheme controlling peak level based on adaptive algorithm. Electron Comm Jpn Pt 1, 89(10):44–55, 2006.

74. Vaananen, O., Vankka, J., and Halonen, K.: Simple algorithm for peak windowing and its application in GSM, EDGE and WCDMA systems. In Proc. of IEE Communications, volume 152, pages 357–362, June 3 2005.

75. Chen, G., Ansari, R., and Yao, Y.: Improved peak windowing for papr reduction in ofdm. In Vehicular Technology Conference, 2009. VTC Spring 2009. IEEE 69th, pages 1–5, 2009.

76. Boyd, S. and Vandenberghe, L.: Convex Optimization. Cambridge University Press, 2004.

77. Dejardin, R., Colas, M., and Gelle, G.: Comparison of iterative receivers mitigating the clipping noise of ofdm based systems. In 13th European Wireless Conference (EW'07), Paris, France, Apr. 2007.

78. Kim, D. and Stuber, G.: Clipping noise mitigation for ofdm by decision-aided reconstruction. Communications Letters, IEEE, 3(1):4–6, January 1999.

CITED LITERATURE (Continued)

79. Saeedi, H., Sharif, M., and Marvasti, F.: Clipping noise cancellation in ofdm systems using oversampled signal reconstruction. Communications Letters, IEEE, 6(2):73–75, February 2002.

80. Chen, H. and Haimovich, A.: An iterative method to restore the performance of clipped and filtered ofdm signals. In Communications, 2003. ICC '03. IEEE International Conference on, volume 5, pages 3438–3442, May 2003.

81. AliHemmati, R. and Azmi, P.: Iterative reconstruction-based method for clipping noise suppression in ofdm systems. Communications, IEE Proceedings, 152(4):452–456, Aug. 2005.

82. Chen, Y., Zhang, J., and Jayalath, A.: Estimation and compensation of clipping noise in ofdma systems. Wireless Communications, IEEE Transactions on, 9(2):523–527, Feb. 2010.

83. Chen, G. and Ansari, R.: Clipping noise suppression in ofdma using frame based alternating projection. In Electro/Information Technology (EIT), 2012 IEEE International Conference on, pages 1–4, Indianapolis, IN, USA, May 2012.

84. Chen, G. and Ansari, R.: Ofdma nonlinear distortion recovery using improved clipping localization and iterative projections. In Wireless Telecommunications Symposium (WTS), 2013, pages 1–5, Phoenix, AZ, USA, April 2013.

85. Proakis, J. and Salehi, M.: Digital Communications. McGraw-Hill Science/Engineering/Math, 2007.

86. Simon, M. K. and Alouini, M.-S.: Digital Communication over Fading Channels: A Unified Approach to Performance Analysis. Wiley-Interscience; 1st edition, 2000.

87. Wang, L. and Tellambura, C.: Analysis of clipping noise and tone-reservation algorithms for peak reduction in ofdm systems. Vehicular Technology, IEEE Transactions on, 57(3):1675–1694, May 2008.

88. Ferreira, P. J. S. G.: Mathematics for multimedia signal processing ii discrete finite frames and signal reconstruction. Signal Processing for Multimedia, pages 35–54, 1999.

89. Farrell, B.: Limiting empirical singular value distribution of restrictions of discrete fourier transform matrices. Journal of Fourier Analysis and Applications, 17(4):733–753, 2011.

90. Erceg, V. et al.: Channel models for fixed wireless applications. IEEE 802.16 Broadband Wireless Access Working Group, Tech. Rep., Jul. 2001.

CITED LITERATURE (Continued)

91. Guan, K.: Opportunistic Sampling by Level-Crossing. Doctoral dissertation, University of Illinois at Urbana-Champaign, 2012.

92. Jayalath, A. D. S. and Athaudage, C. R. N.: On the par reduction of ofdm signals using multiple signal representation. Communications Letters, IEEE, 8(7):425–427, 2004.

93. Krongold, B. and Jones, D.: Par reduction in ofdm via active constellation extension. Broadcasting, IEEE Transactions on, 49(3):258–268, Sept. 2003.

94. Dejardin, R., Colas, M., and Gelle, G.: Soft decision aided suboptimal ml detection receiver for clipped cofdm transmissions. In Global Telecommunications Conference, 2009. GLOBECOM 2009. IEEE, pages 1 –6, 30 2009-dec. 4 2009.

95. Mohammadnia-Avval, M., Ghassemi, A., and Lampe, L.: Compressive sensing recovery of nonlinearly distorted ofdm signals. In Communications (ICC), 2011 IEEE International Conference on, pages 1 –5, june 2011.

96. Al-Safadi, E. and Al-Naffouri, T.: Peak reduction and clipping mitigation in ofdm by augmented compressive sensing. Signal Processing, IEEE Transactions on, 60(7):3834 –3839, july 2012.

97. Fischer, R. F. and Waeckerle, F.: Peak-to-average power ratio reduction in ofdm via sparse signals: Transmitter-side tone reservation vs. receiver-side compressed sensing. OFDM 2012, 17th International OFDM Workshop 2012 (InOWo'12); Proceedings of, pages 1 –8, aug. 2012.

98. Li, H., Jiang, T., and Zhou, Y.: An improved tone reservation scheme with fast convergence for papr reduction in ofdm systems. Broadcasting, IEEE Transactions on, 57(4):902–906, Dec 2011.

99. Liu, Q., Baxley, R., and Zhou, G.: Free subcarrier optimization for peak-to-average power ratio minimization in ofdm systems. In Acoustics, Speech and Signal Processing, 2008. ICASSP 2008. IEEE International Conference on, pages 3073–3076, March 2008.

100. Donoho, D.: Compressed sensing. Information Theory, IEEE Transactions on, 52(4):1289–1306, 2006.

101. Cands, E. J.: The restricted isometry property and its implications for compressed sensing. Comptes Rendus Mathematique, 346(910):589 – 592, 2008.

CITED LITERATURE (Continued)

102. Tibshirani, R.: Regression shrinkage and selection via the lasso: a retrospective. Journal of the Royal Statistical Society: Series B (Statistical Methodology), 73(3):273282, 2011.

103. Needell, D. and Vershynin, R.: Signal recovery from incomplete and inaccurate measurements via regularized orthogonal matching pursuit. Selected Topics in Signal Processing, IEEE Journal of, 4(2):310 –316, april 2010.

104. Candes, E., Romberg, J., and Tao, T.: Robust uncertainty principles: exact signal reconstruction from highly incomplete frequency information. Information Theory, IEEE Transactions on, 52(2):489–509, 2006.

105. Tarokh, V., Seshadri, N., and Calderbank, A. R.: Space-Time Codes for High Data Rate Wireless Communications: Performance Critierion and Code Construction. IEEE Trans. Inf. Theory, 44(3):744–765, March 1998.

106. Xin, Y., Wang, Z., and Giannakis, G. B.: Space-time diversity systems based on linear constellation precoding. IEEE Trans. Wireless Commun., 2(2):294–309, March 2003.

107. Valbonesi, L.: Frame-theoretic approach for improved signal design in Orthogonal Frequency Division Multiplexing. Doctoral dissertation, Univ. of IL. at Chicago, 2005.

108. Valbonesi, L. and Ansari, R.: Frame-based approach for peak-to-average power ratio reduction in ofdm. IEEE Trans. on Commun., 54(9):1604–1613, September 2006.

109. Lee, Y., You, Y., Jeon, W., Paik, J., and Song, H.: Peak-to-average power ratio in MIMO-OFDM systems using selective mapping. IEEE Commun. Lett., 7(12):575–577, December 2003.

110. Woo, G. and Jones, D. L.: Peak power reduction in MIMO-OFDM via active channel extension. In Proc. IEEE Intl. Conf. on Commun., volume 4, pages 2636–2639, May 2005.

111. Chen, G. and Ansari, R.: Frame expansion based peak to average power ratio reduction in mimo ofdm systems. Signal Processing Systems, 2007 IEEE Workshop on, pages 61–66, Oct. 2007.

112. Alamouti, S. M.: A simple transmit diversity technique for wireless communications. IEEE J. Select. Areas Commun., 16(8):1451–1458, October 1998.

113. Goyal, V., Kovacevic, J., and Kelner, J.: Quantized frame expansions with erasure. Applied and Computational Harmonic Analysis, 2001.

CITED LITERATURE (Continued)

114. Rath, G. and Guillemot, C.: Frame-theoretic analysis of dft codes with erasures. IEEE Trans. Signal Processing, 52(2), 2004.

VITA

Name	Guoguang Chen
Education	Ph.D., Electrical and Computer Engineering University of Illinois at Chicago, Chicago, IL 2014
	M.S., Mathematics University of Illinois at Chicago, Chicago, IL 2005
	M.S., Electronic Engineering Tsinghua University, Beijing, China 2002
	B.E., Electronic Engineering Tsinghua University, Beijing, China 1999
Experience	Lemko Corporation Lead Software Engineer 2009 to present
	Motorola Inc. Motorola Labs, Contractor 2006 to 2008
	University of Illinois at Chicago Graduate Assistant 2004 to 2006
	University of Illinois at Chicago Graduate Teaching Assistant 2002 to 2006
Publications	Guoguang Chen and Rashid Ansari, *Clipping noise mitigation in OFDMA using improved peak localization and frame-based alternating projection*, IEEE Transactions on Wireless Communications, submitted.

VITA (Continued)

Publications

Guoguang Chen and Rashid Ansari, *Joint Design on Transmitter and Receiver Schemes of Mitigating Nonlinear Power Amplification Effects in OFDMA*, IEEE Trans. Signal Processing, submitted.

Guoguang Chen and Rashid Ansari, *A New PAPR Reduction Technique Using Improved Peak Windowing in LTE System*, IEEE Transactions on Broadcasting, submitted.

Guoguang Chen and Rashid Ansari, *Frame Expansion Based Peak to Average Power Ratio Reduction in MIMO OFDM Systems*, Signal Processing Systems, 2007 IEEE Workshop on, pp.61-66.

X. Zhang and H. Wang and A. Khokhar and R. Ansari and G. Chen, *Distortion Analysis for Real-Time Data Collection of Correlated Fields in Randomly Distributed Sensor Networks*, Communications, 2008. ICC '08. IEEE International Conference on, pp.2211-2215.

Guoguang Chen and Rashid Ansari and Yingwei Yao, *Improved Peak Windowing for PAPR Reduction in OFDM*, Vehicular Technology Conference, 2009. VTC Spring 2009. IEEE 69th, pp.1-5.

Guoguang Chen and Rashid Ansari, *Clipping noise suppression in OFDMA using frame-based alternating projection*, Electro/Information Technology (EIT), 2012 IEEE International Conference on, May 2012, Indianapolis, IN, USA,pp.1-4.

Guoguang Chen and Rashid Ansari, *OFDMA Nonlinear Distortion Recovery using Improved Clipping Localization and Iterative Projections*, Wireless Telecommunications Symposium (WTS), 2013, Phoenix, AZ, USA, pp.1-5.

Guoguang Chen and Rashid Ansari, *Design of Joint Transmitter and Receiver Schemes for Power Efficiency Improvement in OFDMA*, MilCom'14, to be submitted.

Membership

Member, Communications Society, Signal Processing Society, IEEE, since 2006